Ph.D. Dissertation of Engineering

Selective Use of Fly Ash Nanoparticles in Oil Industry

– Application for CO_2 EOR, Oil Spill Cleanup and Produced Water Treatment –

비산재 나노입자의 석유 산업 내 선별적 활용

–CO_2 기반 석유증진회수, 원유 유출 처리, 생산수 정화에 적용–

February 2019

Graduate School of Engineering
Seoul National University
Energy Resources Engineering Major

Daeyang Lee

Selective Use of Fly Ash Nanoparticles in Oil Industry

- Fly Ash Nanoparticles for CO_2 EOR, Oil Spill Cleanup and Produced Water Treatment -

Adviser: Heechan Cho

Submitting a Ph.D. Dissertation of Public Administration
November 2018

Graduate School of Engineering
Seoul National University
Energy Resources Engineering Major

Daeyang Lee

Confirming the Ph.D. Dissertation written by
Daeyang Lee
December 2018

Chair	민 동 주	(Seal)
Vice Chair	조 희 찬	(Seal)
Examiner	하 전	(Seal)
Examiner	정 은 혜	(Seal)
Examiner	김 정 은	(Seal)

Abstract

In this study, the preparation and application of nanoparticles obtained from fly ash using top-down method were studied. The main objectives of application are to replace the synthetic silica nanoparticles used in CO_2 enhanced oil recovery and remove oil contamination from produced water and oil spills.

The energy cost of producing fly ash nanoparticles with an average particle size of 200 ㎚ was approximately one-tenth the price of synthetic silica. Bare fly ash nanoparticle did not stabilize supercritical CO_2 foam alone, but showed synergy with some surfactants. The synergistic effect of producing more stable foam was observed between nanoparticles obtained from thermally-treated fly ash(TTFA) and surfactants such as dodecyltrimethylammonium bromide (DTAB) or Bioterge AS-40. The resistance factor of foam increased 2 to 4 times when the TTFA nanoparticles were added to the surfactant.

The high carbon content fly ash (HCCFA) nanoparticle dispersant formed very stable aggregates with crude oil, which aided in oil spill cleanup by delaying oil penetration into sand and promoting the separation of oil from sand. This indicates the possibility of using fly

ash as an oil spill cleanup agent, especially when the oil spill occurred near a beach with waves.

HCCFA also showed excellent efficacy in removing micro oil droplets ($d < 10$ ㎛) dispersed in produced water. When HCCFA was added to pollutants at 1:1 ratio, it produced branch-like agglomerates with crude oil and precipitated, and 93–97% of the crude oil micro droplets were removed through this reaction.

This study suggests the possibility of increasing the recycling rate and reducing the environmental impact of fly ash by exploring different application methods of carbonaceous and mineral components of fly ash.

Keywords : Fly ash, Nano-grinding, Enhanced oil recovery, Oil spill cleanup, Produced water treatment, CO_2 foam.
Student Number: 2010-21041

Table of contents

1. Introduction 1
1.1. Importance of Petroleum and Coal for World's Energy Needs... 1
1.2. Thesis Research Objectives, Key Hypotheses and Implementation Tasks 3
1.3. Synopsis of Thesis..... 6
2. Research Background..... 8
2.1. Overview of Gas-based Enhanced Oil Recovery (EOR) 8
2.1.1. CO_2 EOR and WAG process 9
2.1.2. Importance of mobility control..... 15
2.1.3. Improved mobility control by using foam 18
2.1.4. Nanoparticles and foam..... 24
2.2. Oil Spill Cleanup 39
2.3. Produced Water Treatment 42
2.4. Characteristics of Fly Ash and its Utilization..... 45
2.4.1. Coal combustion products and fly ash 46
2.4.2. Fly Ash as construction materials 50
2.4.3. Fly ash as a low-cost absorbent..... 61
2.4.4. Environmental impact of fly ash 78
2.4.5. Fly ash in Korea..... 82
3. Fly ash Particles as CO_2 Foam Stabilizer..... 84
3.1. Materials and Preparation..... 84
3.1.1. Characteristics of raw fly ash samples..... 84
3.1.2. Chemical composition control of fly ash particles 91

3.1.3. Grinding characteristics of fly ash 101
3.1.4. Narrowing the particle size distribution 116
3.1.5. Batch-type emulsion/foam generator 119
3.1.6. Continuous injection equipment 121
3.2. Experimental Results 126
3.2.1. Batch-type emulsion/foam generator 126
3.2.2. Continuous injection test 136
4. Utilization of the Carbonaceous Material in Fly Ash 143
4.1. Fly Ash at the O/W Interface 144
4.2. Oil Spill Cleanup by Using HCCFA 150
4.2.1. Experimental method 150
4.2.2. Experimental results 152
4.3. Treatment of Produced Water by Using HCCFA 158
4.3.1. Experimental method 158
4.3.2. Experimental results 161
5. Conclusions and Recommendations 168
References 174
Appendix 201

List of Figures

Figure 1.1. Oil demand forecast by 2040 (data from OPEC 2017) .. 2
Figure 1.2. Changes in energy demand by 2040 relative to 2017 (OPEC 2017) 2
Figure 2.1. Schematic diagram of the phenomena responsible for the poor sweep efficiency observed in gas flooding: (a) gravity override, (b) viscous fingering, and (c) thief zone. 16
Figure 2.2. Variation of the energy of attachment, E (relative to kT), of a spherical particle of radius R = $1 \times 10\text{-}8$ m at a planar oil–water interphase; $\gamma ow = 36 \times 10\text{-}3$ $N \cdot m\text{-}1$ at 298 K (Binks and Lumsdon, 2000)..... 27
Figure 2.3. Schematic demonstrating the relationship between contact angle (measured with an aqueous phase) and the position of a spherical particle at the planar oil–water interface; for $\theta < 90$ (left), o/w emulsions are favored, whereas for $\theta > 90$ (right), w/o emulsions are expected (Dickson et al., 2004)..... 27
Figure 2.4. Stepwise thinning of a film in the presence of 8 ㎚ silica particles at the effective volume fractions of 0.25 (right) and 0.35 (left). (Sethumadhavan et al., 2001) 34
Figure 2.5. Possible mechanisms of liquid film stabilization: (a) a monolayer of bridging particles; (b) a bilayer of close packed particles; and (c) a network of particle aggregates inside the film. (Horozov, 2008) 34

Figure 2.6. Coal demand growth by major regions, 2015–2040. The demand growth in India is prominent. (OPEC, 2017) 49
Figure 2.7. Annual CCP emissions and recycling rates (American–Coal–Ash–Association., 2018) 49
Figure 2.8. Use of fly ash (a) in the USA in 2012 (modified from (American–Coal–Ash–Association., 2012)) and (b) in India in 2016 (modified from (American–Coal–Ash–Association., 2018)) 51
Figure 2.9. Idealized structure of zeolite framework (Querol et al., 2002) 77
Figure 2.10. Top: Channel diameter of zeolite, which is dependent on the structure. Bottom: Examples of channel sizes for select zeolites, which may be synthesized from fly ash, that are compared with the diameters of some gaseous molecules. (Querol et al., 2002) 77
Figure 3.1. XRD pattern of the fly ash sample obtained from Taean coal power plant in Taean, Korea 86
Figure 3.2. Size distribution of the fly ash sample. 87
Figure 3.3. SEM image of −400 mesh sample 88
Figure 3.4. Results of EDS analysis of spherical mineral particles in fly ash 88
Figure 3.5. SEM image and EDS analysis results of +100 mesh samples. (a) Porous shell–shaped particles. (b) Small spherical minerals in the shell–like particles. (c) EDS result of shell–like particle. 89

Figure 3.6. Measured zeta potential as a function of pH for raw fly ash particles. The particles were ground to an average size of about 5 ㎛ before the analysis..... 90
Figure 3.7. Results of the zeta potential measurements of TTFA samples. 92
Figure 3.8. Change in LOI according to particle size..... 94
Figure 3.9. (a) Schematic of a tensiometer; (b) Results of wettability experiments performed on +140 mesh fly ash and TTFA. 99
Figure 3.10. SEM image of the particles separated by froth flotation. 100
Figure 3.11. The bead mill used in the experiment and a schematic diagram of the flow in the equipment..... 104
Figure 3.12. Median size of fly ash particles per energy input for varying the grinding media size in an attrition mill..... 108
Figure 3.13. Reduction in median size with increasing number of recirculations when grinding a TTFA sample in a bead mill by using three different sizes of grinding media 110
Figure 3.14. Evolution of the size distributions of a TTFA sample upon grinding in a bead mill by using three different sizes of grinding media: (a) 100 ㎛, (b) 300 ㎛, and (c) 500 ㎛..... 111
Figure 3.15. Change in median size according to energy input for different types of fly ashes. 113
Figure 3.16. TEM image of a fly ash with the median particle size of 200 ㎚. 113

Figure 3.17. Effect of the slurry concentration and the rotational speed on the specific energy 115
Figure 3.18. Effect of grinding aid (Calgon) on the specific energy 115
Figure 3.19. Changes in zeta potential with the addition of sodium polyacrylate to fly ash. The TTFA particles were strongly anionic (< -30 mV) in the pH range 6 to 9. 118
Figure 3.20. (a) Schematic of a batch-type emulsion/foam generator, (b) Actual image of the inside of the cell. The magnet stirrer is driven by a specially designed neodymium magnet spinner present on the outside. 120
Figure 3.21. Schematic of continuous injection equipment 125
Figure 3.22. Images of the CO_2/water emulsion stabilized by using three different types of fly ash nanoparticles: (a) TTFA, (b) raw fly ash, and (c) +140 mesh fly ash (generated at 800 psi, 286 K). 127
Figure 3.23. Outline of the CO_2 foam test used to find the synergistic fly ash-surfactant combinations. 130
Figure 3.24. Relative volume of the foam formed through the addition of DTAB into the slurries of the fly ash nanoparticles obtained by grinding three different types of fly ash samples. 130
Figure 3.25. Neither the (a) 0.1% DTAB solution nor (b) 3% TTFA dispersion formed a stable foam with supercritical CO_2, but a stable fine-textured foam was obtained in (c) a mixed solution of 3% TTFA and 0.03% DTAB. 132

Figure 3.26. Supercritical CO_2 foam stabilized with 0.05% DTAB and different fly ash: (a) 5 wt% TTFA, (b) 5 wt% raw fly ash, (c) 5 wt% +70 mesh fly ash mixtures. There are large cavities inside the foam in figure (c); consequently the backlight is visible, while it is invisible in the other samples. 133
Figure 3.27. Foam stabilization effect of oil-coated fly ash obtained from a CO_2 foam test performed under atmospheric pressure. 135
Figure 3.28. When 5 wt% of fly ash (50% LOI) with 0.5 ㎖ of turpentine oil was mixed with supercritical CO_2, no foam was observed 135
Figure 3.29. Supercritical CO_2 injection test results 137
Figure 3.30. Schematic of the core flooding equipment of UT Austin. 139
Figure 3.31. Synergy case of TTFA nanoparticles with an anionic surfactant (Bio-terge AS-40). (Modified from the annual research report of UT Austin, Aug 2014; not published) 141
Figure 3.32. Experimental case where nanoparticles have a negative effect on nonionic surfactants. (Modified from the annual research report of UT Austin, Aug 2014; not published) 142
Figure 4.1. Relative volume of the o/w emulsion phase formed when decane was mixed with the dispersion of fly ash nanoparticles of various solid concentrations after the lapse of 5000 min. 146
Figure 4.2. Visual demonstration of the o/w emulsion phase formed for solid concentrations of (a) 0.31 wt%, (b) 0.62 wt%, and (c) 1.25 wt% in +140 fly ash samples 146

Figure 4.3. (a) Relative volume of the o/w emulsion phase formed when different types of alkanes were mixed with the dispersion of fly ash nanoparticles at various solid concentrations after the lapse of 2000 min. (b) Plots as functions of time for the different alkanes. 148
Figure 4.4. (a) Relative volume of the o/w emulsion phase formed when different types of alkanes were mixed with an anionic surfactant (Bioterge AS-40) at various concentrations after the lapse of 1600 min. (b) Plots as functions of time for the different alkanes. 149
Figure 4.5. Schematic of tidal flushing experiment. 153
Figure 4.6. Schematic of surface-scraping experiment. 154
Figure 4.7. Percentage of oil removed by tidal flushing..... 156
Figure 4.8. (a) The left side shows a sand pack with OHA and brine, and the right side is a sand pack with crude oil and brine; (b) After 24 h, the oil settled at the bottom; (c) The OHA remaining on the surface floated, due to water injection; (d) In the sand pack with crude oil, contaminated brine is elevated, but no oil layer is observed; (e) Top view. 157
Figure 4.9. Appearance of the sample pushed up for surface-scraping (for the case of AEL OHA). 159
Figure 4.10. (a) APW samples with 2000 ppm of crude oil dispersed. AEL is on the left, SOK in the middle, and KWT on the right. (b) After HCCFA was added in 1:1 ratio with oil. (c) After 24 h; and (d) Appearance of the separated supernatant, which is almost transparent..... 163

Figure 4.11. (a) Optical microscopy image of APW with dispersed crude oil at 1000 magnification; (b) HCCFA particles with d50 = 500 ㎚; (c) An image (at 1000 magnification) of the supernatant recovered after HCCFA precipitation reaction; (d) Appearance of the precipitated HCCFA particles. 164
Figure 4.12. Removal efficiency of HCCFA particles corresponding to each BTEX component with different average particle sizes. 166
Figure 4.13. Appearance of the HCCFA particles recovered from the bottom. 166
Figure 4.14. Change of adsorption rate on BTEX by addition of DTAB. In both cases, the average adsorption rate increased from 52% to 75%..... 167

List of Tables

Table 1. Summary of the papers published on the synergy between nanoparticles and surfactants 35
Table 2. Comparison of the normal ranges of the chemical constituents of bituminous coal fly ash with those of lignite coal fly ash and sub−bituminous coal fly ash (Ahmaruzzaman, 2010) 54
Table 3. The chemical composition criteria of Class C and Class F fly ashes, as defined by ASTM C 618 54
Table 4. Ranges of the trace elements released into aqueous solution. From 4:1 to 20:1, water/ash was experimented for 18 h to 24 h (modified from (Theis et al., 1990)) 81
Table 5. Results of XRF analysis of the fly ash sample obtained from Taean coal power plant 86
Table 6. Results of flotation experiments performed at different pH values 100
Table 7. Particle size distribution of stability−enhanced TTFA particles after centrifugation 118
Table 8. Origin and properties of the crude oil used in the experiment 153

1. Introduction

1.1. Importance of Petroleum and Coal for World's Energy Needs

According to OPEC's 2017 data, petroleum accounts for 31% of global energy consumption (OPEC, 2017). Although 95.4 million barrels of oil is consumed every day (OPEC, 2017), opinions on oil depletion are divergent. The main reason people are skeptical about oil depletion is the development of related technologies. Technological development in the field of oil discovery and exploration has enabled the production of oil not only onshore but also offshore. The development of oil production technologies has made available new resources such as shale gas and light tight oil. The world is trying to find alternative energy sources because it is clear that there are environmental problems with oil production and consumption, apart from its depletion. The development of renewable energy and the proliferation of electric vehicles are representative strategies to reduce the dependence on oil. Thanks to these efforts, the dependence on oil in 2040 is projected to decline by 4% to 27%, but oil consumption is expected to increase to 111.1 million barrels per day (Figure 1.1) (OPEC, 2017). Although energy consumption by the developed countries is expected to decrease, there is an enormous requirement for additional energy in developing countries, especially India and China (Figure 1.2) (OPEC, 2017).

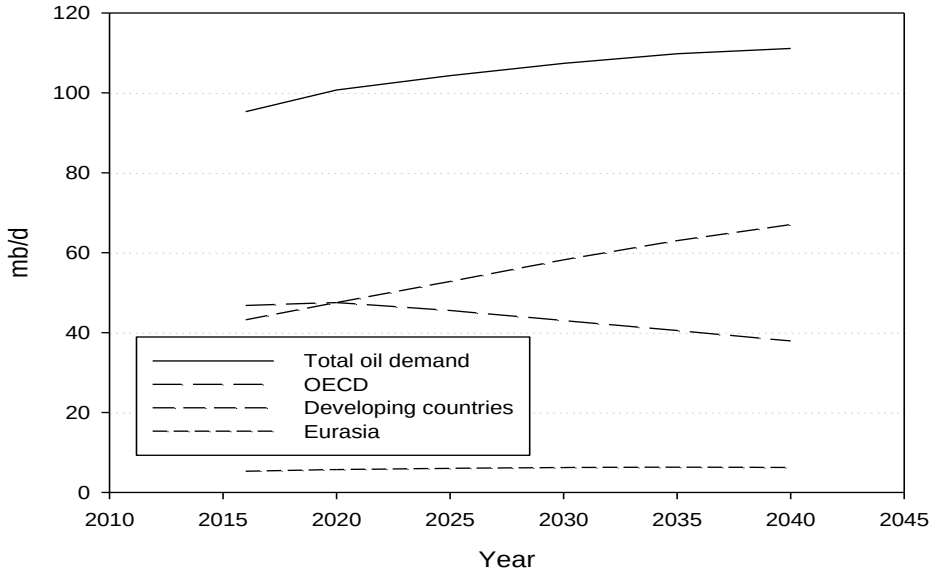

Figure 1.1. Oil demand forecast by 2040 (data from OPEC 2017)

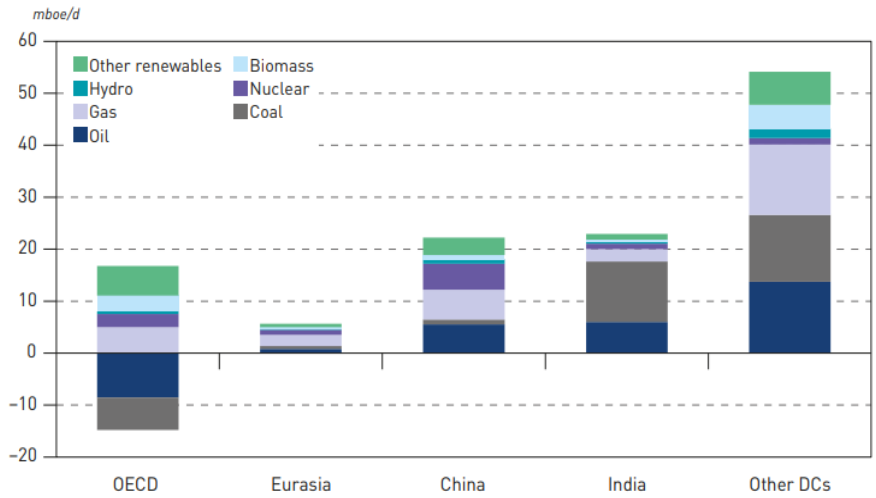

Figure 1.2. Changes in energy demand by 2040 relative to 2017 (OPEC 2017)

Particularly to note from, Figure 1.2 is that coal will also still be a major energy source especially for electricity generation, for the coming tens of years. Since the use of coal generates huge amounts of by-products such as fly ash and bottom ash along with greenhouse gas emissions, minimizing its environmental impacts is a major task that the society has to find solution and act on it. As described in the next sub-section, this thesis research is an attempt to develop a technology that not only helps reduce the environmental impacts from coal usage, but also improves the efficiency of petroleum production.

1.2. Thesis Research Objectives, Key Hypotheses and Implementation Tasks

As reviewed in detail in Section 2.1.4, active research efforts are ongoing to develop silica nanoparticle-stabilized CO_2 foams which can be employed to enhance oil production from the application of CO_2 enhanced oil recovery (EOR) processes (see Section 2.1.1 for overview of CO_2 EOR).

Recognizing that the largest constituent mineral in fly ash is silica, the use of nano-milled fly ash in place of expensive synthesized silica nanoparticles has the potential of not only utilizing waste products from coal-fired power plants but also lowering the cost of foam-stabilizing synthetic nanoparticles.

To achieve this goal, fly ash must undergo several processing steps. First, to reduce its chemical complexity, its mineral or carbonaceous

components were selectively concentrated. A combination of processes such as thermal treatment, particle size classification, and froth flotation resulted in various samples with carbonaceous material content ranging from 0.1% to 71.3%, while the rest are mineral components. Second, each sample was ground to an average particle size of 200 nanometers using an attrition mill and a bead mill. Centrifugation was applied when the particle size distribution had to be further narrowed.

Each fly ash nanoparticle was placed in a batch-type view cell or continuous injection equipment to determine the effects of nanoparticles at the CO_2 and water interface. Experiments were carried out for gas, liquid, and supercritical state CO_2; the temperature, pressure, and solid concentration were variables.

When the nanoparticles alone cannot provide satisfactory results, additives such as surfactants and collectors were added. Studies on the synergistic effects of surfactants and nanoparticles have also been conducted on synthetic silica nanoparticles, and positive results were reported. (see Section 2.1.4.2 for synergistic effects of surfactants and nanoparticles).

In this study, a method to maximize the recycling rate of fly ash was investigated. Fly ash that mainly consists of minerals is recycled as construction materials or for the synthesis of zeolite; however, fly ash with high unburned carbon content is difficult to recycle. Experimental results have shown that fly ash with high carbon

content was well adsorbed on the oil–water interface and exhibited some unique characteristics compared with the surfactant. These characteristics are considered beneficial for oil spill cleanup and produced water treatment.

The use of high carbon content fly ash (HCCFA) for oil spill cleanup has been studied as an alternative to existing solidifiers. Experiments have been conducted to compare the degree to which crude oil agglomerated by HCCFA prevents the penetration of crude oil into sand when it reaches the beach, and how it is separated again by natural low-energy flows such as tides. The removal efficiency of artificial cleanup method such as surface scraping was verified using custom-made equipment.

In order to confirm the feasibility of applying HCCFA in produced water treatment, HCCFA ground to an average particle size of 500 ㎚ was added at 1:1 ratio of the dispersed contaminant mass. Three types of crude oil and a mixture of benzene, toluene, ethylbenzene, and xylene (BTEX), which are the main toxic organic substances in typical produced water, were used as the contaminants for artificial produced water samples. Total petroleum hydrocarbon (TPH) analysis and BTEX analysis were conducted after sedimentation to verify the removal efficiency.

1.3. Synopsis of Thesis

In Section 1.2, the research objective was clarified as use of fly ash in oil industry for various way. The following sections describe three strategies for achieving the research objectives.

Chapter 2 discusses the theoretical and experimental backgrounds. Section 2.1 illustrates the process by which nanoparticles are used for CO_2-based enhanced oil recovery. Gas flooding and foam flooding were mainly summarized for this purpose. Sections 2.2 and 2.3 deal with oil contamination that may occur during oil production, transportation, or storage. Each section deals with current technology and its limitations. In this study, we tried to solve these problems using fly ash. The characteristics and current utilization of fly ash are discussed in Section 2.4.

In Chapter 3, the pretreatment and surface modification processes for the utilization of fly ash as a CO_2 foam stabilizer are described according to the experimental procedure. In Section 3.1.2, various attempts were made to remove or concentrate carbonaceous materials in fly ash. In Section 3.1.3, each sample was ground to an average particle size of 200 ㎚ and the effects of grinding media size and equipment type on the grinding process of fly ash were identified in terms of net energy. In Section 3.2, each sample was injected into batch-type or continuous-type equipment to characterize their behavior at the CO_2-water interface. The nanoparticle dispersion

was mixed with gas, liquid, and supercritical CO_2 in the equipment with or without additives such as oil or surfactant.

Chapter 4 presents new strategies for maximizing the recycling rate of fly ash. Since the main factor that makes fly ash difficult to recycle as construction materials is unburned carbon, the Chapter 4 focuses on how to utilize carbonaceous materials in fly ash. Based on the experimental results, two applications are proposed; as oil spill cleanup agent in Section 4.2 and as absorbent for produced water treatment in Section 4.3.

The results of each chapter are summarized in the conclusion of Chapter 5.

2. Research Background

2.1. Overview of Gas-based Enhanced Oil Recovery (EOR)

Petroleum production from oil fields can be roughly divided into three stages: primary, secondary, and tertiary. Primary recovery is the process of recovering the oil produced by the natural pressure in a reservoir. When the production well reaches the reservoir, the oil in the reservoir expand and naturally flow out through the pipe. The amount obtained through primary recovery is only a small fraction of the total oil present. For example, in Buffalo field in the northwest corner of South Dakota, only 6% of the original oil in place was recovered through primary recovery (Fassihi et al., 1997). In secondary recovery, oil is produced mainly by injecting water into the reservoir to displace oil from reservoir rock pores. The primary and secondary recovery factors range from 20% to 50%, depending on the oil and reservoir properties (Donaldson et al., 1989). For tertiary recovery, often called as EOR, a wide variety of technics has been developed (for review, (Lake, 1989; Sheng, 2013)). When a steady and sufficient source of natural or anthropogenic CO_2 is available, CO_2 injection can be one of the best EOR method. CO_2 injection not only have the advantages as the EOR injection fluid described in Section 2.1.1 below, but also contributes to carbon capture and storage (CCS) by isolating the carbon dioxide in the safe

reservoir. The following is a summary of the advantages, shortcomings, recent work and remaining tasks of CO_2-based EOR.

2.1.1. CO_2 EOR and WAG process

CO_2 EOR is a type of gas flooding. Gas flooding is the most widely used EOR technique since the 2000s (Alvarado and Manrique, 2010). It is as much a traditional EOR technology as thermal method, because it is essentially based on steam flooding technique. Gas flooding involves the injection of hydrocarbon or nonhydrocarbon components into oil reservoirs that are typically water flooded to recover the residual oil. The injection components may include mixtures of hydrocarbons (from methane to propane), and nonhydrocarbon components such as carbon dioxide, nitrogen, and even hydrogen sulfide or other exotic gases such as SO_2 (Sheng, 2013). The primary mechanism of oil recovery by high-pressure gas flooding is mass transfer of the components in the oil between the flowing gas and oil phases, which increases when the gas and the oil become more miscible. Secondary recovery mechanisms include swelling and reduction in oil viscosity as intermediate components in the gas condense into the oil (Sheng, 2013). As a result, gas flooding exhibits better microscopic displacement efficiencies, which lower the residual oil saturation, compared to water flooding (Lake, 1989).

Previously, the injection gas was mainly composed of flue gas or natural air, which is easy to procure in the production field, but now,

nitrogen or carbon dioxide is mainly used for technical stability and protection of the injection equipment.

Nitrogen is an inert, non-toxic, and non-corrosive gas. The biggest advantage of nitrogen is that it can be prepared inexpensively in any location by separation from natural air. Unfortunately, nitrogen has a very high minimum miscibility pressure (MMP), which has limited its usage despite the advantages mentioned above. The reservoir pressure must usually be near or above the MMP to achieve good displacement efficiency (Yellig and Metcalfe, 1980). Because of its high MMP, nitrogen flooding yields good results in a deep light oil reservoir (Taber et al., 1997).

CO_2 is an abundant, nonflammable, and essentially nontoxic, nonpolar solvent that has drawn attention for use in various industrial applications because of its tunable properties (Johnston and Da Rocha, 2009). Unlike nitrogen, carbon dioxide causes corrosion. Nonetheless, CO_2 flooding has been in the global spotlight for many other reasons. From a reservoir engineering point of view, Holm and Josendal summed up the advantages of CO_2 (Holm and Josendal, 1974):

1. It promotes swelling.
2. It reduces oil viscosity.
3. It increases oil density.
4. It is highly soluble in water.

5. It exerts an acidic effect on rocks.

6. It is transported chromatographically through porous rocks.

To be more specific, when a gas bubble is dissolved in oil, the oil–gas mixture has a larger volume than the original oil. The new volume is called "swollen" volume. Some oils can swell by a factor of 1.7 when contacted by CO_2 (Sheng, 2013). If the injected CO_2 produces miscible flooding along with the reservoir fluids after satisfying the miscibility condition, then the interfacial tension becomes negligible and no oil is trapped by the capillary forces (Holm and Josendal, 1974). These phenomena are not uncommon because CO_2 has a very low MMP compared to other gases. A rough "rule of thumb" for oils with bubble point viscosities less than about 10 cP and an API oil gravity of 25 or greater is that CO_2 becomes miscible with the oil when the reservoir pressure is above 1000 psia, while methane becomes miscible with light oils at pressures greater than about 3000 psia, and nitrogen at pressures greater than about 5000 psia (Sheng, 2013).

In addition, CO_2 forms a dense or supercritical phase at the typical reservoir pressure and temperature conditions. The critical pressure of CO_2 is 1073 psia and the critical temperature is 31.0 ℃. When both the temperature and the pressure of the reservoir exceed the respective critical values, the CO_2 becomes supercritical, and, if the pressure in the reservoir is greater than the critical pressure, while

the temperature is below the critical temperature, then CO_2 exists in a dense state. This dense or supercritical CO_2 has a high density and viscosity, compared to other gases, which renders the displacement of the front more stable by naturally mitigating gravity segregation and viscous fingering to certain extents during gas flooding (Sheng, 2013).

Furthermore, CO_2 flooding is also associated with CCS technology. It is believed that the CO_2 emissions produced by human activities represented about 82.0% of the total greenhouse gas emissions in the United States in 2015 (USEPA, 2017). A reservoir guarantees long-term sequestration of CO_2 because a high-temperature, high-pressure fluid has been kept isolated in it for millions of years. Dooley and his colleagues (Dooley et al., 2010) have described CO_2-EOR as "a stepping stone to the long-term sequestration program for climate change risk mitigation."

Despite these advantages, CO_2 flooding did not rapidly gain popularity owing to the technical limitations of general gas flooding. Ideally, miscible flow should be piston-like which means whatever volume of gas is injected an approximately equal volume of the reservoir hydrocarbon fluid is displaced. Unfortunately, in real field applications, such piston-like behavior does not occur because reservoir heterogeneities and gravity override, causing the gas to cycle through one or more high-permeability layers (Sheng, 2013). For this reason, the recovery efficiency of gas flooding may not be

high even though the microscopic displacement efficiency for miscible floods at the field scale is often of the order of 70−90%.

Displacement instabilities and poor mobility control during gas injection can be attributed to the low viscosities and densities of most gases, as well as to the geological differences in the reservoir (Heller, 1994). Although CO_2 has a higher density and viscosity than other gases, these values may still be insufficient for effective oil recovery or may be significantly reduced, depending on the reservoir environment.

At the underground temperature and pressure of interest, the density of supercritical CO_2 varies between 600 kg/m³ (at 30 ℃, 8 ㎫) and 800 kg/m³ (at 160 ℃, 70 ㎫) (Van der Meer, 2005). These values seem to be sufficient to sweep light oils, but the situation is different if there is contamination due to methane in the reservoir. At the pressure of 19.3 ㎫ and the temperature of 60 ℃, the presence of only 3% methane can reduce the density of CO_2 from 700 kg/m³ to 500 kg/m³ (Van der Meer, 2005). A fluid with a low density gradually floats as it moves through a denser fluid, and this phenomenon is called "gravity override."

The viscosity of supercritical CO_2 in the typical reservoir condition varies from about 0.04 cP (at 30 ℃, 8 ㎫) to 0.08 cP (at 160 ℃, 70 ㎫) (Van der Meer, 2005). Considering that the viscosity of water is about 0.2 cP and that of oil about 0.5 cP to several tens of cP under similar conditions, the viscosity of supercritical CO_2 is quite low.

When low-viscosity fluids flow into fluids with higher viscosities, they split into several strands, and this phenomenon is called "viscous fingering." The larger the viscosity contrast between the fluids the more severe is the viscous fingering, therefore, the viscosity of reservoir oil is an important criterion in gas flooding screening. In the case of CO_2 flooding, the limit of reservoir oil viscosity is assumed to be about 10 cP, and it is recommended that this technique be applied to reservoirs with oil viscosities less than 1.5 cP (Taber et al., 1997).

The negative effect of reservoir condition on sweep efficiency is largely due to the heterogeneity of the permeability. If there are both high-permeability and low-permeability zones in the reservoir, the injection fluid moves intensively through the high-permeability zones. This phenomenon is called "gas channeling" and, when it occurs, the high-permeability zone is often called "thief zone" (summarized in Figure 2.1).

Attempts to solve the abovementioned problems have been made in various ways, and water-alternating-gas (WAG) is one of the conventional methods. For WAG, injection takes place for a number of gas-water cycles. This has several advantages, one of which is the ability to reduce the consumption of gas by injecting water, which is usually cheaper than gas (Sheng, 2013). WAG has also been proven to be a very effective mobility control measure, which implies that it delays breakthrough of the gas and reduces gas cycling through the high-permeability layers (Sheng, 2013). Although WAG

does increase the recoveries, the gas can still flow upward in the formation, away from the wells, while water can move downward because of gravity segregation (Jarrell et al., 2002). This may be less serious than a simple gravity override, but it still presents an unfavorable situation. Adjusting the volumes of water and gas injected during WAG can improve the recovery efficiency (Sheng, 2013), but it is not a fundamental solution.

2.1.2. Importance of mobility control

In the EOR process, the recovery efficiency, E_R, of a fluid displacement process is the product of the microscopic displacement efficiency, E_D, and the volumetric sweep, E_V, of the injected fluid(s) (Lake, 1989):

$$E_R = E_D * E_V \qquad \text{Eq. } 2-1$$

The two important parameters for increasing E_R during fluid displacement are the capillary number and the mobility ratio.

The capillary number, N_c, is a dimensionless quantity that is used to represent the balance between the viscous drag forces and the capillary forces acting in the porous media during flooding. Various definitions of the capillary number are available, with one common definition being Eq. 2-2 (Shi et al., 2018)

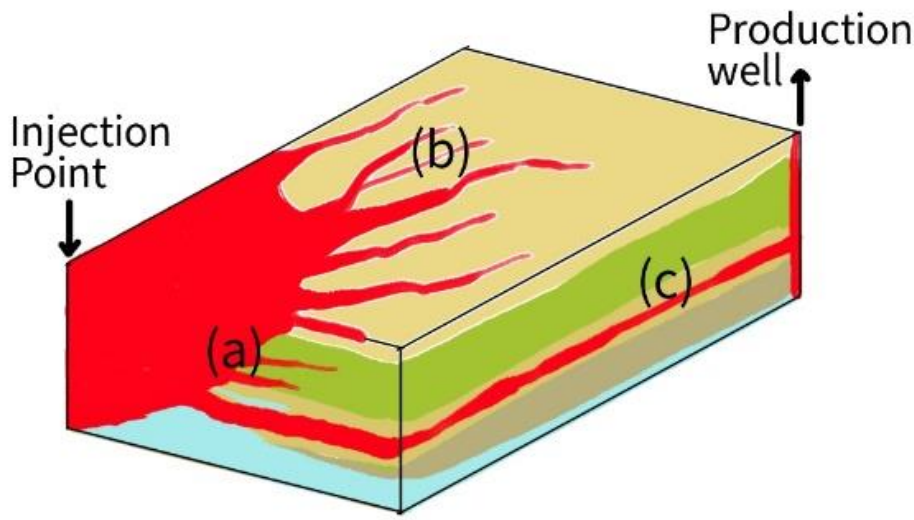

Figure 2.1. Schematic diagram of the phenomena responsible for the poor sweep efficiency observed in gas flooding: (a) gravity override, (b) viscous fingering, and (c) thief zone.

$$N_c = \frac{\mu V}{\sigma} \qquad \text{Eq. 2-2}$$

where μ is the viscosity of the displacing fluid, V is a characteristic velocity, and σ is the interfacial/surface tension between the displacing fluid and the fluid being displaced.

Mobility, $\boldsymbol{\lambda_1}$, is the ability of a fluid to flow through porous media, and is defined as Eq. 2-3;

$$\lambda_1 = \frac{\kappa_{r1}}{\mu_1} K \qquad \text{Eq. 2-3}$$

where κ_{r1} is the relative permeability of the fluid, K is the absolute permeability of the porous medium, and μ_1 is the viscosity of the fluid.

The mobility ratio M is defined as the ratio of the mobilities of the displacing fluid, λ_1, and the displaced fluid, λ_2:

$$M = \frac{\lambda_1}{\lambda_2} = \frac{\kappa_{r1}/\mu_1}{\kappa_{r2}/\mu_2} \qquad \text{Eq. 2-4}$$

All EOR processes and technologies aim to increase N_c or improve M in order to increase the overall E_R.

2.1.3. Improved mobility control by using foam

Foam is a potential solution for alleviating the abovementioned challenges associated with gas flooding. The concept of using foams as mobility control agents was first proposed by Boud and Holbrook in 1958 (Boud and Holbrook, 1958). Foam is defined as a dispersion of a relatively large volume of gas in a small volume of liquid or solid (Weaire and Hutzler, 1999), and is generally characterized by its quality and bubble size (Lake, 1989). Foam is commonly encountered in our daily lives (e.g., soap bubbles or detergent foam), but its theory is very complicated. The basic properties of foam were studied by 19th century scientists such as Joseph Plateau (1801–1883), but it was only in the 1970s that academic studies on foam stability, coarsening, and drainage commenced, which are called foam physics (Princen et al., 1980; Princen and Science, 1979).

The main mechanism of using foam in EOR, which overcomes the disadvantages of gas flooding, is the increase in apparent viscosity. In the case of CO_2, the apparent viscosity in porous media may be increased by factors of 10 to 100+ through foam formation (Rossen, 1996). The principal factors affecting the apparent viscosity of foam in porous media are the dynamic changes occurring at the gas/liquid interfaces. Hirasaki and Lawson summarized the reasons as follows (Hirasaki and Lawson, 1985):

1. Slugs of liquid between gas bubbles resist flow.
2. Viscous and capillary forces result in interfaces that are deformed against the restoring force of surface tension. The extent of this deformation and the resulting bubble shape partially determine the apparent viscosity as a function of the flow rate.
3. Another factor determining the apparent viscosity as a function of velocity is the expansion of the interface at the leading end of a bubble, which is accompanied by a compression at the trailing end.

Hirasaki and Lawson assumed a uniform capillary for their theoretical approach, but foam has a greater advantage in heterogeneous porous media. Its ability to overcome heterogeneities can be attributed to its sensitivity to capillary pressure. Foam films are more stable in high-permeability layers owing to the low capillary pressure environment, whereas these films are less stable in low-permeability layers owing to the high capillary pressure environment. This phenomenon can be equally explained through a limiting water saturation, which the foam films cannot survive owing to the lack of an aqueous phase (Sheng, 2013). This characteristic allows stable foams to reside in the high-permeability layer and helps in diverting flowing fluids into the low-permeability layer. Foam can also mitigate the gravity override of oil-rich zones and/or selective channeling through high-permeability streaks owing to its

high apparent viscosity, this improving the volumetric displacement efficiency(Kovscek et al., 1997).

2.1.3.1. Evaluation of foam flooding efficiency

There is a parameter called mobility reduction factor (MRF) that represents the overall effect of foam. MRF is a dimensionless value that is used for comparing the changes in mobility during gas-liquid two-phase flow in porous media. According to Darcy's law, the drop in pressure (ΔP) as the fluid travels through a porous medium with cross sectional area A and length L is given by

$$\frac{q_q}{A} = \frac{kk_{rg}^{o}(S_w)\Delta P}{\mu_g^o \; L} = \lambda_g^o(S_w)\frac{\Delta P}{L} = k\lambda_{rg}^o(S_w)\frac{\Delta P}{L} \qquad \text{Eq. 2-5}$$

and

$$\frac{q_q}{A} = \frac{kk_{rg}^{o}(S_w)\Delta P}{\mu_g^o \; L} = \lambda_g^o(S_w)\frac{\Delta P}{L} = k\lambda_{rg}^o(S_w)\frac{\Delta P}{L} \qquad \text{Eq. 2-6}$$

where, q, k_r , S, μ, λ, and λ_r represent the flow rate, relative permeability, saturation, viscosity, mobility, and relative mobility. The subscripts "w" and "g" represent water and the gas phase,

respectively, whereas the superscript "o" represents the state of a porous medium with no foam.

Previous studies show that the presence of a foam film alters the gas-phase mobility significantly, but not the liquid-phase flow mobility (de Vries and Wit, 1990; Friedmann et al., 1991). This means that when foam is present, the part of Darcy's equation that is related to the gas phase must be modified. Mobility is the ratio of relative permeability to phase viscosity, so the superscript "f" is added to indicate the values corresponding to the presence of foam.

$$\frac{q_q}{A} = \frac{kk_{rg}^{f}(S_w)\Delta P}{\mu_g^f \; L} = \lambda_g^f(S_w)\frac{\Delta P}{L} = k\lambda_{rg}^f(S_w)\frac{\Delta P}{L} \qquad \text{Eq. 2-7}$$

In order to specifically define each effect, the effective gas relative permeability or effective gas viscosity may be introduced, but MRF more simply represents the overall effect of the foam as a single value:

$$\frac{q_q}{A} = \frac{kk_{rg}^{f}(S_w)\Delta P}{\mu_g^f \; L} = \frac{1}{MRF}\frac{kk_{rg}^{fo}(S_w)\Delta P}{\mu_g^o \; L} \qquad \text{Eq. 2-8}$$

MRF = 1 if foam is not present in the medium, and MRF > 1 if foams exist and propagate in the medium. Typically, MRF can range from 1 to as high as more than 100,000 (Sheng, 2013).

For simulation studies, MRF allows sufficiently simplified comparisons of the results, but, in experimental studies, simpler and more explicit values are often useful, such as the foam resistance factor (RF). Experiments performed at the same injection rate in the same core sample can eliminate many terms that require information about the rocks. Assuming that the water saturation in the core is also changed by the foam, RF is simply defined as

$$\mathrm{RF} = \frac{\Delta P^f}{\Delta P^o} \qquad \text{Eq. } 2-9$$

where ΔP^f is the pressure drop with gas and water along with some foaming agents and ΔP^o is the pressure drop with just water and gas co-injection. RF = 1 indicates no increase in the resistance. That is, no foam is formed during the injection. If the foaming agent works properly, RF will have a value greater than one.

As mentioned above, MRF or RF can be 1 when there is no foam. Since all foams are thermodynamically unstable (Ewers and Sutherland, 1952; Pugh, 1996), proper foaming agents are required to maintain effective foam. This is the main problem with using foam for EOR.

2.1.3.2. Surfactant and foam

Surfactant is one of the representative foaming agents. The term "surfactant" is an abbreviated form of surface-active agents. Surfactants are usually organic compounds that are amphiphilic, meaning they are composed of a hydrophilic head and a hydrophobic tail. They adsorb onto or concentrate at a surface or fluid-fluid interface and reduce the surface or interfacial tension (Sheng, 2013). Since the interface referred to here also includes the oil-water interface, surfactant flooding aimed at lowering the interfacial tension of oil without using foam had been proposed earlier (Wolcott, 1923). Surfactant flooding has been studied extensively since the 1970s owing to the physical and chemical complexities of the surfactants and the harsh heterogeneous conditions of the reservoir. Even today, surfactant flooding is the most risky EOR process, as it involves the most difficult design decisions and large capital investments (Lake et al., 1992). The foam stabilized via a surfactant has the property of resisting certain physical environmental changes. For example, when foam is exposed to sudden expansion due to an external force or the spatial heterogeneity of the reservoir, it prevents film rupture through the following process (Schramm and Hepler, 1994):

1. The surfactant concentration in the expanded portion of the film will decrease.
2. Non-uniform surfactant distribution along the expanded surface leads to a local increase in the surface tension.

3. The gradient in surface tension induces a spontaneous contraction of the surface, which causes the surfactant to flow toward the film thinning area, while suppressing the liquid flow from this area.

These mass transfers are mainly caused by the Gibbs-Marangoni effect (Marangoni, 1865) and lead to the foam film exhibiting elasticity.

On the other hand, surfactants are vulnerable to heat, salinity, and surrounding ions. Most surfactants display optimal performances in a narrow salinity range, and adsorption or retention can occur through ionic exchange with the reservoir rocks after injection (Lake et al., 1992). When the reservoir temperature is as high as 180 ℃, some surfactants decompose, with half lives of a few days (Handy et al., 1982). Above all, the problem is that the oil in the reservoir acts as a typical antifoaming agent for surfactant-stabilized foam (Denkov, 2004). When a surfactant-containing foam is contacted with oil, the surfactant molecules move away from the gas-water interface to the oil phase, and the stability of the foam decreases as the surfactant concentration decreases (Jensen and Friedmann, 1987).

2.1.4. Nanoparticles and foam

Recently, attempts have been made to use nanoparticles as foaming agents to solve the abovementioned problems. The idea of stabilizing

foams and emulsions by using particles was first conceived by Ramsden in 1903 and Pickering in 1907 (Pickering, 1907; Ramsden, 1903). They found that durable emulsions and foams can be formed by the adsorption and accumulation of colloidal particles at the liquid–liquid interface of macroemulsions and the gas–liquid interface of foams. Since then, Kam and Rossen theoretically demonstrated in 1999 that solid particles could be used to stabilize foam without any surfactants (Kam and Rossen, 1999).

The major mechanisms of foam stabilization with particles have been identified in previous studies as high particle detachment energy, particle arrangement during film drainage, reduced capillary pressure, and increased maximum capillary pressure of coalescence (Hunter et al., 2008).

The detachment energy is the energy required to remove the solid adsorbed at the interface. When a particle (that is small enough so that the influence of buoyancy or gravity can be ignored) with radius R and contact angle θ is adsorbed on an interface with the interfacial tension of γ_{aw}, the detachment energy is as follows (Binks and Lumsdon, 2000):

$$E = \pi R^2 \gamma_{aw} (1 - |\cos\theta|)^2 \qquad \text{Eq. 2-10}$$

Assuming a particle diameter of 10 ㎚ and calculating the energy at the water and air interface, the obtained value exceeds 10^3 kT at a contact angle of about 60° to 120° (Figure 2.2) (Binks and Lumsdon, 2000). From a thermodynamic point of view, this value implies complete irreversible adsorption. The contact angle determines not only the detachment energy, but also which fluid will be the continuous phase or the dispersed phase. When nanoparticles with appropriate contact angles are dispersed to the oil and water interface, the oil-in-water (o/w) emulsion, in which water is the continuous phase, or the water-in-oil (w/o) emulsion, in which oil is the continuous phase, is stabilized (Figure 2.3) (Dickson et al., 2004).

Of course, not all solids adsorb stably at the interface. Particularly, a change in the contact angle sharply decreases the detachment energy. At $\theta < 20°$ or $\theta > 160°$, the contact energy is only 10 kT or less (Binks and Lumsdon, 2000). which is about the same or smaller than the detachment energies of common surfactant molecules (Binks, 2002). If the diameter of a particle increases, the detachment energy also increases as R^2, but the gravity effect increases much more rapidly as R^3. As a result, the accumulation of micron-sized particles at the film interface results in rapid coalescence of bubbles (Li et al., 2012).

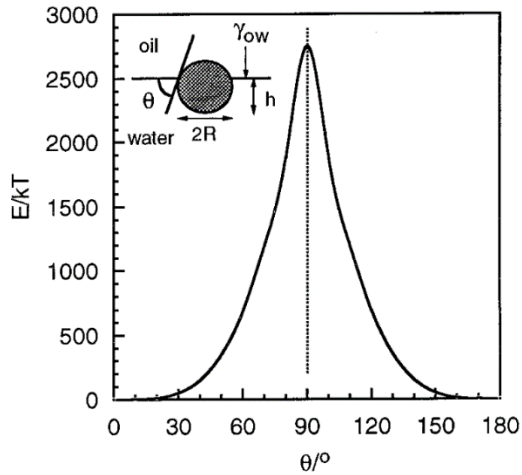

Figure 2.2. Variation of the energy of attachment, E (relative to kT), of a spherical particle of radius R = $\mathbf{1 \times 10^{-8}}$ m at a planar oil–water interphase; $\boldsymbol{\gamma_{ow} = 36 \times 10^{-3}\ N \cdot m^{-1}}$ at 298 K (Binks and Lumsdon, 2000).

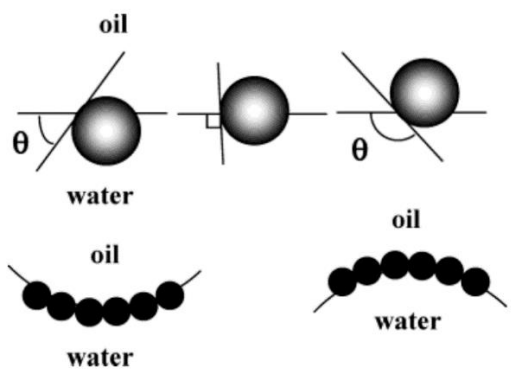

Figure 2.3. Schematic demonstrating the relationship between contact angle (measured with an aqueous phase) and the position of a spherical particle at the planar oil–water interface; for $\theta < 90$ (left), o/w emulsions are favored, whereas for $\theta > 90$ (right), w/o emulsions are expected (Dickson et al., 2004).

2.1.4.1. Surface treatment of nanoparticles

With advances in nanotechnology and surface treatment technology, the theory of Ramsden and Pickering has been proven experimentally. Because many studies are aimed at EOR application (Emrani et al. 2017, Kim et al. 2016, Singh et al. 2015), water-in-CO_2 foam or CO_2-in-water (C/W) foam is being studied extensively. As solids, silica nanoparticles are the most widely used because of their size and homogeneity. Since bare silica nanoparticles are too hydrophilic to stabilize the C/W foam (Worthen et al., 2013a), most studies stabilize the foam through surface treatment or the assistance of a surfactant. Although some studies (e.g. (Mo et al., 2012)) have succeeded in stabilizing the foam without the apparent need for any surface modification, the commercial silica particles used in the experiments may have been subjected to surface treatments that the experimenter may not be aware of.

In addition to increasing the interfacial adsorption properties of nanoparticles, surface treatment has the effect of increasing their dispersity. For the nanoparticles applied to EOR, they will inevitably come in contact with brine, which reduces the Debye length drastically. As the Debye length decreases, the electrical repulsions between the particles decrease and the gap between the nanoparticles narrows. When the nanoparticles are too close to each other, they are aggregated by Van der Waals forces. Surface treatment is the process of attaching a polymer substance to the

surface of a nanoparticle to form a steric barrier. A typical surface treatment method for silica is PEG coating and silanization.

PEG is the abbreviation for polyethylene glycol, which is a non-degradable polyether of the monomer ethylene glycol. Since ethylene glycol is a hydrophobic molecule that is used to produce the non-ionic surfactant, PEG also has hydrophobicity. PEG is easily and strongly attached to the silica surface because its etheric oxygen chemically combines with the hydroxyls on the silica surface to form hydrogen bonds (Derosa and Trapasso, 2002). PEG can be coated either during the synthesis of silica nanoparticles (Xu et al., 2003) or after the synthesis (Andreani et al., 2014). PEG-coated silica nanoparticles have successfully produced stable foams in many studies (Griffith and Daigle, 2017; Singh and Mohanty, 2017; Worthen et al., 2013c; Worthen et al., 2016).

Silanization is the process of coating a surface with organofunctional alkoxysilane molecules. Silanization is used in various studies besides silica (Britt and Hlady, 1996; Chovelon et al., 1995; Liu et al., 2013) because it can form strong covalent bonds on most mineral or metal surfaces that contain a hydroxyl group. There are many variants of alkoxysilane molecules, such as methylsilyl(amine) (Yekeen et al., 2017), (3-Glycidyloxypropyl)-trimetho-xysilane (Singh and Mohanty, 2017), (2-[methoxy-(polyethyleneoxy)6-9propyl]-trimethoxysilane (Worthen et al., 2016), and (3-aminopropyl)-trimethoxysilane (Ranka et al., 2015; Worthen et al., 2013b), compared to PEG, which exhibits only molecular weight

differences. All these materials increase the steric repulsions on the surface of the silica nanoparticles and impart hydrophobicity through silanization.

The biggest advantage of silanization is that the degree of coating can be controlled. The first successful generation of stable aqueous foams by using silica nanoparticles with different degrees of hydrophobicity was carried out by Binks and Horozov (Binks and Horozov, 2005). They prepared nanoparticles of different hydrophobicities by using a silane reaction and expressed the degree as the percentage of SiOH exposed on the surface. Experimental results show that nanoparticles with 20% and 32% SiOH successfully formed stable foams, whereas 42% SiOH produced a very small amount of foam, and no foam was formed above 51% SiOH. The results of this experiment are of great value because nanoparticles were used to synthesize foam without the aid of a surfactant.

2.1.4.2. Co-application of nanoparticles and surfactants

Until now, many studies have used surfactants while studying foam formation by using nanoparticles (AlYousef et al., 2017; Babamahmoudi and Riahi, 2018; Emrani and Nasr-El-Din, 2017; Pichot et al., 2012; Singh and Mohanty, 2015; Yekeen et al., 2017; Yusuf et al., 2013). Yet, there has been no successful case of stabilizing foam with high quality and in large volume (e.g., several times the height of the liquid phase) by using only nanoparticles.

Fortunately, nanoparticles are often reported to have positive synergies with surfactants.

There are several representative methods available for identifying the synergistic effects of nanoparticles. The first is to compare foam stabilities. The foam stability is measured in terms of either the time it takes for the height of the foam to decrease by half or the resistance to antifoaming agents such as crude oil. The second method measures the foam RF. As described earlier in Section 2.1.3.1, the original RF is a value that is used for comparing the cases of w/ and w/o foams. To confirm the effect of nanoparticles, we can simply compare the RF values w/ and w/o the nanoparticles.

Although the details are different, most studies reveal increased foam stability as a result of nanoparticle–surfactant synergy (Table 1). It is known that the nanoparticles adsorbed improve the foam stability by reducing gas diffusion and the direct contact between the fluids and by decreasing the rate of film rupture and bubble coarsening (Karakashev et al., 2011; Maestro et al., 2014).

However, this alone does not explain the results listed in Table 1. Certain experiments employed a concentration of nanoparticles as high as 7% (Yusuf et al., 2013), though most experiments used nanoparticles with the concentration of around 1%, which seems to be too low to efficiently prevent direct contact.

Another reason why nanoparticles enhance the stability of bubbles can be found in the study using plane parallel films that contain

nanoparticles (Sethumadhavan et al., 2001). As the effective volume fraction of the nanoparticles in the film increased, larger number of steps were required for film collapse by thinning of films. This indicates that not only the interface but also the nanoparticles inside the film affect the stability of foams.

The nanoparticles present in the lamella are divided into three types; monolayer, bilayer, and a network of particle aggregates (Horozov, 2008). In some articles (Kaptay, 2003), the structures are classified into six subdivisions, according to whether they are clustered or bridged. For microsized colloidal particles, studies by Velikov and his colleagues found that colloidal particles at the interface should cover 50% of the surface to form a bridged network instead of a single cluster (Velikov et al., 1998). Because they used latex particles of diameter 70 ㎛, it was possible to accurately observe the arrangement of the particles on the surface, however, actual imaging of the nanoparticle network in the film is difficult with current technology.

Recently, attempts have been made to image the nanoparticles at the interface by using fluorescent nanoparticles (Singh and Mohanty, 2015). The researchers obtained an image of nanoparticles that were concentrated in the plateau borders, but the structure of the network was not identified, therefore, the distinctions in the nanoparticle structure seemed to depend on the discretion of the researcher for a while.

Yekeen and colleagues believed that the synergistic effects of nanoparticles and surfactants on foam stability are due to lamella thickness (Yekeen et al., 2017). They visually confirmed that the addition of 1% nanoparticles to a 3% sodium dodecyl sulfate (SDS) solution rendered the lamella approximately four times thicker. The drainage rate is affected by various factors such as the surface tension gradients, surfactant concentration, and electrostatic repulsive interactions (Pugh, 1996), but thicker lamella guarantees high stability if other conditions are similar, since thin liquid films gradually become thinner and may eventually rupture after drainage below the critical thickness (Pugh, 1996).

The results of observing finer and more homogeneous foam textures in the presence of nanoparticles can also be found in several articles (Xue et al., 2016; Yekeen et al., 2017). Sarma and Khilar found that a more uniform bubble-size distribution and a high initial gas volume fraction afforded more stable foams because of reduced interbubble diffusion rate (Sarma et al., 1988).

Despite these studies, the reason why nanoparticles are difficult to apply to EOR lies in the economics. Unlike the other applications where nanotechnology has been introduced in the petroleum industry (e.g., drilling fluid (Hoelscher et al., 2012; Mao et al., 2015), oil well cement (Choolaei et al., 2012), and water invasion barrier (Cai et al., 2012; Ershadi et al., 2011)), EOR applications require enormous volumes of nanoparticles. Even with a highly positive assumption that 1% concentration of nanosilica solution is used to recover 10%

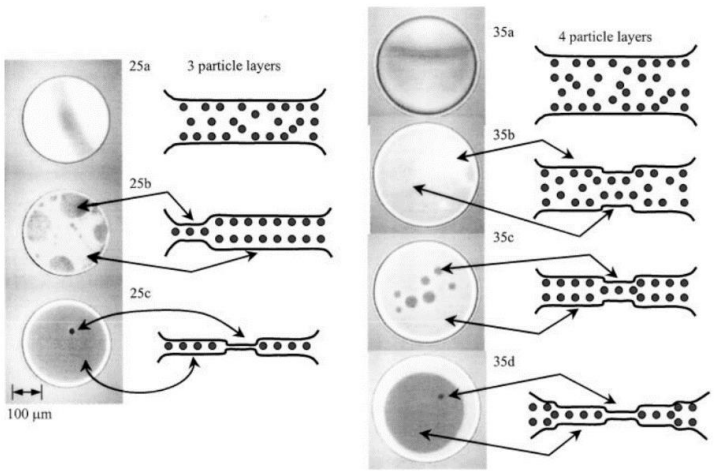

Figure 2.4. Stepwise thinning of a film in the presence of 8 ㎚ silica particles at the effective volume fractions of 0.25 (right) and 0.35 (left). (Sethumadhavan et al., 2001)

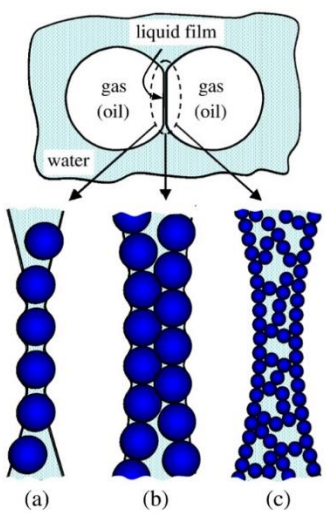

Figure 2.5. Possible mechanisms of liquid film stabilization: (a) a monolayer of bridging particles; (b) a bilayer of close packed particles; and (c) a network of particle aggregates inside the film. (Horozov, 2008)

Table 1. Summary of the papers published on the synergy between nanoparticles and surfactants

Source	NP type	Experimental conditions	Summary of results
Alyousef et al., 2017	30 ㎚, commercial silica	Surfactant: AOS Static foam test Core flood 1200 psi, 50 ℃	No significant change in static foam test w/o crude oil; Enhanced foam stability in the presence of crude oil; 10% increased recovery
Babamahmoudi and Riahi, 2018	20−30 ㎚, commercial silica	Surfactant: SDS Static foam test	40% increased half−life; Improved stability depending on oil API (no effect with light oil)
Emrani et al., 2017	140 ㎚ commercial silica	Surfactant: AOS Static foam test − 25 and 65 ℃, 300 psi Core flood − 25 and 121 ℃	Enhanced foam stability at 65 ℃ Increase in RF from 3 to 8 at 65 ℃; No change was observed at 121 ℃
Singh and Mohanty, 2015	10 ㎚ PEG coated silica	Surfactant: AS−40 Static foam test Core flood 90 ℃, 1500 psi	Dramatically increased stability above 0.3% NP concentration; MRF increased from 4000 to 8700; 10% increased oil recovery

Source	NP type	Experimental conditions	Summary of results
Worthen et al., 2013	28 ± 2 ㎚ Bare silica	Surfactant: CAPB bead pack flood 50 ℃, 19.4 MPa	Increased apparent viscosity; Synergistic foam formation under conditions where neither the surfactant nor the NPs alone generate foam.
Xue et al., 2016	Non-ionic steric stabilizer bonded commercial silica (size not mentioned)	Surfactant: LAPB, AOS, Bioterge AS-40; and Polymers; Dynamic flood: 3000 psia, 50 ℃	Synergies slow down the Oswald ripening of the SC CO_2 foam by a factor of 30.
Yekeen et al., 2017	15-20 ㎚ hydrophilic silica (θ = 52.17°) 12 ㎚ 50% silanized silica (θ = 88.48°)	Surfactant: SDS Static foam test Dynamic foam test	Increased apparent viscosity, especially at low flow rates; Thicker lamella; Smaller, more uniform foam size; Decreased foamability

Source	NP type	Experimental conditions	Summary of results
Yusuf et al., 2013	60–70 ㎚ commercial silica (as powder)	Surfactant: Triton X100 Static foam test	The silica concentration at which synergy occurs depends on the concentration of TX100. (The most stable foam is obtained at TX 0.1% and NP 7% condition.)
Singh and Mohanty, 2017	20 ㎚ PEG coated; 12 ㎚ silanized silica	2D heterogeneous sand pack, 110 psi	Less oil recovery (80–>60%), but cross-flow prevention effect from the low-permeability zone to the high-permeability zone was observed

of the original oil in place with 75% foam quality and 25% recovery efficiency at the typical oil reservoir size of 300 million barrels, about 50000 tons of nanosilica particles are needed. Silica particles may be used only as a part of the EOR process, as gas flooding in WAG does, but the assumption is still valid, because the other indicators that increase silica consumption could be much worse. There have also been a number of studies on lowering the cost of nanosilica (Lazaro et al., 2012; Liou and Yang, 2011), but its price (at hundreds of dollars per ton of solution, or more than $ 1500 per ton of solids) is still too high for this purpose.

One of the objectives of this research was to investigate the feasibility of replacing such "engineered" silica nanoparticles with nano-milled fly ash by utilizing the learnings from the earlier research on the use of silica and other well-defined nanoparticles. Fly ash is an industrial waste that has practically negative value, but it becomes more attractive when the environmental value of recycling it is considered.

2.2. Oil Spill Cleanup

Oil spill refers to the release of liquid petroleum hydrocarbons into the environment due to human activities. The well-known oil spills include the Kuwaiti Oil Fires in 1991, Gulf War Oil Spill in 1991, and Deep Water Horizon in 2010. Millions to billions of barrels of oil were released into the ecosystem, which caused major disasters in the vicinities.

In Korea, there was a large oil spill called Hebei Spirit oil spill in December 2007, in which 10800 tons of crude oil leaked from a tanker and a significant amount of them landed at the Korean coast, resulting in at least five beaches being contaminated with large tar lumps. About 330 million US dollars were spent on the cleanup, and hundreds of thousands of volunteers, soldiers, local residents, civil servants, and even students had worked to clean up the spill. Thanks to this effort, the oil concentration in intertidal seawater 15 days after the spill was as high as 16600 μg/L, but it reported to be below the Korean marine water quality standard of 10 μg/L at most sites 10 months after the spill (Kim et al., 2010).

The efficiency of cleanup of an oil spill depends on various conditions such as the type of oil, temperature, wind speed, location, quantity, water temperature, and accessibility. For instance, in the case of Tsesis oil spill (Teal and Howarth, 1984), about 65% of the oil was recovered because the heavy bunker

oil leaked along with No. 5 fuel oil in cold weather. On the other hand, the Hebei Spirit oil spill occurred in hotter weather and stronger winds than usual, therefore, the damage was much bigger than expected. In the case of Argo merchant oil spill, they even failed to burn the oil and the recorded cleanup rate was 0% (Teal and Howarth, 1984).

To cope with this situation, various dispersants, absorbents, solidifiers, booms, and skimmers have been developed and applied. Dispersants break the oil to small droplets and disperse the oil to lower its concentration, thereby promoting its biodegradation and reducing the environmental damage. The aim of absorbents is to isolate the oil from the ecosystem through absorption and collection. Solidifiers are dry granular or hydrophobic polymers that convert the oil into a cohesive, solidified mass that floats in water and can be easily recovered. Booms are devices used to prevent the movement of oil and confine it to a particular place. Skimmers are tools employed to recover the oil from the water surface.

Each method has its own advantages, disadvantages, and certain limitations. For example, the solidifier has the advantage of separating oil from the ecosystem, but its high price and long reaction time are disadvantages, and it is also difficult to apply to heavy oil (Dahl et al., 1996). If the solidifier does not combine with the oil owing to cold weather or strong waves, it is dispersed

in the environment, which can cause additional environmental pollution.

Owing to these problems, research on adsorbents that use natural fibers and natural minerals has been carried out (Choi et al., 1993; Stowe, 1991; Sun et al., 2004). Adsorbents using natural fibers such as wool or straw can be biodegraded easily even if they are lost during the cleanup process, thus minimizing the impact on the environment. Various approaches have also been attempted to increase the recovery rate. Bryk and Yakovenco (Bryk and Yakovenko, 1987) used clays with high contents of iron oxide as an absorbent to recover the aggregates through magnetic forces.

If a cleanup eventually fails owing to circumstantial limitations, the self-purification effect of nature can be expected; nature sometimes shows a much better resilience than what is expected. During the cleanup operations following the Exxon Valdez spill in Prince William Sound, Alaska, 1989, scientists noticed that the oil was removed from natural low-energy flows such as tides or waves. To explain this phenomenon, they postulated that a process of "clay-oil flocculation" resulted in the natural cleaning and removal of the stranded oil (Lee et al., 1997). Clay-oil flocculation is a phenomenon by which solid-stabilized emulsion are naturally formed through interactions between clay particles and the buried oil, and the clay-oil flocculants easily escape from the beach through natural low-energy sources such

as waves and tidal flushes. In many subsequent studies, it has been found that this phenomenon does not guaranteed by mineral types or sizes only (Lee, 1998), but is determined by various conditions such as appropriate salinity (Le Floch et al., 2002). This combination of natural conditions for effective oil removal emerged just by coincidence, but it is an important phenomenon that we can effectively exploit by artificially creating it.

2.3. Produced Water Treatment

"Produced water" is a broad term that includes all waters that are generated directly or indirectly during the oil and gas production processes. The global production of produced water is estimated at around 300 million barrels per day (Ferro and Smith, 2007), compared with around 80 million barrels per day for oil. Some of the factors affecting the quantity of produced water include the method of drilling the well, its location, the type of water separation technology, water injection or water flooding for enhancing oil recovery, poor mechanical integrity, and underground communication (Reynolds and Kiker, 2003). In general, most of the produced water is from the oil/water separation process during oil production.

Crude oil when produced often contains water in the form of w/o emulsion droplets. The water increases the volume of the oil and lowers the purity; therefore, the water and dissolved salts

present in the emulsion must be separated before the further transportation and processing in a refinery (Kelland, 2014). The w/o emulsions are stabilized by the solid particles, resins, naphthenic acids, and/or asphaltenes present in the crude oil (Grutters et al., 2007). Thus, various physicochemical demulsification processes are required to recover the oil.

Emulsions are usually less stable at higher temperatures, therefore, heating is one of the most widely used demulsification processes. Heating generally works well, because heat renders the oil less viscous and helps the water droplets sink by gravity, unless carboxylates or naphthenates stabilized emulsions are involved (Graham, 1988). In such cases, heating usually causes the pH to increase and makes the surfactants more polar. Consequently, heating undesirably enhances the performance of the surfactant and stabilizes the emulsion even further.

Another typical method is gravity separation. Since most oils are lighter than water, they are separated by gravity if they are kept still. If oil is dispersed as very small droplets and it takes too long to separate, hydrocyclones or induced gas flotation equipment can be used (Veil et al., 2004).

Electrostatic demulsification is a method of destabilizing o/w emulsions by neutralizing the electrostatic repulsions between dispersed oil droplets. High-valent metal salts such as iron (Ⅲ), zinc (Ⅱ), and aluminum (Ⅲ) salts, and cationic or anionic

polymers are commonly utilized in electrostatic demulsification. The charge density of the ionic polymer is an important factor in this process, since too high charge density can reverse the charges on the particles and restabilize them (Kelland, 2014).

The typical water separated out from oilfield-processing facilities is still contains residual oil and finely dispersed solids. The oil is present as an oil dispersion in water, i.e., an o/w emulsion. The concentration of the residual oil is usually too high to allow discharge of the water into the environment; the residual oil also has economic value (Kelland, 2014). For the treatment of produced water, heating, gravity separation, electrostatic neutralization, and addition of other chemicals, including flocculants, are commonly employed.

For the produced water to be discharged after treatment, it must meet the regional environmental standards. These standards usually consist of the oil and grease concentrations and toxicity assessments. Benzene, toluene, ethylbenzene, and xylene are the main ingredients that affect the toxicity of produced water, and are abbreviated as BTEX.

The produced water that meets environmental and other appropriate standards can be reused for various purposes. The reuse and recycling of produced water include its underground injection to increase oil production, use for irrigation, livestock or wildlife watering and for habitats, and various industrial uses

such as dust control, vehicle washing, power plant makeup water, and fire control (Sirivedhin et al., 2004; Veil et al., 2004).

However, the problem is with the produced water that contains highly stable, micron-scale oil droplets whose treatment is difficult to meet the value corresponding to the standard. If too much chemical is consumed during the treatment, it may affect the pH and the metal ion concentration of the produced water, resulting in a secondary problem that the treated water still does not meet environmental standards. On the other hand, physical processing does not cause secondary contamination, but requires special equipment such as hydrocyclones, centrifuges, media filters, and even membrane filters (Lee and Frankiewicz, 2005), which have issues related to cost and processing capacity. Therefore, in this study we explore the possibility of using high carbonaceous materials in fly ash as an inexpensive adsorbent for produced water, which is difficult to treat.

2.4. Characteristics of Fly Ash and its Utilization

As stated earlier, emission of fly ash will continue to increase with increased use of coal over the next decade. The study of fly ash cannot be separated from environmental enforcement. Crystalline silica or lime, which is the main component of fly ash, is harmful to humans when it dispersed in the form of small particles in the air (Morawska and Zhang, 2002; Warheit et al.,

2008). For this reason, electrostatic separation or other filtering technologies for collecting fly ash particles were first studied. Most of the particles collected over the last decades have been buried in ponds to minimize fugitive dust. However, as a result of several ash spills, social concerns about pond reclamation have increased (Lemly, 2015; Ruhl et al., 2010). As environmental standards for water quality and the atmosphere continue to strengthen, environmental costs for fly ash emissions continue to increase. Above all, for sustainable growth and human health, fly ash should be treated more appropriately. This study aims to maximize the recycling rate of fly ash and utilize it as a source for products of high added value. Section 2.4 summarizes the general characteristics of fly ash and the existing studies on recycling and environmental impacts of fly ash. This will help identify the applicability and limitations of fly ash recycling and present new possibilities.

2.4.1. Coal combustion products and fly ash

While coal is one of the oldest fossil fuels used by mankind, it is still, and also for many years to come, a major energy source around the world. Unlike oil, coal reserves are available in over 70 countries worldwide, the largest reserves are found in North America, Russia, Europe, China, and Australia, in that order which account for more than 80% of the global reserves (Heidrich et al., 2013). However, concerns regarding global

warming have led to a rapid decline in coal use in the developed countries, even though coal is still an important energy source for developing countries such as India, where the demand is increasing. According to OPEC's energy forecasts (OPEC, 2017), coal consumption will peak in 2030 and then decline gradually (Figure 2.6).

In recent years, about 90% of coal consumption is in coal-fired power plants. According to the 2018 EIA report, coal-fired power plants produce 1200 billion kWh of electricity, which accounts for 37% of the global electricity generation (2018a). For this purpose, about 7 billion metric tons of coal are produced and burned each year. As mentioned above, since coal is an abundant resource in many countries, 85% of coal is used in the country in which it is produced, with the remaining 15% being exported (Heidrich et al., 2013). The disadvantage of coal compared to other fossil fuels is that large amounts of coal combustion products (CCPs) are generated from its usage.

CCPs are produced primarily as the furnace residue from combustion of coal, but also from the cleaning of stack gases. In 2010, the annual production of CCPs was estimated to be 777 Mt, and fly ash accounted for about 85% of it, with the rest being bottom ash, boiler slag, fluidized-bed combustion ash, or flue gas desulfurization (FGD) materials (Heidrich et al., 2013). The recycling rate of the total CCPs varies from 96.4% to less than 10% depending on the country, with an average of 53% being

recycled (Heidrich et al., 2013). This indicates that about 300 Mt of CCP waste is generated each year, but fortunately, the recycling rate of CCPs has improved significantly over the past several decades (Figure 2.7) (American-Coal-Ash-Association., 2018).

Fly ash is composed of particles that are generally spherical in shape and range in size from 0.5 ㎛ to 300 ㎛. As mentioned above, since fly ash accounts for the majority of the CCPs, it can be considered as the world's fifth largest raw material resource (Mukherjee et al., 2008). Therefore, if not utilized, enormous landfill costs are incurred. The unit cost for a landfill is increasing more and more owing to the enforcement of environmental regulations. Because of the reason, active research has been and being carried out on the recycling of fly ash.

Recycling of fly ash has been actively considered since the 1940s. In 1953, the American Society for Testing and Materials (ASTM) first defined C350-54t that enable fly ash to be used as a fine aggregate admixture in concrete. Since then, the utilization of fly ash has been steadily expanded and its application refined. Fly ash is mainly used as an ingredient in construction material, replacing the traditional clay, sand, limestone, and gravel. More specifically, it is used as a mixture in concrete or cement, and as a foundation material for roads or coal mine backfills. Some applications can use fly ash as is, while others may require specific modification, or need fly ash with a

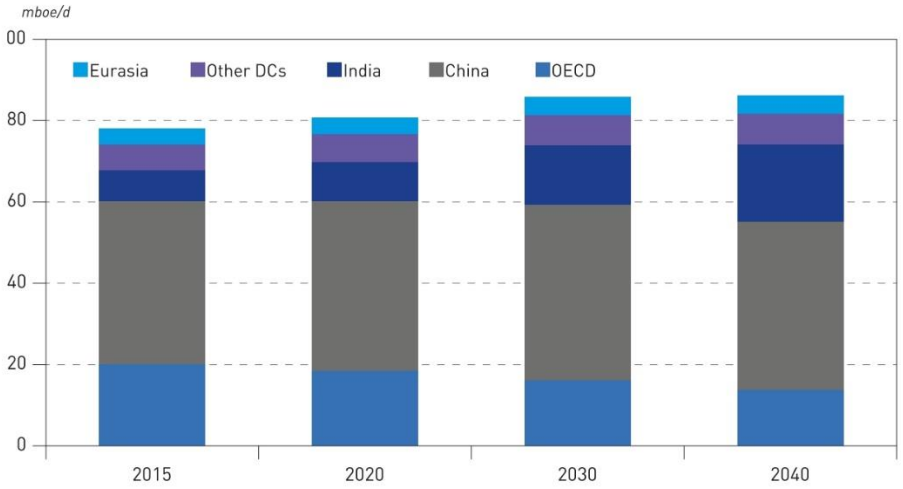

Figure 2.6. Coal demand growth by major regions, 2015-2040. The demand growth in India is prominent. (OPEC, 2017)

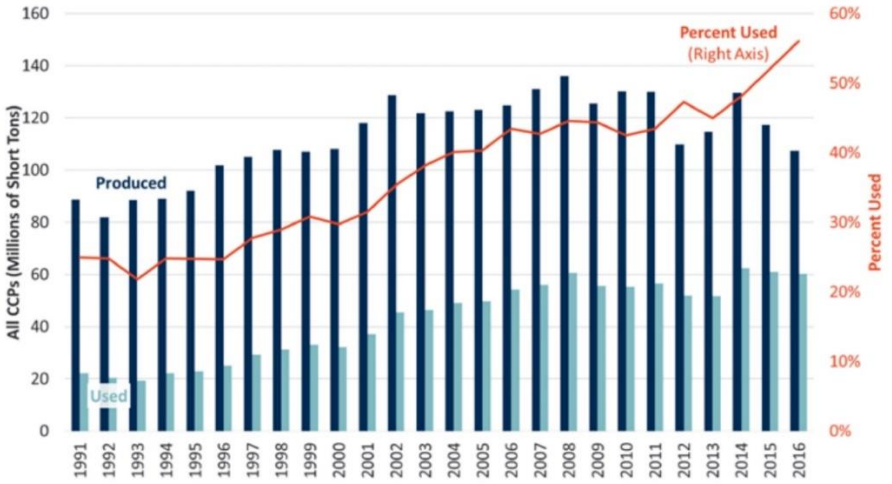

Figure 2.7. Annual CCP emissions and recycling rates (American-Coal-Ash-Association., 2018)

particular classification, since the chemical characteristics of fly ash are widely varying because they are heavily influenced by the combustion coal type and combustion conditions. In addition, the demand and regulatory requirements for construction materials also vary by country and region. For these reasons, the utilization of fly ash depends on the country (Figure 2.8).

In addition to the items shown in Figure 2.8, considerable research efforts are underway to utilize fly ash in a variety of ways, such as in zeolite synthesis, pollution control, and heavy metal adsorption. The research will lead to enhanced utilization of fly ash, based on the better understanding of the physical and chemical characteristics of the wide variety of fly ash.

2.4.2. Fly Ash as construction materials

2.4.2.1. Concrete and cement

Fly ash was recognized to be a pozzolanic ingredient of concrete in 1914, and the first comprehensive study was carried out by Davis et al. in 1937 (Joshi and Lohita, 1997). Since then, many investigations have been performed to utilize fly ash as a construction material. After the first ASTM specification, C350-54t, for the use of fly ash as a concrete admixture was released in 1953, the fly ash specification criteria have become more diverse and refined based on the subsequent studies. Since 1977, ASTM C 618 (2017a) provides the criteria for class F and class

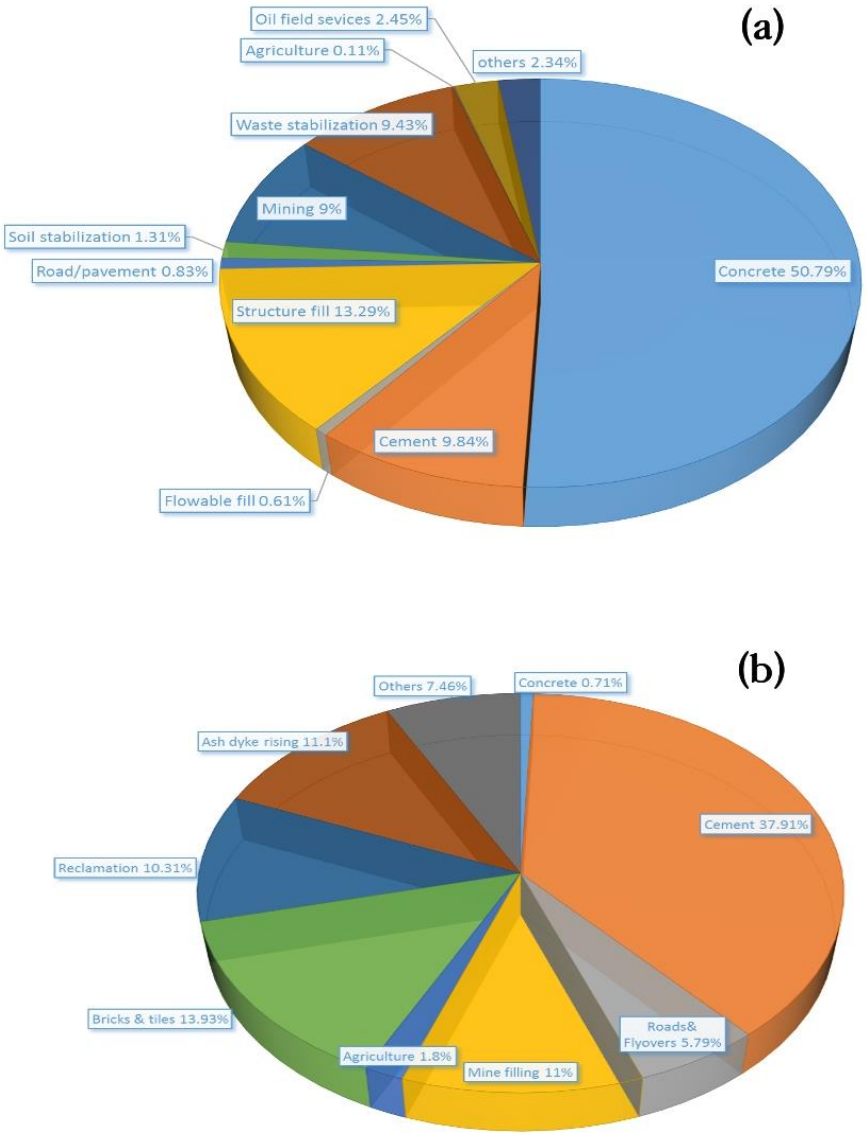

Figure 2.8. Use of fly ash (a) in the USA in 2012 (modified from (American-Coal-Ash-Association., 2012)) and (b) in India in 2016 (modified from (American-Coal-Ash-Association., 2018)).

C fly ash. Both classes have pozzolanic properties, with class C also exhibiting some cementitious properties. This difference is mainly due to the lime (CaO) content of the fly ash component, which is a result of the difference in the composition based on the coal type.

There are four types of coals: anthracite, bituminous, sub-bituminous, and lignite. Fly ash with high CaO contents is mainly obtained from lignite and sub-bituminous coals. Bituminous coal fly ash is characterized by relatively high contents of silica, iron oxide, and carbon. Anthracite is rarely used in coal-fired power plants, therefore, the characteristics of anthracite fly ash are not well known, but this fly ash is more similar to bituminous coal fly ash than sub-bituminous coal fly ash. The normal ranges of the fly ash components corresponding to each type of coal are shown in Table 2.

Class F fly ash typically has less than 7% CaO, whereas Class C fly ash occasionally has more than 20% CaO. Alkali and sulfate (SO_4) contents are also usually higher in Class C. Comparing with the data presented in Table 2, Class C fly ash is likely to be produced from lignite or subbituminous coal, whereas class F fly ash is likely to be produced from bituminous coal. In practice, many fly ashes obtained from lignite or subbituminous coal also satisfy the criteria of Class F, therefore, the type of raw coal cannot be directly used as a classification criterion for fly ash.

Detailed information on the ASTM C 618 criteria for Class C and Class F ashes is provided in Table 3.

Because of the pozzolanic effect and the cementitious properties of fly ash, 20−30% of Class F fly ash and 20−35% of Class C fly ash can be substituted for Portland cement. Mixing less than 20% does not cause any issues related to the properties nor is it prohibited by law, but such a mixture cannot be called fly ash mixed concrete.

Cement is one of the six largest energy−intensive industry after the steel, chemical, glass, paper, and non−ferrous metal industries. The production of 1 metric ton of cement requires energy equivalent to the production of 0.40 metric tons of CO_2 from fossil fuels. In addition, calcium carbonate emits 0.50 metric tons of CO_2 directly during the chemical reaction in Eq. 2−11, for cement manufacturing (Davidovits, 1994)

$$5\ CaCO_3 + 2\ SiO_2 \rightarrow (3CaO, SiO_2)(2CaO, SiO_2) + 5CO_2 \qquad \text{Eq. 2−11}$$

With the global demand for cement increasing each year (American−Coal−Ash−Association., 2018), the CO_2 emissions from cement manufacturing are a major concern with regard to

Table 2. Comparison of the normal ranges of the chemical constituents of bituminous coal fly ash with those of lignite coal fly ash and sub-bituminous coal fly ash (Ahmaruzzaman, 2010)

Component (wt%)	Bituminous	Sub-bituminous	Lignite
SiO_2	20-60	40-60	15-45
Al_2O_3	5-35	20-30	10-25
Fe_2O_3	10-40	4-10	4-15
CaO	1-12	5-30	15-40
MgO	0-5	1-6	3-10
SO_3	0-4	0-2	0-10
Na_2O	0-4	0-2	0-6
K_2O	0-3	0-4	0-4
LOI	0-15	0-3	0-5

Table 3. The chemical composition criteria of Class C and Class F fly ashes, as defined by ASTM C 618

	ASTM C 618 Requirements (wt%)	
	Class C Fly Ash	Class F Fly Ash
$SiO_2+Al_2O_3+Fe_2O_3$, min	50	70
SO_3, max	5	5
Moisture, max	3	3
LOI, max	6	6

global warming. Since fly ash is used as a cement substitute after a simple screening process, the CO_2 emissions during the manufacturing process are negligible. In short, replacing 1 ton of cement with fly ash reduces CO_2 emissions by one metric ton. From an energy-saving point of view, each ton of fly ash used to replace a ton of cement saves the equivalent of nearly one barrel of oil (Shi and Qian, 2003).

Despite these advantages, the existence of stringent standards for the application of fly ash is a priority for ensuring safety in the construction industry. Since concrete is used in the construction of large structures such as dams and bridges, a failure to realize the required physical strength and durability can lead to major disasters.

After the ASTM C 618 standard was established, Tikalsky et al. (Tikalsky et al., 1988) studied the freeze-thaw resistance, flexural strength, compressive strength, creep, shrinkage, and abrasion resistance based on more than 1600 laboratory and field tests over a three-year period to prove that concrete containing fly ash can be proportioned having equal strength properties and adequate durability when a suitable ASTM C 618 Class C or F fly ash is used at appropriate proportions.

The limitation on the ratio of fly ash in concrete is mostly due to the decrease in strength at early stage of construction, which is mainly attributed to the low reactivity of fly ash during cement

hydration. Several methods, such as elevated temperature curing of fly ash concrete, grinding of fly ash, and the addition of chemical activator(s) to fly ash concrete mixtures, have been investigated to enhance the reactivity of fly ash and improve the early properties of concrete containing high volumes of fly ash (Shi and Qian, 2003). Usually, elevated temperature curing increases the strength development rate, but decreases the ultimate strength of concrete. Grinding is an energy-intensive process that requires complicated facilities, which offsets the benefits of applying fly ash inplace of cement. Obla et al. (Obla et al., 2003) tried to solve this problem by selecting ultrafine particles from fly ash by using air classification instead of grinding. Concrete containing ultrafine fly ash could be produced with only 50% of the high-range water reducer dosage required for a comparable silica fume concrete, and exhibited similar early strengths and durability. The addition of chemical activators such as Na_2SO_4 or $CaCl_2$ accelerates pozzolanic reactions and changes the pozzolanic reaction mechanisms between fly ash and lime, which results in decreased setting time, accelerated strength development, and increased strength of the materials containing fly ash, especially those with high percentages of fly ash (Shi and Qian, 2003). Antiohos et al. (Antiohos et al., 2008) chemically activated high-calcium fly ash by adding industrially produced quicklime. Quicklime had a positive effect only during the very early stages of hydration, with the effect subsequently

becoming inhibitive with respect to the development of the reactivity of the fly ash.

These efforts have been fairly successful in overcoming the disadvantages of fly ash mixed concrete and broadening its usage. Some attempts with fly ash have been successful that do not meet the ASTM C 618 standard. Atiş et al. (Atiş et al., 2004) obtained strength properties with a non-standard high-calcium fly ash that were comparable or higher to those of the corresponding normal Portland cement concrete. Pei-Wei et al. (Pei-Wei et al., 2007) showed that the compressive strength after 90 days was improved when 50% of fly ash was added to dam concrete, and the shrinkage and expansion were reduced by 33% and 40%, respectively, compared to a concrete not containing fly ash. Oner et al. (Oner et al., 2005) showed that the optimal blend proportion of fly ash was 40%, which is higher than the current standard (up to 30% to 35%, depending on the class of fly ash), in their experiments where using 28 different concrete mixtures. In fact, experiments on concrete with fly ash contents higher than the standard have been steadily increasing since the introduction of ASTM C 618 (Giaccio and Malhotra, 1988; Maslehuddin et al., 1989; Ravina and Mehta, 1986). These studies involved replacing as little as 40% to as much as 56% of cement or sand with fly ash to obtained some positive results. However, standards cannot be easily altered, simply because

there are a few exceptions, and it seems that further effort will still need to be made to develop the optimal application criteria.

2.4.2.2. Brick and other construction applications

Fly ash, in addition its use in concrete and cement, can be used as a substitute for sand or clay and sometimes gravel. The manufacturing process in which clay is consumed in large quantities is clay-fired brick production. The sintering temperature of bricks with high fly ash content is 50 ℃ to 100 ℃ higher than that of traditional clay bricks (Lingling et al., 2005), but it has several advantages.

First, fly ash bricks are lighter than ordinary bricks. The typical brick densities are 2 g/cm^3 for clay bricks and 1.6-1.8 g/cm^3 for calcium silicate bricks, while fly ash sand lime bricks can be 1.14 g/cm^3 or lighter (Cicek and Tanrıverdi, 2007). Lightweight bricks dramatically reduce the freight costs of shipping, resulting in more economic benefits than any differences in the manufacturing costs.

Second, fly ash bricks have better physical properties than the typical clay bricks. In the experiments of Lingling et al. (Lingling et al., 2005), fly ash bricks showed the advantages of higher compressive strength, lower water absorption, no cracking due to lime, no frost, and high resistance to frost melting. Higher

durability of fly ash bricks was also observed in the experiments conducted by Cultrone and Sebastián (Cultrone and Sebastián, 2009). They found less decay in fly ash bricks due to salt crystallization. This is because fly ash reduces the proportion of micropores in brick, which are most vulnerable to salt-induced structural decay.

Third, fly ash is obtained as an inevitable by-product from coal-fired power plants, which are usually not far from the urban areas, and brick-making facilities near such power plants can dramatically reduce the material procurement and transportation costs of the products (Ahmaruzzaman, 2010). With increasing development of recycling applications, the recent price of fly ash is similar to that of the common clay (about $ 15 per ton), but, the stable supply of large quantities from nearby sources makes fly ash more economically attractive.

Fly ash is also used in construction sites where large volumes of materials are required, such as highway embankment. Fly ash offers an attractive alternative to the use of other materials because substantial economic savings can be obtained through reductions in the ash disposal costs and through the conservation of natural soils and lands (Kim et al., 2005). The use of fly ash in road works results in a reduction in construction cost of about 10-20% (Ahmaruzzaman, 2010). Fly ash/bottom ash mixture may be more compressible than the typical compacted sands at the same compaction levels, mainly due to the higher crushability

of bottom ash. Ash mixtures required compaction of 95% of the maximum density obtained from the standard proctor compaction test to have similar behavior of sandy soils in dense states(Kim et al., 2005).

Another area that requires a large amount of construction materials is mine backfills. Backfilling or sand stowing has been the method followed for decades to counter ground subsidence, as well as to improve pillar recovery (Mishra and Karanam, 2006). Upon the extraction of minerals from the ore, there is a very large amount of crushed rocks in the form of tailings that need to be disposed of. The most sensible thing to do is to send them back to where they came from (Rankine, 2007). For this purpose, the most common types of materials used for backfilling are waste rocks, mill tailings, quarried rocks, sand, and gravel (Mishra and Karanam, 2006). However, these alone usually do not provide enough structural strength to support the mine and exhibit poor injection, therefore, cement or other supportive materials are also injected to fill the empty spaces, increase the strength, and enhance injectivity. Cement is quite expensive for this purpose; the cost of cemented backfill tends to be 10–20% of the total operating cost of a mine, and cement can represent up to 75% of that cost (Grice, 1998). The criteria for mine backfill materials vary depending on the characteristics of the region (such as depth, re-mining potential, residential proximity, and surrounding land intensity), but the common requirement is

that the target compressive strength must be reached at the curing age of 28 days and beyond. As introduced in Section 2.4.2.1, when using fly ash as the substitute for cement, the problem is the low initial strength during the first 9 days rather than that after 28 days, since the strength at 28 days or later is often higher than that of ordinary cement. For this reason, fly ash is recycled as a mine backfill material in countries where the mining industry is active. For example, over 10% of recycled fly ash is being used for mine backfilling in India (American-Coal-Ash-Association., 2018). The fly ash injection process would also reduce acid mine drainage (AMD) through a two-fold approach: by neutralizing AMD and by preventing contact between water and pyritic materials (Ahmaruzzaman, 2010).

2.4.3. Fly ash as a low-cost absorbent

2.4.3.1. Water treatment by using fly ash

Fly ash has potential application in wastewater treatment because of its major chemical components, which include alumina, silica, ferric oxide, calcium oxide, magnesium oxide, and carbon, and owing to its physical properties such as porosity, particle size distribution, and surface area. Moreover, the alkaline nature of fly ash makes it a good neutralizing agent (Ahmaruzzaman, 2010).

Removal of phosphates

Water treatment by using fly ash has been tried since the 1970s. The waters obtained from hydraulic removal of the ash from power plants revealed excellent results when used for the treatment of municipal wastes, food industry wastes (meat, diary, and fish), and tannery wastes. Ash water reduced the biochemical oxygen demand (BOD) by 45% to 90% and the chemical oxygen demand (COD) by 92% (Kuziemska, 1980).

This is obtained because the water extracts of fly ash contain soluble ash components such as the hydroxides and sulphates of calcium, sodium, potassium, iron, and aluminum. It was found that phosphate precipitation occurs immediately after the introduction of aqueous extract of fly ash because of the very high total alkalinity of the extract. The addition of fly ash to water produces insoluble or low-solubility salts when combined with phosphates (Kuziemska, 1980). Phosphates are one of the main causes of eutrophication problem, therefore, their removal from water significantly reduces the BOD and COD values.

Cheung and Venkitachalam (Cheung and Venkitachalam, 2000) have shown through their study that weathered fly ash, which is abandoned in lagoons (they called it lagoon fly ash), can also be used as a good phosphorus absorbent. Lagoon fly ash was inferior to precipitator fly ash with respect to phosphate removal, probably owing to its relatively low exchangeable calcium

concentration. However, this result is highly promising in its possibility of recycling the fly ash that abandoned a long time ago.

Removal of phenol

Water treatment by using fly ash has been tried for many organic compounds besides phosphates, and phenol is one of them. Khanna and Malhotra (Khanna and Malhotra, 1977) first examined the potential of fly ash for the removal of phenol. They reported the kinetics and mechanism of phenol removal by using fly ash and provided useful data for the design of phenol–fly ash adsorption systems. Kumar et al. (Kumar et al., 1987) conducted a batch experiment on the phenol adsorption of fly ash and compared the results with those of activated carbon. The results show that the adsorption of phenol on fly ash is quite satisfactory; however, the contact times required to reach adsorption equilibrium on fly ash are roughly twice those on activated carbon.

According to followup studies, the removal of phenol depends markedly on the temperature and pH of the treatment solution (Alemany et al., 1996), particle diameter, carbon content, and specific surface area (Kao et al., 2000). More adsorption takes place with a fly ash of higher carbon content and larger specific surface area; and the affinity of phenolic compounds for fly ash is much above the expected amount corresponding to monolayer

coverage (Akgerman and Zardkoohi, 1996). In the experiments of Akgerman and Zardkoohi (Akgerman and Zardkoohi, 1996), fly ash had a surface area of only 1.87 m^2/g and a rough estimate of the amount required for monolayer coverage of the fly ash surface by phenol was 0.62 ㎎/g. However, fly ash adsorbed 67 ㎎/g of phenol in their experiment. They concluded that this is due to the strong hydroxyl functional group of phenol that vertically aligns the molecules on the surface as a result of interaction with the fly ash surface.

In all these adsorption experiments, the most prominent advantage of using fly ash was its low price compared to that of activated carbon, though another important advantage was pointed out by Batabyal et al. (Batabyal et al., 1995). In their research, the desorption of saturated fly ash was tested with aqueous solutions of hydrogen peroxide at 324 K, and the regenerated fly ash was reused for adsorption. It was found that the adsorption rate and the time to attain equilibrium were the same as those of the fresh fly ash particles, although about 30% of the used activated carbon is lost during the conventional thermal regeneration process; the regenerated carbon has a lower adsorption capacity than the virgin one.

Removal of heavy metals

In 1988, Gashi and his colleagues studied the removal of lead, zinc, cadmium, and copper by using reverse osmosis (Gashi et al., 1988), targeting removal of the heavy metals generated from the battery manufacturing, the fertilizer industry, zinc electrolysis, and sulfuric acid production. They needed low-cost agents to neutralize the acidic components. They tried to solve this problem by including a fly ash pack in the pretreatment step of the reverse osmosis process, but most of the heavy metals were adsorbed by the fly ash before entering the reverse osmosis process. The heavy metal removal efficiency varied from 73.1% to 96.84% in their research.

Rio et al. (Rio et al., 2002) examined the efficiencies of removing Pb^{2+}, Cu^{2+}, Cr^{3+}, Ni^{2+}, Zn^{2+} and Cr^{4+} from two types of fly ashes: silico-aluminous fly ash and sulfo-calcic fly ash. The silico-aluminous fly ash gave the removal efficiency sequence: $Pb^{2+} > Cu^{2+} > Cr^{3+} > Zn^{2+} > Ni^{2+} > Cr^{4+}$, going from the best removal efficiency (95%) to the worst (5%); whereas the sulfo-calcic fly ash's removal efficiency sequence was $Pb^{2+} > Cu^{2+} > Ni^{2+} > Cr^{3+} > Zn^{2+} > Cr^{4+}$, with the efficiencies ranging from 95% to 9%. They compared the removal efficiencies of fly ash with activated carbon or other low-cost sorbents and concluded that fly ash could be a viable alternative to them.

In a removal experiment on As (V), Diamadopoulos et al. (Diamadopoulos et al., 1993) found that As (V) is strongly adsorbed on fly ash and that the adsorption is almost irreversible. Therefore, they suggested that arsenic fixation could be achieved with fly ash. Kılınçkale et al. (Kılınçkale et al., 1997) went one step further and tried to realize more secure immobilization by processing fly ash that adsorbed heavy metals onto concrete blocks. They improved the setting, hardening, and mechanical properties of the final concrete block by adding $NaAlO_2$, $Ca_3(PO_4)_2$, or $Ca_3(PO_4)_2+CaCl_2$ at optimal dosages to eliminate the negative effect of lead; lead is the leading metal in causing fixation problems by disrupting the matrix in cement-based pozzolanic processes. These various attempts are expected to contribute to improving the environment by preventing the desorption of heavy metals from adsorbents.

2.4.3.2. Air purification by using fly ash

Activated carbon is one of the most popular adsorbents for air purification. It is obtained from carbonaceous source materials such as wood, bamboo, and coal. The physical or chemical activation process greatly increases the surface area of the material. Activated carbon almost exclusively adsorbs nonpolar materials, though it adsorbs a large amount of them (in terms of unit mass) because of its very large specific surface area.

The biggest disadvantage of activated carbon is its high prices, ranging from $ 500 up to $ 4,000 per metric ton (Maroto-Valer et al., 1999). Activated carbon cannot be permanently used and must undergo a periodic regeneration process. 10-15% loss occurs during every regeneration process (Kumar et al., 1987) and the adsorption efficiency also gradually decreases (Batabyal et al., 1995). For this reason, many researchers are looking for an inexpensive substitute for activated carbon.

The substitute of activated carbon should be cheap, exist in large quantities, have a low mineral content, and should be easily activated. The unburned carbon in the ash furnishes satisfactorily in all the conditions; since it can be easily obtained from the utility industries as a byproduct, it can be beneficiated from fly ash through the commercially available techniques. Note that it has already undergone a devolatilization process in the combustor and, therefore, it only requires activation (Maroto-Valer et al., 1999).

Usually, the unburned carbon content in fly ash is in the range 2-12%. However, with the introduction of the 1990 Clean Air Act Amendments, caps have been established on the emission of nitrogen oxides (NO_X). Consequently, many coal-fired utilities have begun to retrofit with low NO_X burners to meet the emission requirements. As a result of such a transition, the carbon content of fly ash generally increased significantly, up to 20% in some cases, due to the low oxygen and/or low

temperature combustion conditions required in those low NO_X combustion units (Ahmaruzzaman, 2010).

Another reason for the increase in unburned carbon content is the increase in the price of bituminous coal. Bituminous coal was priced at less than $ 30 per metric ton until the early 2000s, but then, it sharply rose to around $ 60. The average price of bituminous coal in 2017 is $ 55.84 per metric ton, which is more than thrice the price of sub-bituminous coal, $ 14.29 per metric ton(EIA, 2018). Since the 1970s when sub-bituminous coal began to be used (EIA, 2012), more and more coal-fired power plants have been increasingly using it for economic reasons, and in 2017, the production of sub-bituminous coal was slightly higher than that of bituminous coal; being 45.4% and 45.3% of total production(EIA, 2018). Most sub-bituminous coals contain more than 20% moisture, and this moisture results in a lower combustion efficiency and a higher conversion ratio of nitrogen fuel to NO_X in pulverized coal combustion, compared with a coal having the same fuel ratio but with little moisture. On the other hand, the concentration of unburned carbon in fly ash during blended combustion is also higher than that during non-blended combustion of each coal (Kurihara et al., 2003).

For this reason, the increase in the amount of unburned carbon contained in fly ash is a big problem in the operation of coal-fired power plants, but it also suggests that the substitute of activated carbon will be abundant for the time being. The

remaining issue is to identify the right way to use them in the right place.

Removal of NO_X and mercury by using fly ash

As mentioned above, NO_X is becoming a new obstacle in coal-fired power plants. To reduce NO_X emissions, power plants are sacrificing the combustion efficiency of coal and restricting the use of sub-bituminous coal, which is much cheaper than bituminous coal. NO_X abatement can be achieved by reducing the amount of emissions during combustion, but also be achieved by removing the NO_X after the combustion. Reducing the NO_X emission has disadvantages as mentioned above, so the post-treatment methods have been intensively studied, removal NO_X by using fly ash is one of them.

Another typical toxic substance that is observed in coal combustion is mercury. Mercury is cycled both in the terrestrial and aquatic environments on regional and global scales and has many adverse effects on the ecosystem (Schroeder and Munthe, 1998). In coal-combustion flue gas, mercury is emitted mainly as $HgCl_2$ but also as Hg(g), Hg(p), and HgO (Galbreath and Zygarlicke, 2000).

Since fly ash contains too much of mineral components, a sufficient surface area cannot be obtained by the conventional

method of activation. Rubel et al. (Rubel et al., 2005) therefore attempted to utilize fly/bottom ash as a mercury and NO_X adsorbent by steam activation at 875 ℃, but only a poor performance was realized.

Davini (Davini, 2002) modified the fly ash which came from an oil-fired plant, into activated carbon through the concentration and activation processes, and tried to adsorb NO_X. He used two types of acidic solutions to remove the ash component in fly ash and increased the unburned carbon content up to 85.5%, then activated it at 900 ℃ under CO_2 condition. The general properties obtained were the same as those of the typical activated carbon, and, of course, NO_X was well adsorbed.

Rubio et al. (Rubio et al., 2007) also obtained activated carbon from fly ash through a similar process. The only difference was that steam was used instead of CO_2 during the activation process. They tried NO removal with ammonia by using activated carbon as the catalyst at a low temperature. The obtained activated carbon performed well in this reaction, and the performance was agreement with the BET-measured surface area of the activated carbon.

Hower et al. (Hower et al., 2000) separated carbon from fly ash by using density gradient centrifugation with a lithium hetero-polytungstate high-density medium. They achieved a surface area of up to 36 m^2/g by concentrating the carbon content up to

the 77% without an additional activation process. The exact adsorption proportion of mercury is not reported in their paper, but the concentration of mercury vapor through the fly ash carbon packs was reduced from 12 ppm to 0.18 ppm in the best case.

Removal of organic vapors by using fly ash

Until NO_X and CO_2 became a social issue, organic vapors were identified as the main cause of air pollution. Research on the adsorption of organic vapor by using fly ash was performed much earlier than on NO_X.

In 1983, Peloso et al. (Peloso et al., 1983) used aggregation reaction with phosphoric acid and a low-temperature activation process (at 450 ℃) to increase the specific surface area of fly ash, in order to utilize it as a toluene vapor adsorbent. The specific surface area of the initial sample, which had a loss on ignition (LOI) of 8.9%, was 7.2 m^2/g, but it was reduced to 3.4 m^2/g upon heating to 650 ℃ during sample processing. Finally, a surface area of about 40 m^2/g was obtained after the activation process. The experiment showed that toluene was adsorbed in proportion to the specific surface area up to 3.8% by weight of fly ash. It seems that the concept of using the carbon content of fly ash was not known at that time because they even heated the sample to remove the unburned carbon.

Rothenberg et al.(Rothenberg et al., 1991) studied the adsorption kinetics of aromatic hydrocarbons and m-xylene on fly ash. They suggested that the adsorption was diffusion-controlled from analysis of the effects of temperature and vapor pressure on the adsorption.

Studies on organic vapors are less popular than those on combustion gases, therefore, no recent research can be found. In recent study (Maroto-Valer et al., 1999), however, the surface area of fly ash was increased to more than 400 m^2/g, which is about 10 times that obtained from Peloso's study (Peloso et al., 1983). Therefore, organic vapor adsorption experiments using fly ash are expected to show much better results than in earlier years, if conducted.

Removal of SO_X by using fly ash

The removal of SO_X is quite different from the other air purification processes described above. Until now, air purification has mainly used the large surface area of fly ash and has been based on unburned carbon, but the removal of SO_X uses the mineral component of fly ash.

A typical method for removing SO_X is to install FGD equipment. The most common FGD involves a wet scrubber that uses limestone. The working principle of the wet scrubber are shown below (Buecker, 2011).

$$SO_2 + H_2O \leftrightarrow H_2SO_3 \quad \text{Eq. 2-12}$$

$$H_2SO_3 \leftrightarrow H^+ + HSO_3^- \leftrightarrow 2H^+ + SO_3^{-2} \quad \text{Eq. 2-13}$$

$$CaCO_3 + H^+ \rightarrow Ca^{+2} + HCO_3^- \quad \text{Eq. 2-14}$$

When the three equations are combined, Eq. 2-15, the fundamental limestone scrubbing process, is obtained.

$$CaCO_3 + 2H^+ + SO_3^{-2} \rightarrow Ca^{+2} + SO_3^{-2} + H_2O + CO_2 \uparrow \quad \text{Eq. 2-15}$$

There are several drawbacks to this process. First, a large amount of water is required to scrub SO_2. The water used in the process contains sulfonic acid or calcium ions, therefore, it causes a certain amount of water pollution when it is discharged. As an alternative, gypsum ($CaSO_4$) can be recovered, as a byproduct, but the emission of CO_2 cannot be avoided .

Dry FGD is an alternative to the wet scrubber process that can solve this problem. Dry FGD uses calcium hydroxide ($Ca(OH)_2$) to immobilize SO_2 gas as gypsum (Kikuchi, 1999), as shown below:

$$NO + \frac{1}{2} O_2 \rightarrow NO_2 \qquad \text{Eq. 2-16}$$

$$SO_2 + NO_2 \rightarrow SO_3 + NO \qquad \text{Eq. 2-17}$$

$$Ca(OH)_2 + SO_3 \rightarrow CaSO_4 + H_2O \qquad \text{Eq. 2-18}$$

Fly ash can be used as a raw material for dry FGD because it is capable of supplying sufficient calcium to SO_2 in the form of calcium oxide. The key chemical reaction, for dry FGD, between the treated fly ash and SO_2 in excess O_2 is expressed by the Eq. 2-19 (Al-Shawabkeh et al., 1995):

$$CaO \cdot SiO_2 + SO_2 + \frac{1}{2} O_2 \rightarrow CaSO_4 + SiO_2 \qquad \text{Eq. 2-19}$$

Since fly ash is much cheaper than calcium hydroxide, massive introduction of fly ash can alleviate the disadvantages of dry FGD, which are a low SO_2 removal efficiency and a high maintenance cost.

The FGD process using coal ash has been commercialized, and some industrial plants have achieved $DeSO_x$ efficiencies of over 90%, such as the Ebetsu power station (50000 Nm^3/h) in Hokkaido, Japan, and the Tomato-atsuma power station

(644000 Nm^3/h) in Hokkaido, Japan, under high molar ratios of calcium to sulfur (1.0–1.2) (Kikuchi, 1999).

2.4.3.3. Zeolite synthesis by using fly ash

Zeolites are porous aluminosilicate minerals that are widely used as adsorbents and catalysts, like activated carbon. The first method to synthesize zeolite with fly ash was developed by Holler and Wirsching (Holler and Wirsching, 1985) in 1985. Since their initial study, many patents and technical articles reported different hydrothermal activation methods to synthesize different zeolites from fly ash (Querol et al., 2002). All the methodologies developed are based on the dissolution of aluminum–silicon–bearing fly ash into alkaline solutions (mainly NaOH and KOH) and the subsequent precipitation of zeolitic material, but various forms of zeolite are synthesized, depending on the activation agent, concentration, temperature, and solution/fly ash ratio (Querol et al., 2002).

Zeolites are crystalline aluminum silicates. Their structure is a framework of $[SiO_4]^{4-}$ and $[AlO_4]^{5-}$ tetrahedra that are linked to each other at the corners through sharing of their oxygen atoms (Figure 2.9). The tetrahedra form a three–dimensional network with plenty of voids in the network structure. The voids define the many special properties of zeolites, such as the adsorption of molecules in their huge number of internal channels (Figure

2.10). The substitution of Si (IV) by Al (III) in the tetrahedra results in a negative charge in the structure (Figure 2.9), which gives rise to a high cation exchange capacity (CEC; of up to 5 meq/g) when the open spaces allow access to the cations (Querol et al., 2002). These properties make zeolite a molecular sieve or a high cation exchange material. Since zeolite can be used either in aqueous (Erdem et al., 2004; Querol et al., 2002; Zorpas et al., 2000) or atmospheric conditions (Aguado et al., 2004; Khan and Kr. Ghoshal, 2000) and even in soils (Querol et al., 2006), it performs all the roles of an adsorbent, mentioned in Sections 2.4.3.1-2.

Since zeolite has different orders of affinity for different ions, it is advantageous in heavy metal adsorption in a certain manner. According to Moreno et al. (Moreno et al., 2001) a tentative order for cation adsorption preference of 4A and NaP1 type zeolite is as below;

$$Fe^{3+} = Al^{3+} \geq Cu^{2+} \geq Pb^{2+} \geq Cd^{+} = Ti^{+} > Zn^{2+} > Mn^{2+} > Ca^{2+} = Sr^{2+} > Mg^{2+}$$

This means that the zeolite selectively adsorbs heavy metal ions or other environmentally harmful ions in a calcium- or magnesium-rich solution (Moreno et al., 2001). This reduces the consumption of the adsorbent significantly, which makes it

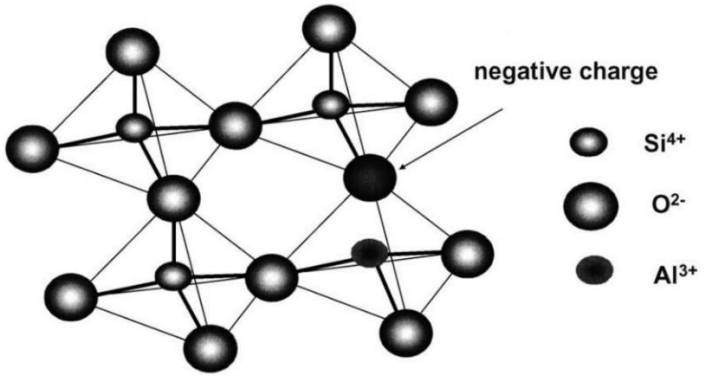

Figure 2.9. Idealized structure of zeolite framework (Querol et al., 2002)

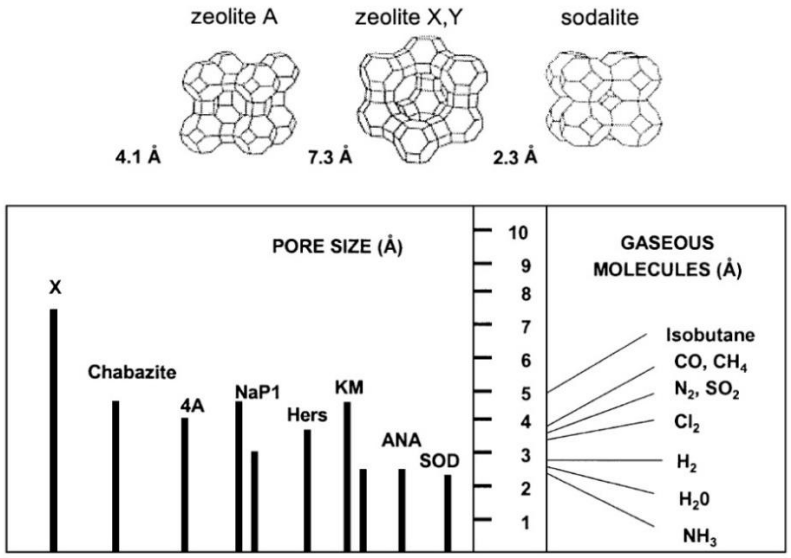

Figure 2.10. Top: Channel diameter of zeolite, which is dependent on the structure. Bottom: Examples of channel sizes for select zeolites, which may be synthesized from fly ash, that are compared with the diameters of some gaseous molecules. (Querol et al., 2002)

economically advantageous.

Another feature of zeolites is the high CEC. However, since ion exchange in zeolites is almost non-selective, it cannot be used as a catalyst (Ahmaruzzaman, 2010).

2.4.4. Environmental impact of fly ash

The utilization of fly ash in water raises concern on the potential leaching of some elements into water, with the possibility of secondary environmental pollution. The surface layer of the fly ash particles, probably of microns thickness, contains a significant amount of readily leachable material that is deposited during cooling after combustion. Therefore, the charge on the surface of the fly ash particles and the formation of a diffuse double layer play a significant role in leaching. The elements present are divided into two groups based on the concentration dependence of particle size (Reijnders, 2005). The elements manganese, barium, vanadium, cobalt, chromium, nickel, gadolinium, neodymium, arsenic, antimony, tin, bromine, zinc, selenium, lead, mercury, and sulfur are usually volatile to a significant extent during the combustion process. The volatility of these elements is inversely proportional to the particle size. Elements such as magnesium, sodium, potassium, molybdenum, cerium, rubidium, cesium, and niobium display smaller volatilized fractions during coal combustion.

In the case of applying coal ashes to soil or water, arsenic, boron, beryllium, chromium, manganese, molybdenum, lead, sulfur, antimony, selenium, vanadium, and zinc could be significant environmental burdens (Reijnders, 2005). Table 4 gives the representative values for the trace elements released from ash materials into distilled water under comparable conditions. There appears to be a trend toward the greatest release of cationic elements by the acidic ashes (cadmium, copper, manganese, nickel, lead, zinc), while the anionic species are released largely in the case of the alkaline ashes (chromium, molybdenum, selenium). Arsenic may be an exception to this trend, although it has been noted that its solubility increases as the pH rises above neutrality (Theis et al., 1990). Since the amount of leached elements differs depending on the type of ash, it is difficult to generalize the environmental impacts. The most remarkable point is that the leaching rate of materials such as arsenic, barium, chromium, copper, and zinc, which are abundant in fly ash, is not very high. In fact, the arsenic, barium, copper, and zinc concentrations measured in the study of groundwater quality near various ash-disposal ponds, revealed that all samples satisfied the quality criteria for domestic water supply, as prescribed by the EPA (Simsiman et al., 1987). Conversely, the boron concentration exceeded the baseline in all the samples during the research.

In addition to these elements, fly ash contains organic compounds that are harmful to the environment. Most of the carbonaceous material in fly ash is chemically irregular; however, some of them are substance with environmental concern. In general, these can be divided into five classes: polyaromatic hydrocarbons (PAH), polychlorinated dibenzo dioxins and polychlorinated dibenzo furans (PCDD and PCDF), polychlorinated biphenyls (PCB), chlorobenzenes and chlorophenols, and phthalates. Since PCDD and PCDF are not stable at high temperatures, they are mostly removed through an efficient combustion process. However, the problems caused by organic compounds remain because new dioxins, furans, and PAHs can form during the combustion process. Fortunately, the most toxic of the organic compounds found in ash materials are among the least soluble in water. In many assays, the detected concentrations were only a few hundred nanograms per liter. Nevertheless, it is likely that the solubility of these compounds can be increased substantially over that in distilled water owing to the presence of other non-toxic organic and inorganic substances that are present in the environment (Theis et al., 1990).

Based on the above studies, the environmental impact of fly ash is deemed to be generally benign, but potential risks still remain. In the case of ashes where leaching is a concern, ponding should be avoided and the fly ash should be disposed through the monofill method. Pickles and his colleagues (Pickles et al., 1990)

Table 4. Ranges of the trace elements released into aqueous solution. From 4:1 to 20:1, water/ash was experimented for 18 h to 24 h (modified from (Theis et al., 1990))

	Fly ash component (μg/kg)	Elements released into aqueous solution (μg/L)	
		Acidic pH 3.9−5.1	Alkaline pH 8.16−12.4
As	6,000−1,200,000	20−4,500	100−400
B	10,000−600,000	39,100−72,000	33,200−109,000
Ba	100,000−1,074,000		72
Cd	290−51,000	<10−3,210	<10−80
Cl	50,000−1,000,000		
Co	6,300−35,000		
Cr	15,000−900,000	<10−1,000	200−1,800
Cu	16,000−400,000	<10−5,700	<10−150
F	120,000−671,000		
Hg	40−100		
Mn	100,000−1,000,000	<10−700	<10−150
Mo	8,400−33,000	10−470	1610−10,500
Ni	1,800−13,000	20−1,750	<20−120
Pb	11,000−800,000	<50−2,000	<10−200
Se	6,900−760,000	<40	130−280
V	73,000−256,000		
Zn	50,000−9,000,000	50−27,500	<10−120

tried to extract valuable metals from fly ash by using an extended arc flash reactor. They targeted the aluminum, silicon, iron, germanium, gallium, vanadium, and nickel present in the fly ash. Based on the same logic, selective removal of harmful components may be possible.

2.4.5. Fly ash in Korea

In Korea, about 6.4 million tons of fly ash is generated annually (Jung and Chu, 2016), about 50% of which is recycled as concrete admixtures, low-cost adsorbent for combustion gas or wastewater, construction materials, and as lightweight aggregates.

Similar to ASTM C 618, KSL 5405 is the Korean standard specification for the fly ash, which is used as an admixture in concrete or mortar. The standard includes silicon dioxide content, LOI, CaO content, density, activity index, and so on. KSL 5405 classifies fly ashes from Class 1 to Class 4; and the particle size, activity factor and LOI value are the main criteria. Class 1 fly ash has the lowest LOI value and the highest specific surface area, resulting in the highest activity factor. The fly ash with a reactive CaO content of more than 10% cannot be recycled because the classified fly ash is mainly used for the low heat of hydration concrete in Korea. Some of the fly ashes with high free-lime

contents will produce false sets and rapid heat rises in concrete mixes (Manz, 1999).

Since about 1% of the global fly ash production occurs in Korea and landfill space is relatively insufficient, studies on the environmental impacts and recyclability of fly ash have been conducted steadily. Recent investigations include the extraction of the rare earth elements from fly ash (김강주 et al., 2012; 이종근 and 김재영, 2013), fly ash application to 3D printing technology(Lee et al., 2017), and utilization of fly ash as a heat-resistant material (Kang et al., 2012).

3. Fly ash Particles as CO_2 Foam Stabilizer

3.1. Materials and Preparation

As explained in Section 2.4, chemical characteristics of fly ash are widely varying, because they are heavily influenced by the combustion coal type and combustion conditions. In order to ensure the reproducibility of the experiment and to improve the objectivity, it is necessary to characterize the fly ash before the experiment.

3.1.1. Characteristics of raw fly ash samples

Fly ash was obtained from Taean coal power plant in Korea. X-ray diffraction analysis (XRD) showed that the fly ash was mainly composed of mullite, quartz, and anorthite (Figure 3.1). The average value of the LOI measured by using a thermal gravimetric analyzer (TGA-701, Leco, USA) at 950 ℃ was 3.5%. From the result of X-ray fluorescence (XRF) analysis, a slightly higher silicon content than that corresponding to the typical case was observed (Table 5).

Particle size analysis was performed through the standard sieve test (for >75 ㎛ particles, +200 mesh) and laser diffraction (for <75 ㎛ particles) (Mastersizer 2000, Malvern Instruments, Worcestershire, UK), which showed that the median size of the

raw fly ash sample was about 20 ㎛ and that 90% of the particles were smaller than 65 ㎛ (Figure 3.2).

Various shapes of the particles can be identified from the scanning electron microscopy (SEM) images. The most frequently observed particles in the fly ash are the fine spherical mineral particles (Figure 3.3). Aluminum and silicon oxides are mainly detected during energy dispersive spectroscopy (EDS) analysis (Figure 3.4).

In the case of particles with large grain sizes, their shapes are much more varied. The most distinctive particles are of porous shell type (Figure 3.5a). EDS analysis of these particles shows that the particles are mostly composed of carbon (Figure 3.5c). The inside of the shell is occasionally filled with small spherical mineral particles, as shown in Figure 3.3 (Figure 3.5b). In addition, particles that are wrinkled, distorted, or fairly close to the spheres are observed. EDS analysis of each particle shows that the particles with smooth surfaces are mineral particles that are composed of silica and aluminum oxide, whereas those with porous or corrugated surfaces mainly comprise carbon.

The measured zeta potential (Nano-ZS, Malvern Instruments, Worcestershire, UK) of the fly ash particles was -20 mV near the neutral pH, and the point of zero charge (PZC) was pH 4.5.

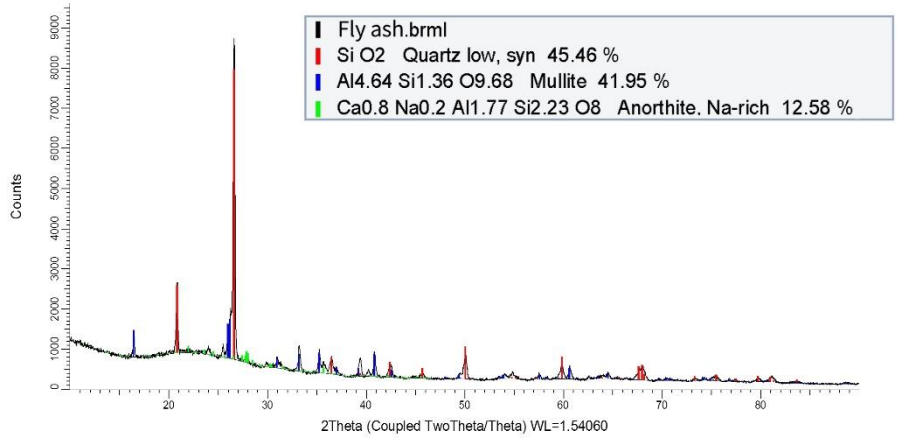

Figure 3.1. XRD pattern of the fly ash sample obtained from Taean coal power plant in Taean, Korea.

Table 5. Results of XRF analysis of the fly ash sample obtained from Taean coal power plant

Formula	SiO_2	Al_2O_3	Fe_2O_3	CaO	MgO	P_2O_5	K_2O
Concentration (%)	63.35	20.7	5.521	4.17	1.56	1.26	1.03
Formula	TiO_2	Na_2O	SO_3	SrO	ZnO	ZrO_2	MnO
Concentration (%)	0.963	0.833	0.25	0.142	0.081	0.073	0.055

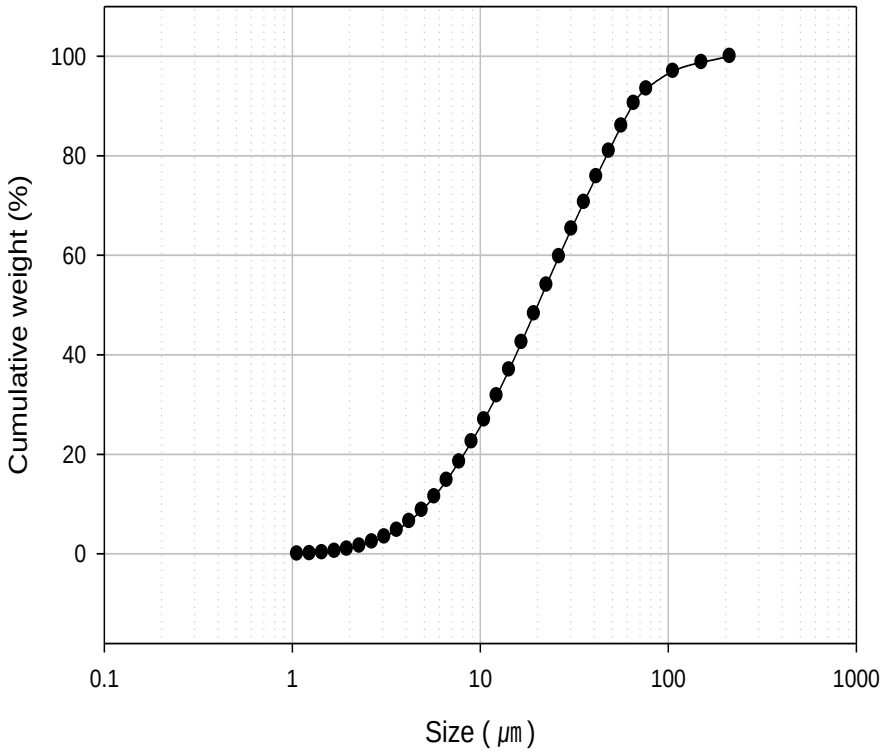

Figure 3.2. Size distribution of the fly ash sample.

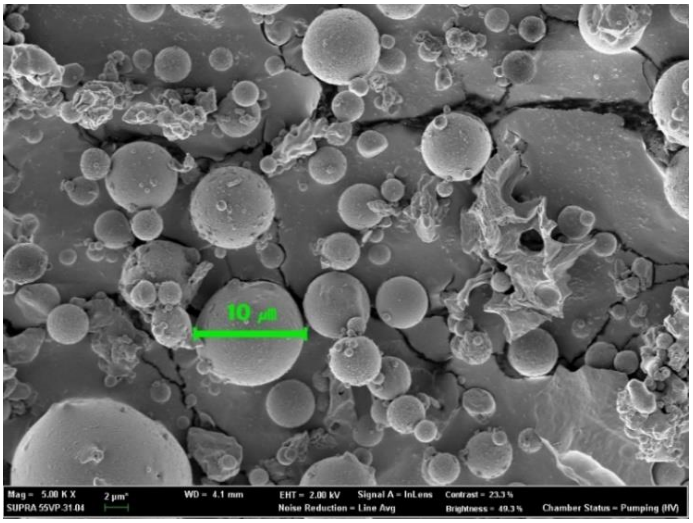

Figure 3.3. SEM image of −400 mesh sample.

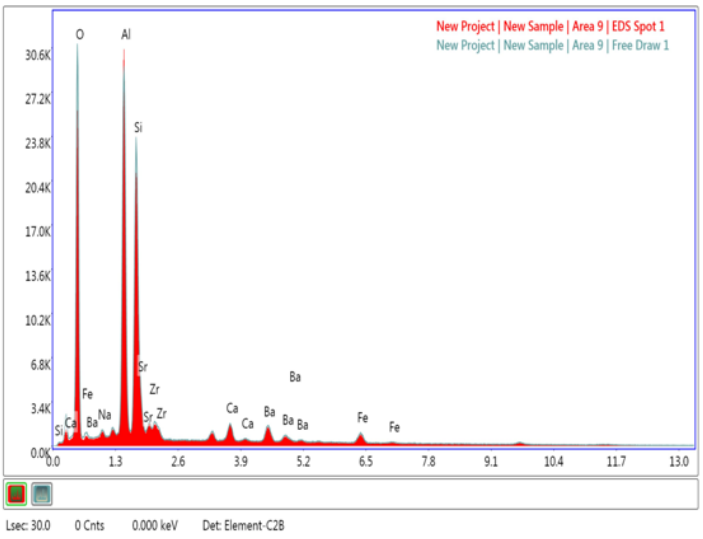

Figure 3.4. Results of EDS analysis of spherical mineral particles in fly ash.

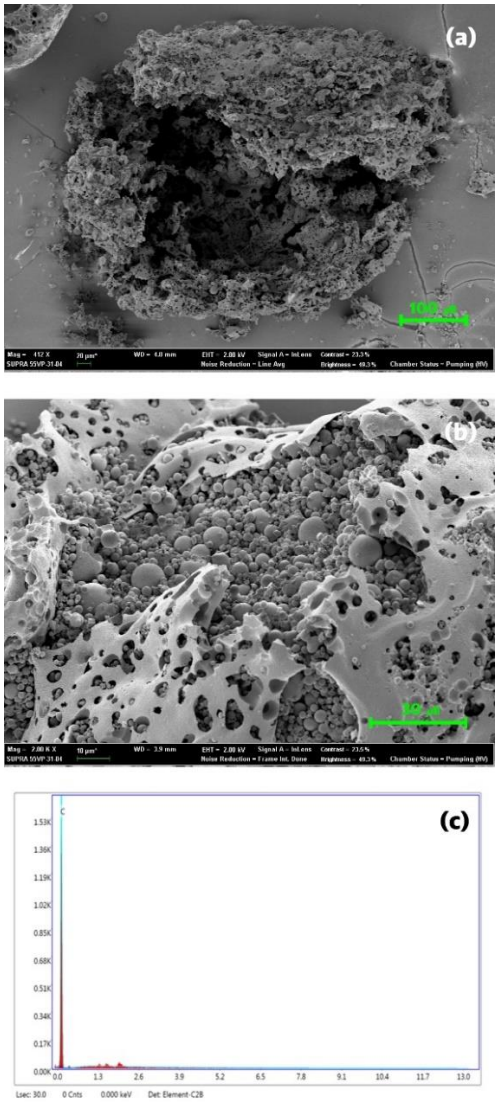

Figure 3.5. SEM image and EDS analysis results of +100 mesh samples. (a) Porous shell-shaped particles. (b) Small spherical minerals in the shell-like particles. (c) EDS result of shell-like particle.

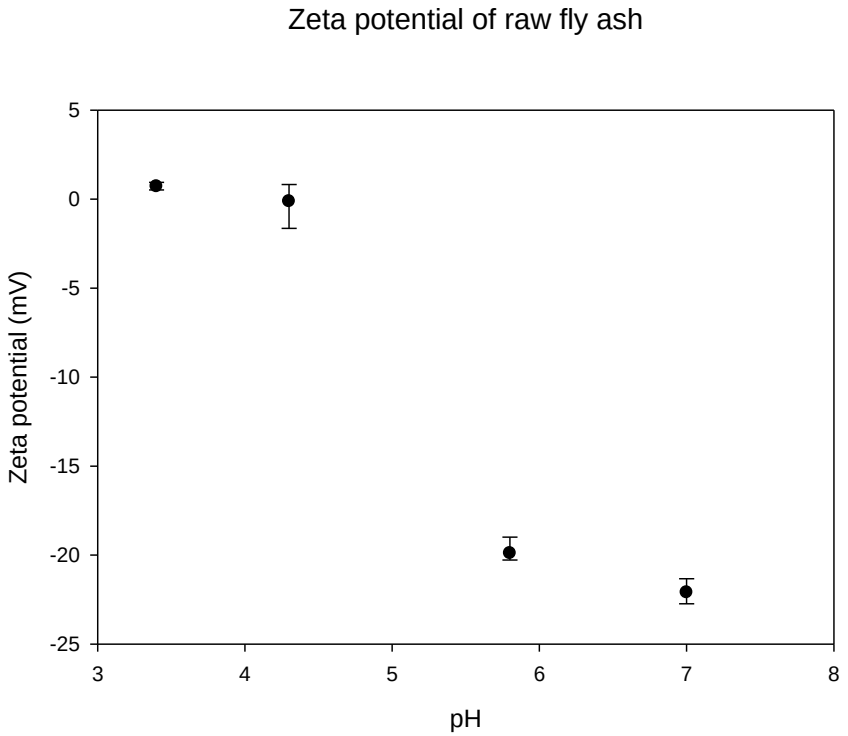

Figure 3.6. Measured zeta potential as a function of pH for raw fly ash particles. The particles were ground to an average size of about 5 ㎛ before the analysis.

3.1.2. Chemical composition control of fly ash particles

As can be seen from the analysis of Section 3.1.1, fly ash can be divided into two major components; minerals and carbon. A sample in which a specific component is concentrated can be obtained by removing either one of them or by selectively sorting them.

3.1.2.1. Thermally-treated fly ash (TTFA)

The easiest way to remove carbon is to burn it away. Since fly ash has already passed the high-temperature combustion process, changes other than the change in the carbon content are not significant. The most notable of the other changes is that the additional oxidation of iron turns the color from light gray to bright orange. The carbon removal process was carried out in an electric furnace at 900 ℃ under ambient air for 20 min. As a result of the carbon removal treatment, TTFA consisting of a concentrated mineral components was obtained.

Among the differences in the physical properties of TTFA and the raw samples, the difference in the zeta potential was outstanding. The zeta potential of TTFA near neutral pH was below −25 mV and the minimum value was −29 mV. Typically, nanoparticles with zeta potentials greater than +30 mV or less than −30 mV are considered to be strongly cationic and

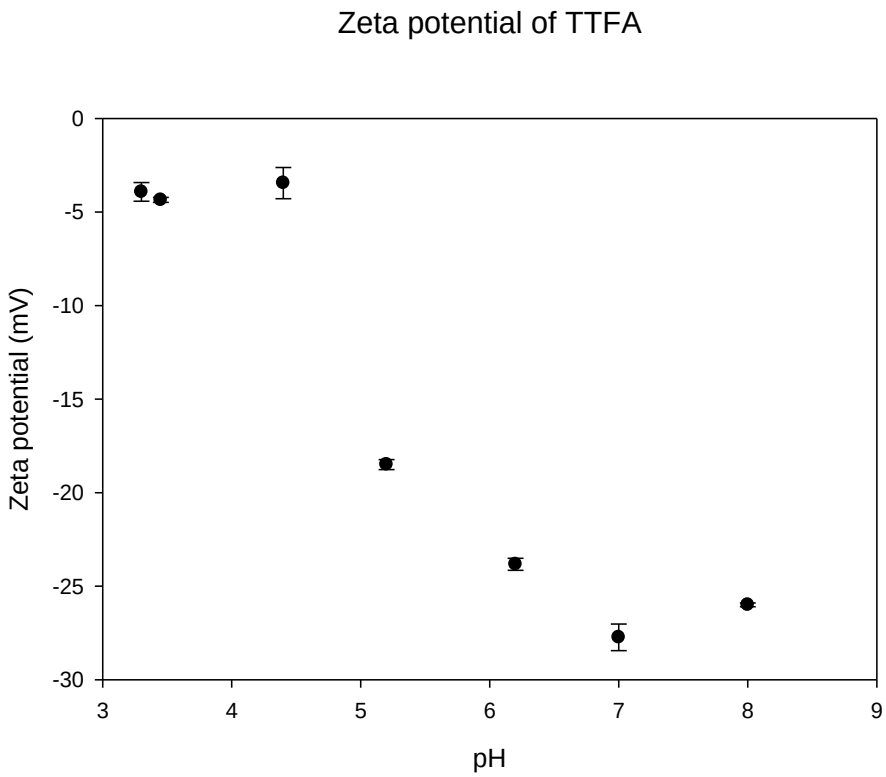

Figure 3.7. Results of the zeta potential measurements of TTFA samples.

strong anionic (Clogston and Patri, 2011), respectively, because they can be maintained in a dispersion by electrical repulsion. These values indicate that when TTFA becomes nanoparticles, there is a high possibility of maintaining a stable dispersion near neutral pH.

3.1.2.2. High carbon content fly ash (HCCFA)

The concentration of carbon components is more difficult and complicated compared to their removal. Although there is an already proven method to removing the mineral components with HCl and HF solutions to obtain a high concentration of the carbon components (Davini, 2002), it is costly and produces environmentally undesirable acidic byproducts.

Carbon enrichment by sieving

One of the easiest attempts to concentrate the carbon was based on size. As can be seen from the SEM image analysis in Section 3.1.1, carbon components with porous or corrugated surfaces are more often observed in large grain size samples. Analysis of the LOI of the samples separated by the standard sieve revealed that the LOI increased as the particle size increased, with the increase being up to 28% in the in the sample with the largest particle size (+70 mesh). On the other hand, the LOI of the −400 mesh sample, which passed through the finest sieve,

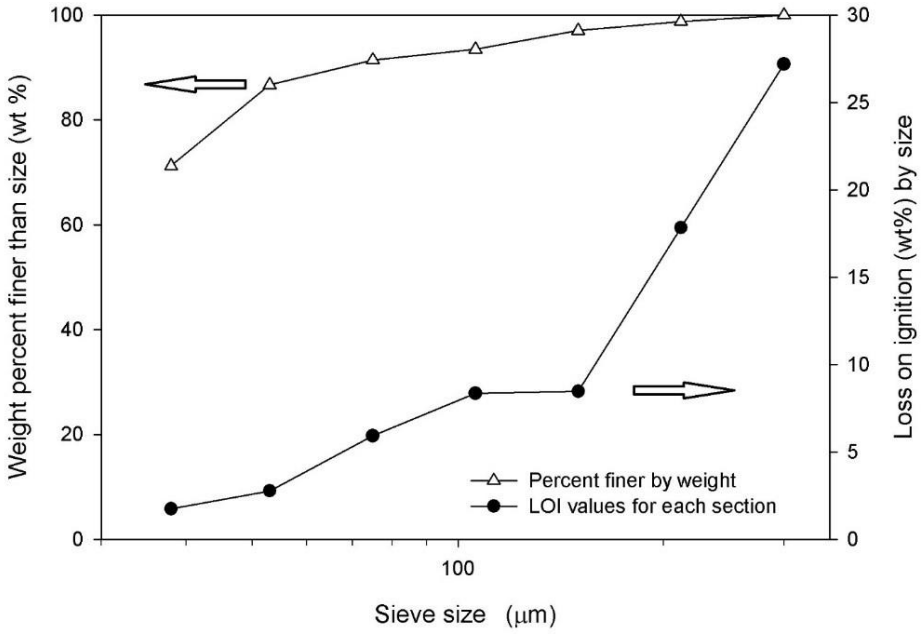

Figure 3.8. Change in LOI according to particle size.

decreased to about half (2%). The biggest disadvantage of this method is that the maximum carbon concentration that can be achieved is limited, as the relative fraction of recoverable particles decreases sharply. For example, the yield of the +70 mesh sample is only 1.2 wt% of the weight of the total sample.

The advantage of this method is that the small particles rejected in the process will have better material properties (lower LOI, smaller and more uniform particle sizes) as a construction material, and thus, the overall recyclability is enhanced.

Carbon enrichment by hindered settling

Density difference is one of the major properties that can be used for additional carbon enrichment. The difference in the density between the mineral and carbon components can be estimated from the chemical composition and the particle shape. It should be noted that amorphous solid carbon(2 g/㎤) is much lighter than aluminum oxide(3.95 g/㎤) or quartz (2.65 g/㎤). Moreover, as can be seen in the corresponding SEM image, the unburned carbon particles have a lot of voids both on the surface and inside, therefore, the apparent density is lower than the actual density.

Hindered settling due to density difference is a typical classification method. Experiments were carried out to separate the carbon components from a sample with an average LOI of 13% by using a custom made hindered settler. The best result among

the trials was obtained when the upstream speed was set to 7 ㎝/min. An overall yield was 1.5 wt% and the average LOI 52.2% was obtained. Although the LOI value is remarkably superior to that obtained by separation based on the size, it is not an efficient process, considering the recovery rate of the total carbon. The average LOI of the input sample is about 13%, which means that 55.2% LOI at the yield of 1.5% could only recover about 6% of the total carbon in the sample. The recovery rate can be improved slightly by optimizing the process, but there is a fundamental limit to the application of the hindered settler. In the hindered settling process, the settling velocity of the particles is proportional to the $(\text{size})^2 \times (\textit{density difference})$. Since fly ash samples have particle size differences that are of several orders of magnitude, compared to the density differences, which are in the tens of percent scale, the particles with high densities and small sizes are easily mixed with the low-density large-sized particles. Therefore, the use of hindered settling for carbon enrichment is quite inefficient.

Carbon enrichment by froth flotation

Further analysis has been carried out on the properties of the sample after sizing, to better explore the enrichment methods. The greatest differences between the carbon-free TTFA

samples and the carbon-enriched samples were in the hydrophobicity and the density.

The hydrophobicity of the particles was measured by using a tensiometer (Sigma 700, KSV instruments, Finland), which is a device that measures the contact angles of particles based on the Washburn equation:

$$T = \left(\frac{\mu}{C \ \rho^2 \gamma \ cos\theta} \right) M^2 \qquad \text{Eq. 3-1}$$

where T is the time after contact, μ the viscosity of liquid, C a material constant characteristic of the solid sample, ρ the density of the liquid, γ the surface tension of the liquid, and M the mass of liquid penetrated into the particle pack. However, this equation is not suitable for evaluating the hydrophobicity of fly ash because it can be used only for a single substance having a single contact angle. The useful information available from this equipment is the wettability of the powder to a liquid, which can be compared for various liquids.

Two different fluids were used in the wetting experiments: water and hexane. There is no change in liquid weight without the penetration due to the capillary pressure because the powder sample is on top of the liquid surface and in contact with the liquid through a fine metallic mesh screen (Figure 3.9a).

As a result, the raw fly ash and TTFA showed wettability to water, but did not absorb hexane. The +140 mesh fly ash, which had relatively high carbon contents, showed wettability in both hexane and water (Figure 3.9b). Since the total absorbed amount can vary depending on the particle size, surface area, and porosity, the absorption tendency should be compared based on the initial slope of the graph. From the experiments, it can be seen that the unburned carbon of fly ash is mainly composed of hydrophobic components.

Froth flotation is a separation method that utilizes both the hydrophilic and hydrophobic properties of a particle surface. When air bubbles are injected into a slurry, the hydrophobic particles tend to adhere to the air bubble and float. Therefore, these particles can be recovered from the water surface. The LOI of the recovered fly ash was increased up to 71.3% by flotation, when the pH was adjusted to 3.0, by using methyl isobutyl carbinol (MIBC) as the frother and kerosene as the collector. Among the 16% recovered sample, 87.7% of the total carbon was contained. The detailed conditions and results are summarized in Table 6.

This is a very effective and remarkable result compared to the hindered settling method. The total recovery of the froth and the tailing was 98.88% of the input sample, which is similar to the normal loss rate observed in the washing and filtering process, therefore, there was almost no effect of the concentration, owing

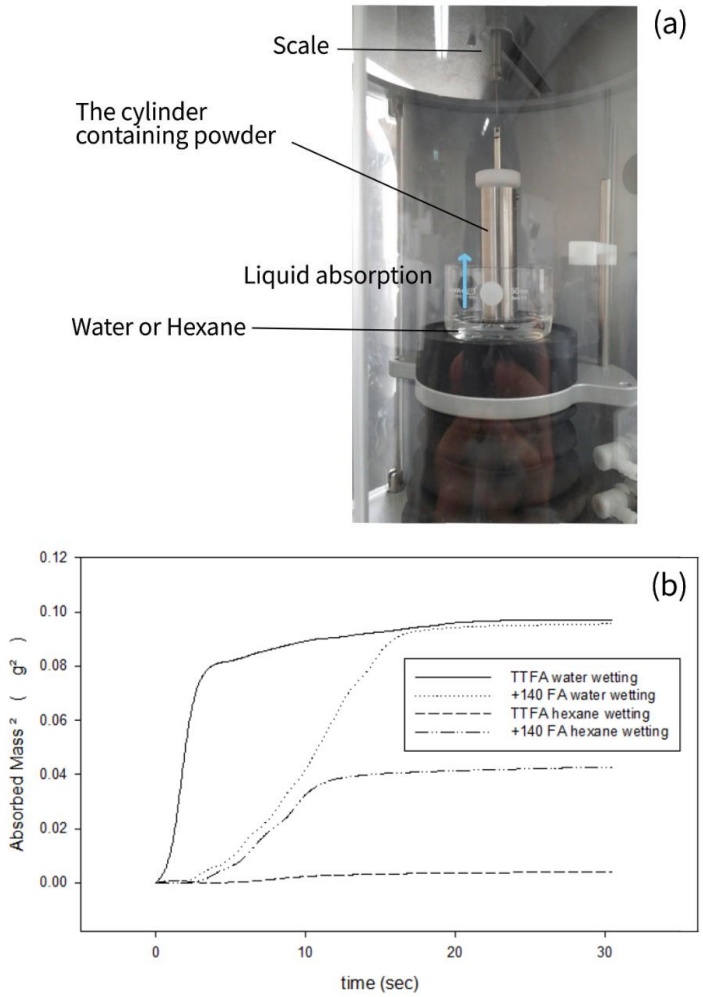

Figure 3.9. (a) Schematic of a tensiometer; (b) Results of wettability experiments performed on +140 mesh fly ash and TTFA.

Table 6. Results of flotation experiments performed at different pH values

Input	Frother	Collector	pH	Product	Wt%	LOI
LOI 13.1% 8 wt% slurry 2200 ㎖	MIBC 1.5 ㎖	Kerosene 1.5 ㎖	3.0	(a)Froth	16.1	71.3
				Tailing	82.8	2.57
				Total	98.9	−
			6.2	(b)Froth	13.4	70.4
				Tailing	85.6	4.7
				Total	99.0	−

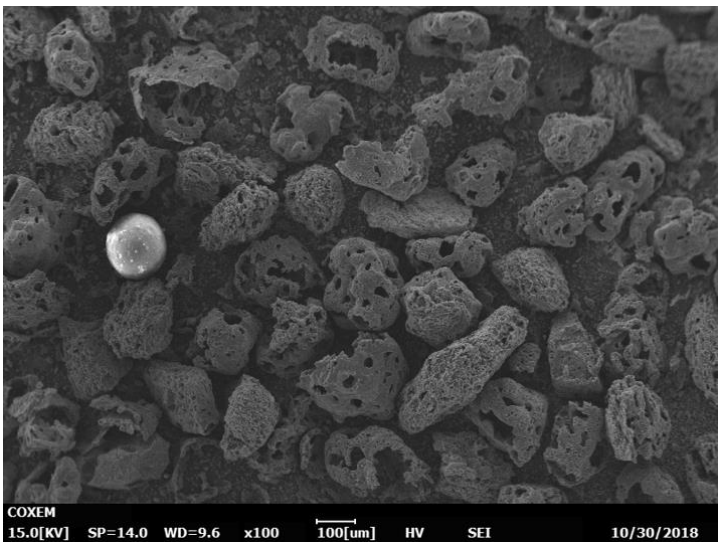

Figure 3.10. SEM image of the particles separated by froth flotation.

to the dissolution of the mineral component by the acid. SEM image analysis showed the effect of flotation (Figure 3.10). Almost all particle have the characteristics of the carbon particles as seen in Figure 3.5a, and mineral particles are rarely observed. The reason for the relatively low LOI value compared with that for the image analysis is presumed to be the mineral component embedded in the carbon particles, shown in Figure 3.5b. A sample that is concentrated to have a LOI of 50% or more by using the flotation technique is called HCCFA.

3.1.3. Grinding characteristics of fly ash

The main purpose of this study is to stabilize the CO_2-in-Water foam using fly ash particles. As explained in Section 2.1.4, micron-sized particles promote the collapse of the films rather than stabilizing them (Li et al., 2012). Furthermore, for EOR applications, the particles must be small enough to pass through the voids of the reservoir. Since nanogrinding is a very energy-intensive process, the target particle size cannot be reduced indefinitely. The target average particle size of the fly ash nanoparticles (from consultation with the CO_2 EOR experts at University of Texas at Austin, an international collaborative partner in this study) was 200 ㎚ with the particle size distribution as narrow as possible.

3.1.3.1. Grinding equipment and analyzers

Wet grinding is one of the top-down approaches used to produce mineral nanoparticles. Among the various ultrafine grinding devices, stirred ball mills are known to be advantageous for nanoparticle production owing to the ease of operation, simplicity of construction, high size reduction rate, and relatively low energy consumption (Gao and Forssberg, 1993). A stirred ball mill consumes 40–60% less energy than an unstirred ball mill because of the efficient use of the grinding media, where a force 30–33 times greater than the gravitational force is applied.

In order to operate a stirred ball mill, various parameters such as the media load, media size, media density, tip speed, grinding time, and slurry concentration must be set. Among these factors, the media size and the tip speed are the primary factors that have the greatest influence on the grinding efficiency. As the media size decreases, the collision frequency between the grinding media and the target material increases, but the kinetic energy decreases as the mass of the media decreases. Therefore, the number of effective collisions may be reduced if the grinding media size is too small. The approach to increasing the kinetic energy of the grinding media when its mass is reduced is to increase the tip speed. It is important to set the tip speed such that it matches the grinding media size; the smaller the media, the higher is the tip speed that can be matched. Too high a tip speed for large grinding media can significantly accelerate the

wear of the operating parts or the consumption of the grinding media or may even cause equipment failure through blade breakage.

Therefore, grinding was conducted in two stages by using two different types of stirred ball mills. The first-stage grinding was performed in a small laboratory-scale attrition mill (KMAM-1B, KMtech, Korea), with the main purpose being to reduce the size of the fly sample particles to the micron range. The 1030 ㎖ (10 cm in diameter) grinding chamber was filled with 800 ㎖ of zirconia balls having the diameters of 1, 2, and 3 ㎜ and the density of 5.9 g/㎤. Wet grinding was carried out for 30% solids (by weight) by using 320 ㎖ of the slurry to fill 80% of the mill chamber. A stirrer axis fitted with four bars was rotated at 800 rpm (13.3 $s^{-1,}$ stirrer tip speed 3.55 m/s).

The second-stage grinding was conducted in a bead mill (Fine mill 0.15, Daega Powder System, Korea). This apparatus had a built-in centrifugal classifier in the chamber to prevent grinding media leakage, which allows the usage of very fine grinding media (Figure 3.11). The mill was loaded with 0.4 kg of zirconia balls, corresponding to 65% of the mill volume being filled with the ball bed. Three different sizes of zirconia beads (100, 300, and 500 ㎛ in diameter) were tested as the grinding media. The 210 ㎖ milling chamber contained a rotor (a shaft with attached pins) rotating at 3750 rpm (62.5 s^{-1}, stirrer tip speed 8.55 m/s).

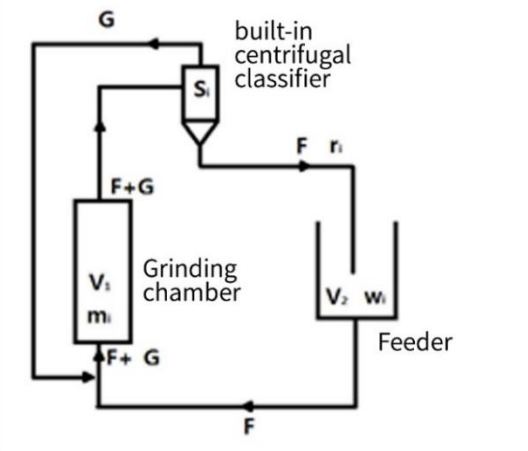

Figure 3.11. The bead mill used in the experiment and a schematic diagram of the flow in the equipment.

The mill was operated in the recirculation mode: the product from the first-stage grinding was passed into the feed vessel and repeatedly pumped back to the milling chamber with an integrated, continuously adjustable pumping and stirring system. The slurry pumping speed was 100 ㎖/min and the mean residence time for each pass-through was 78 s. The concentration of solids in the slurry was 5 wt%. Samples were taken from the outlet of the mill at regular intervals (after a predetermined number of recirculation passes).

The scale-up experiment was carried out using a 3-liter bead mill (KM-3, KMtech, Korea). This equipment has simpler structure without mechanical seal and a higher maximum input concentration that make it energy efficient. 300 ㎛ zirconia beads were selected as the grinding media due to steady particle size reduction and narrow size distribution, 80% of the mill chamber was charged with the media. The rotation speed was 1530 rpm (25.5 s-1, stirrer tip speed 8.72 m/s) and 2000rpm (33.3 s-1, stirrer tip speed 11.4m/s). Sodium hexameta phosphate (Calgon, Sigma-Aldrich, USA) was used to investigate the effect of milling aid on grinding energy.

Size distribution of samples were analyzed using laser diffractometry (Mastersizer 2000, Malvern Instruments, Worcestershire, UK) and dynamic light scattering (Nano-S, Malvern Instruments, Worcestershire, UK). An ultrasonicator (VC505, Sonics & Materials, USA) and a non-ionic dispersant

(IGEPAL-CA630, Sigma-Aldrich, USA) were used to improve the reliability and reproducibility of the size analysis.

The energy consumption during grinding was measured directly by using a power meter (WT-130, Yokogawa Electric Corporation, JP) and a three-phase energy logger (Fluke 1730, fluke corporation, US). The net grinding energy was determined by deducting the idle energy consumed by an empty chamber from the measured values.

3.1.3.2. Grinding results

Attrition mill

In the case of pulverizing fly ash by using an attrition mill, the grinding media d = 3 ㎜ showed the best efficiency during the early stage (Figure 3.12). In the case of using the 3 ㎜ grinding media, the particles reached the median size of 4 ㎛ at half the energy compared to the case of using the 1 ㎜ grinding media. However, as the median size approached 2 ㎛, the grinding efficiency began to drop significantly. When about 1200 kJ/㎏ of energy was applied, the three graphs almost passed through the same point, and smaller grinding medias resulted in smaller median sizes after that point. This is because as the size of the target material becomes smaller, the number of collisions affects the grinding efficiency more significantly than the kinetic energy of each grinding media. The number of collisions is proportional

to the total contact points between the grinding media, and this total number of contact points is inversely proportional to the cube of the diameter of the grinding media. However, as mentioned earlier, it is necessary to find the optimum size because the collision force also decreases when the media size decreases. Since the 1 ㎜ grinding media is also too large to realize average particle sizes that are in the several hundred nanometers range, a reduction in the grinding efficiency is observed before the target particle size is reached.

This was the main reason for employing a different type of mill during the second-stage grinding.

Bead mill

The samples obtained from the first stage ($d_{50} \approx 4$ ㎛ and $d_{90} \approx 10$ ㎛) were placed in a bead mill during the second-stage. In the bead mill, the grinding media of sizes 100, 300, and 500 ㎛ were used for testing the TTFA samples.

Figure 3.13 shows the effect of grinding the TTFA samples in the bead mill on median size. The smaller media are generally known to be more effective in grinding finer particles. However, the results showed an opposite trend. The grinding with 300 ㎛ and 500 ㎛ media showed higher rates of size reduction than that obtained with the 100 ㎛ media. During the later stage of

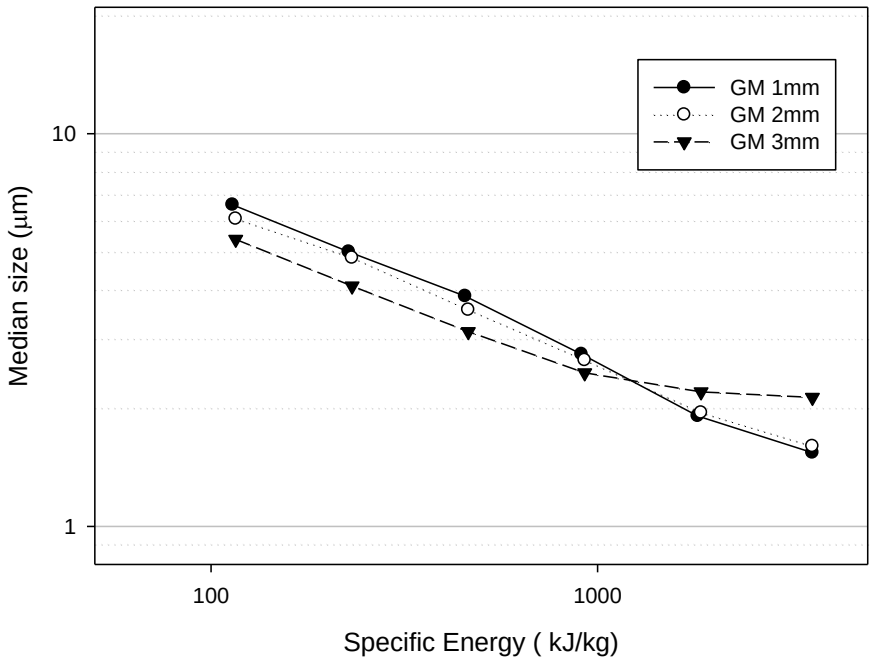

Figure 3.12. Median size of fly ash particles per energy input for varying the grinding media size in an attrition mill.

grinding, the rate of size reduction decreased, approaching the grinding limit of approximately 200 ㎚. In the submicron particle size range, the viscosity of the product suspension increased owing to strong particle-particle interactions. It seems that the 100 ㎛ grinding media was too light to overcome the hydrodynamic force exerted by the viscous suspension and impart a sufficient impact force on the particles for breakage.

Figure 3.14 shows the size distribution as a function of grinding media size for different numbers of passes. In the case of the 500 ㎛ grinding media (Figure 3.14c), a bimodal size distribution is observed during the first-stage because many small fragments were produced through high-stress interactions with the media. However, the distribution became unimodal as the coarse particles were broken down. On a similar note, the product size distribution obtained by using the 100 ㎛ grinding media exhibits a bimodal size distribution (Figure 3.14a). This is typical when the size of the grinding media is too small compared to the particle size. In this case, minor particle breakage occurs, resulting in fragments whose sizes are close to those of the original particles. The primary size reduction mechanism is abrasion rather than breakage, which results in very fine particles. The 300 ㎛ media had the advantage of a narrow size distribution by maintaining the unimodal distribution continuously (Figure 3.14b), but the initial efficiency was lower than that of the 500 ㎛ media.

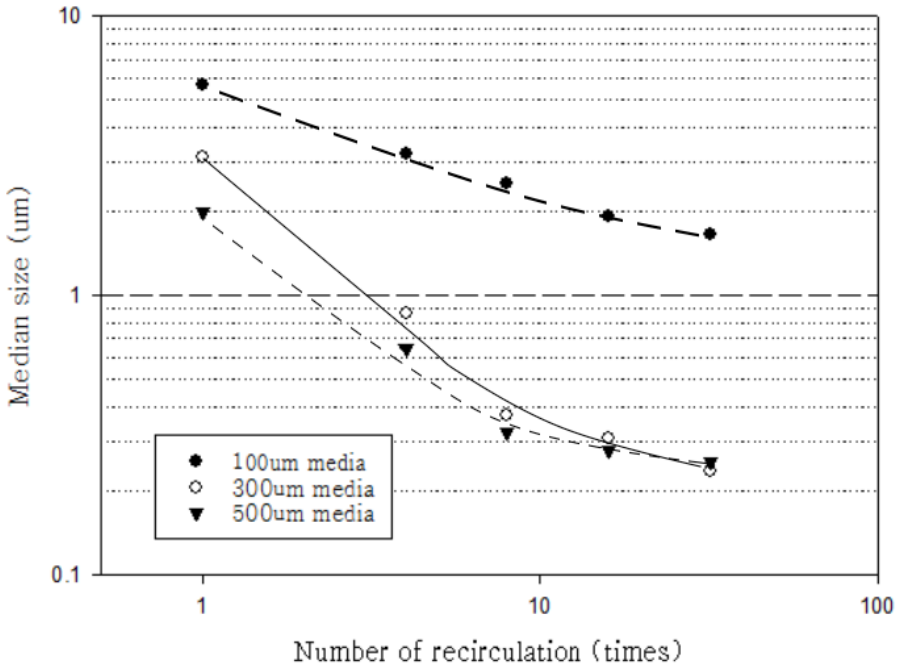

Figure 3.13. Reduction in median size with increasing number of recirculation when grinding a TTFA sample in a bead mill by using three different sizes of grinding media

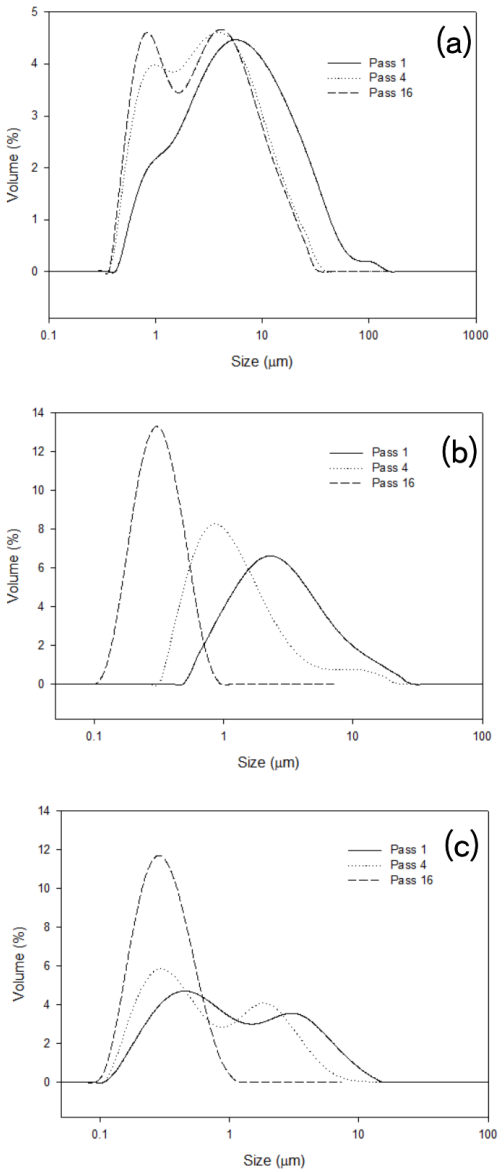

Figure 3.14. Evolution of the size distributions of a TTFA sample upon grinding in a bead mill by using three different sizes of grinding media: (a) 100 ㎛, (b) 300 ㎛, and (c) 500 ㎛.

Two-stage grinding

Based on the results presented above, two-stage grinding was performed for each fly ash sample. Figure 3.15 shows the variation in the median size of the fly ash particles as a function of the energy input during the two-stage grinding with 3 ㎜ / 500 ㎛ grinding media combination.

In the first-stage grinding, the +70 mesh fly ash sample showed the fastest size reduction. This may be because the relatively weaker carbonaceous materials were concentrated in the +70 mesh fly ash sample. However, all three samples showed almost the same particle size (5 ㎛) at the end of the first-stage grinding because the grinding rate decreased in this size range.

After the first-stage grinding, it can be seen from the slope of the curve that the grinding rate significantly increased initially during the second-stage grinding, but it decreased as the grinding proceeded. Obviously, it became more difficult to grind the particles as the size approached the nanometer range. In terms of the size reduction rate, there was not much difference between the three fly ash samples, as they all followed the same curve. The final median size of the particles after recirculating the samples 64 times was approximately 200 ㎚ at the specific energy of approximately 10^5 kJ kg-1. Figure 3.16 shows a TEM image of the particles, most of which are less than 500 ㎚ in size.

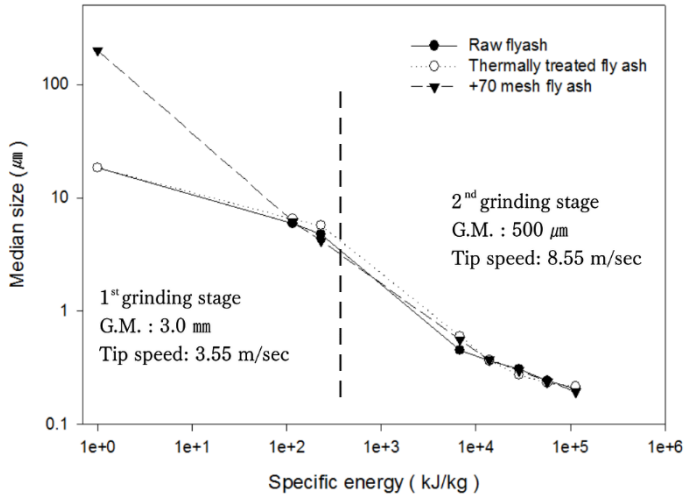

Figure 3.15. Change in median size according to energy input for different types of fly ashes.

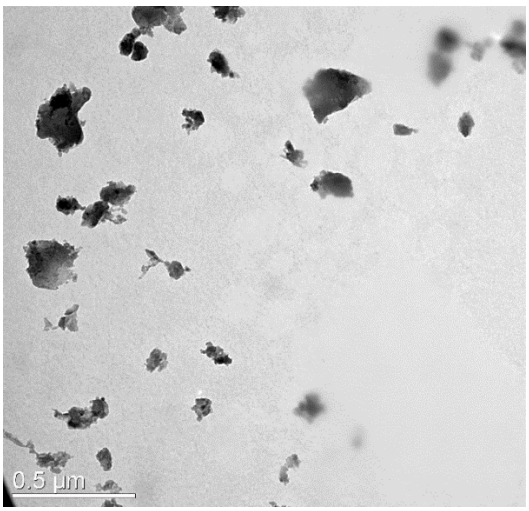

Figure 3.16. TEM image of a fly ash with the median particle size of 200 ㎚.

Scale-up effect and Economic evaluation

Energy costs can vary depending on the country and season, but $10^5\ kJ\ kg^{-1}$ is too high for economical production. To reduce the specific energy required to reach the median size of 200 ㎚, grinding was carried out at higher slurry concentrations in large-scale equipment.

The experimental results showed that 15 wt% slurry could be pulverized, but the specific energy tended to increase at concentrations above 10 wt% due to increased viscosity, especially when tip speed also increased (Figure 3.17).

The results of the experiment on the effectiveness of the grinding aid showed that calgon was the most effective in lowering the specific energy among the tested surfactants (ammonium lauryl sulfate, sodium dodecyl benzene sulfonate, IGEPAL-CA630, Tergitol NP-10, dodecyltrimethylammonium bromide, and cetyltrimethylammonium chloride). When 5% calgon was added, the highest grinding efficiency was obtained, and the grinding on 20% slurry resulted in specific energy consumption of 8000 $kJ\ kg^{-1}$ to achieve a median size of 200 ㎚ (Figure 3.18). Under conditions with milling aids, the faster tip speed did not reduce the specific energy, but increased the throughput and produced twice as many nanoparticles as when no dispersant was added. Approximate energy costs are covered in the appendix.

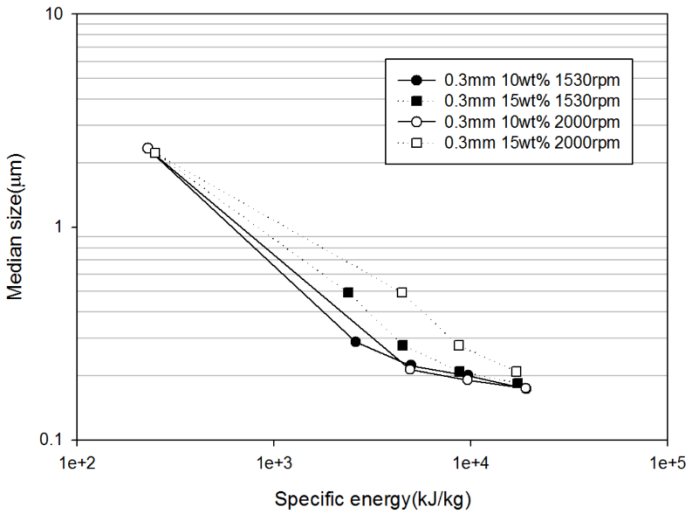

Figure 3.17. Effect of the slurry concentration and the rotational speed on the specific energy.

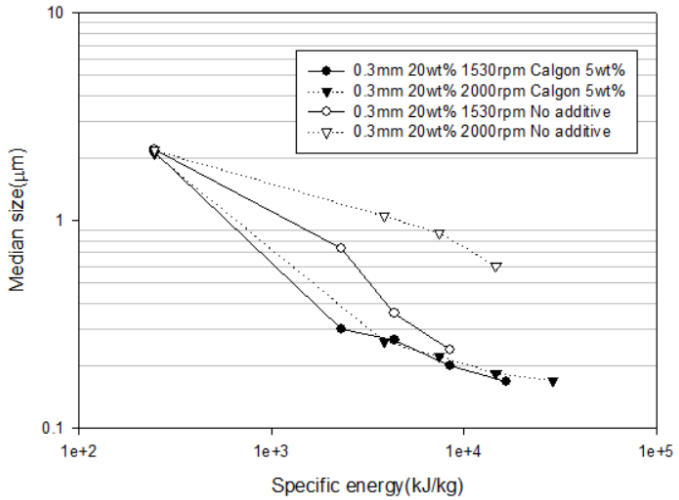

Figure 3.18. Effect of grinding aid (Calgon) on the specific energy

3.1.4. Narrowing the particle size distribution

For the nanoparticles to be stably injected into the oil reservoir, it is very important to reduce their size distribution. Even if the average particle size is small enough, if some large particles are present, they may block the pores near the injection well and cause plugging problem. If the grinding time is infinitely long, the particle size distribution will be concentrated near the grinding limit, but this method has a very poor energy efficiency.

Centrifugation can be used as an alternative to reduce the particle size distribution. Nanoparticles remain dispersed in an aqueous solution when there are sufficient steric or electrostatic repulsion among the particles; but if both are absent or deficient, the particles are agglomerated by Van der Waals attraction. The fly ash nanoparticles that have not been surface treated experience only electrostatic repulsion, which is usually not sufficient (less than 30 mV of surface charge in absolute value) for their long-term dispersion stability. When centrifugation is performed in this state, the electrostatic repulsion is constant, but a centrifugal force that is much stronger than the gravitational force is applied, so that many particles aggregate and sink. This will certainly leave only small particles in the solution, but very low yields can cause energy efficiency problems.

To mitigate this problem, anionic polymers are used to temporarily increase the zeta potential and serve as a steric

barrier. Sodium polyacrylate (SPA) is a sodium salt of polyacrylic acid with the chemical formula $[-CH_2-CH(CO_2Na)-]_n$. It is an anionic polymer, but it adsorbs weakly to anionic particles (Flood et al., 2007). The addition of 2 wt% SPA in fly ash results in a zeta potential value lower than −30 mV between the pH values of 6 and 9 (Figure 3.19).

Stability-enhanced TTFA was centrifuged at 3000 rpm for 30 min. A semi-transparent brown liquid with a volume of about 10% of the original volume was obtained at the top side. A slurry having a lower solid concentration than the original and a small volume of the precipitated particles was also obtained. The samples were divided into five compartments and dried to measure the concentrations of solids after size analysis. The detailed analysis results are summarized in Table 7.

The median size and the slurry concentration increased with the sample from closer to the bottom, and the d_{90} value decreased to less than 300 ㎚ in all the dispersion samples. The recovery of 58.8% of the total nanoparticles seemed to be effective way in improving the energy efficiency. Unfortunately, these weakly adsorbed SPA molecules are easily desorbed when cations such as Ca^{2+} or Mg^{2+} are present in the solution, therefore, the stability-enhancing effect is unlikely to be maintained under the conditions of mixing with brine and other high-ionic materials in reservoirs.

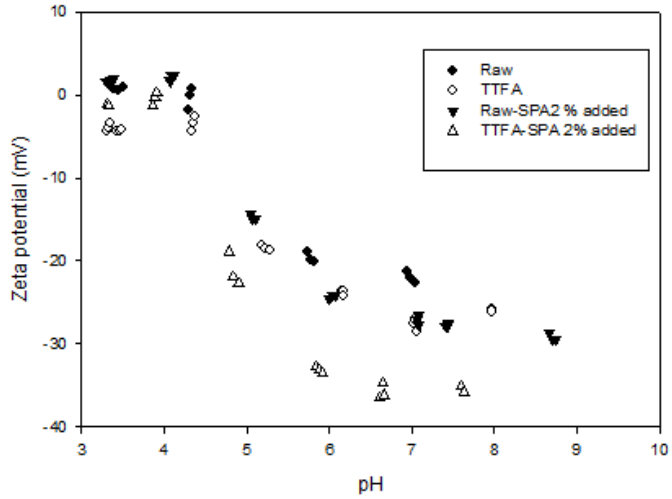

Figure 3.19. Changes in zeta potential with the addition of sodium polyacrylate to fly ash. The TTFA particles were strongly anionic (< -30 **mV**) in the pH range 6 to 9.

Table 7. Particle size distribution of stability-enhanced TTFA particles after centrifugation

Depth from the surface (%)	Slurry conc. (wt%)	Yield (%)	d_{10} (nm)	d_{50} (nm)	d_{90} (nm)
<10	1.07	2.39	61	107	196
10-40	2.38	12.46	96	150	234
40-70	2.52	13.33	108	161	240
70-99	5.08	30.04	120	182	280
Sediments		41.79			

3.1.5. Batch-type emulsion/foam generator

Figure 3.20 shows a schematic of the batch cell used for producing CO_2 emulsion and foam. The cell was composed of a cylindrical aluminum shell with the thickness of 38 ㎜, with inner diameter of 34 ㎜, and depth of 20 ㎜. Both sides of the cylinder are covered with polycarbonate glass so that the emulsion/foam generation could be examined visually. The cell had a built-in magnetic stirrer.

Tests were conducted in the following sequence. First, the cell was purged with CO_2 gas at atmospheric pressure. Then, 8 ㎖ of an aqueous nanoparticle dispersion was injected into the cell by using a syringe. The valve B was closed and CO_2 was injected at 800 psi. The cell was then chilled in a bath of ice water in order to liquefy the CO_2. The pressure of the final state could be roughly controlled through the amount of liquefied CO_2. After liquefaction, both the valves A and B were closed so that the cell could be sealed completely and heated to the target temperature in a hot water bath. After the target temperature and pressure were reached, the cell was agitated with the built-in magnetic stirrer at 1350 rpm for 1 min. A spinner with two powerful neodymium magnets was also custom-built to operate the built-in magnetic stirrer.

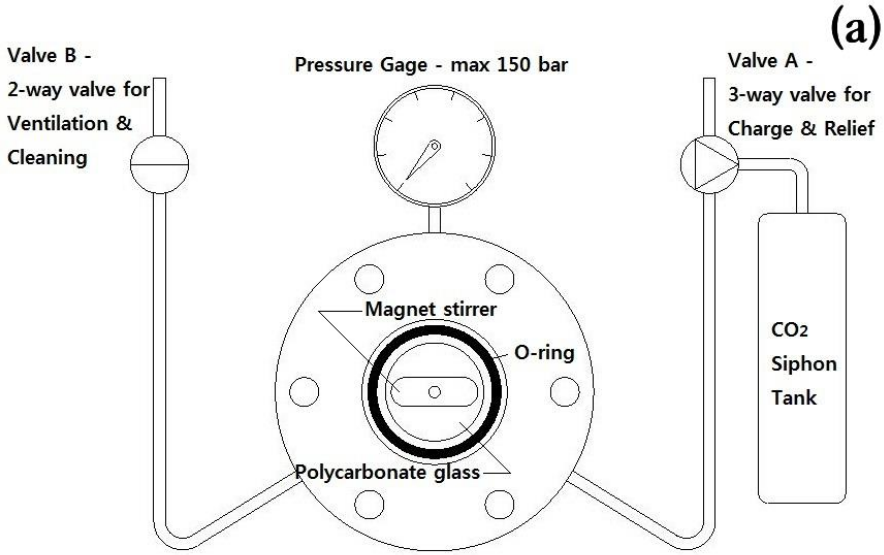

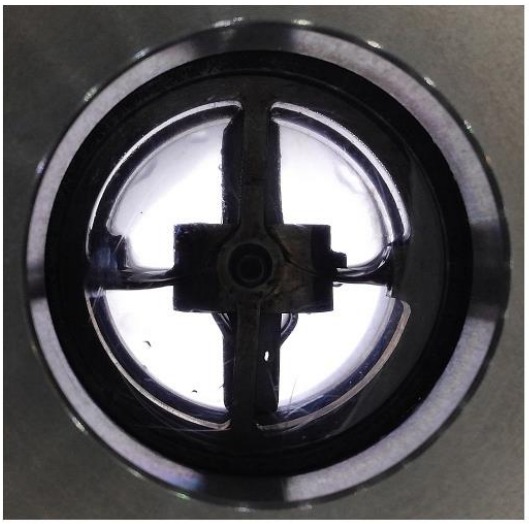

Figure 3.20. (a) Schematic of a batch-type emulsion/foam generator, (b) Actual image of the inside of the cell. The magnet stirrer is driven by a specially designed neodymium magnet spinner present on the outside.

3.1.6. Continuous injection equipment

In actual foam generation experiments, both CO_2 and water are injected through separated port; the two liquids mix with each other as they progress through the porous bead pack and foam is produced by the shear force generated. Generally, the fluid injected into a reservoir travels only about 1 to 4 ft/day, therefore, the shear force generated during the progress can be very small compared to that of the dynamic stirring in the laboratory experiment. Therefore, after the batch cell test, the samples were injected into the continuous injection equipment to confirm that the shear force generated during the injection could also produce the foam.

Figure 3.21 presents a schematic diagram of the apparatus used for the continuous injection experiment. The details of each part are as follows.

a. Pumps: The pumps used in the experiment are syringe pumps obtained from ISCO (500D, Teledyne ISCO, US). The pumps can operate in both the constant pressure mode and constant flow mode, and can circulate water in the temperature jacket, allowing the temperature of the injection liquid to be adjusted before the experiment. Most of the experiments were conducted in the constant flow mode, and the pressure was

controlled by using a backpressure regulator at the end of the circuit.

b. Nanoparticle dispersion tank: Syringe pumps cannot be disassembled and cleaned, therefore, there is the risk of cross contamination when using several types of nanoparticles. Nanoparticles can also damage the cylinder or piston surface of the syringe pump. The nanoparticle dispersion tank is a 1/2−inch diameter stainless steel pipe of length 110 ㎝, and a piston with two O−rings is placed in the pipe.

c. Bead pack: The bead pack is intended to simulate porous media such as sandstone. It is composed of pipes of length 10 ㎝ and diameter 3.86 ㎜ and is filled with 300 ㎛ zirconia beads. Both its ends are clogged with metal filters to prevent outflow of the beads. The average porosity is 38% and the shear stress of 3554 s^{-1} is applied for **10 ㎖/min** injection.

d. Pressure gauges: Three pressure gauges are installed as part of the equipment. Two of the gauges show the pressure inside the test equipment, and the differential pressure gauge that connects them displays the pressure difference between both ends of the capillary. The differential pressure meter automatically transmits and records the values in a computer every second.

e. Capillary: The capillary tube is set up to measure the dynamic apparent viscosity of the foam based on the Hagen–Poiseuille equation:

$$\Delta P = \frac{8\mu_{app} L Q}{\pi R^4} \qquad \text{Eq. 3-2}$$

where ΔP is the pressure difference measured by the differential pressure meter, L is the length of the capillary tube, which is 1 m, Q is the flow rate supplied by the pump, 10 mℓ/min for out experiments, and R is the inner diameter of the capillary tube, which is 1.75 ㎜. From the above formula, the apparent viscosity μ_{app} can be obtained.

f. View cell: The view cell serves to visually confirm that foam is successfully generated during the injection. The observation window has a diameter of 25 ㎜. The polycarbonate discs installed on both sides have a diameter of 40 ㎜ and a thickness of 10 ㎜.

g. Accumulator: The accumulator prevents the nanoparticles from flowing directly into the back-pressure regulator. The inside of the accumulator is filled with about 350 mℓ of water and the piston with two O-rings separates the front and the rear. When the nanoparticle dispersion and CO_2 are

introduced from the front, the piston is pushed back and the water is sent to the back-pressure regulator.

h. Back-pressure regulator: The back-pressure regulator regulates the pressure across the entire system. When the pressure exceeds the set pressure, the valve opens automatically and a small amount of liquid is discharged to lower the pressure.

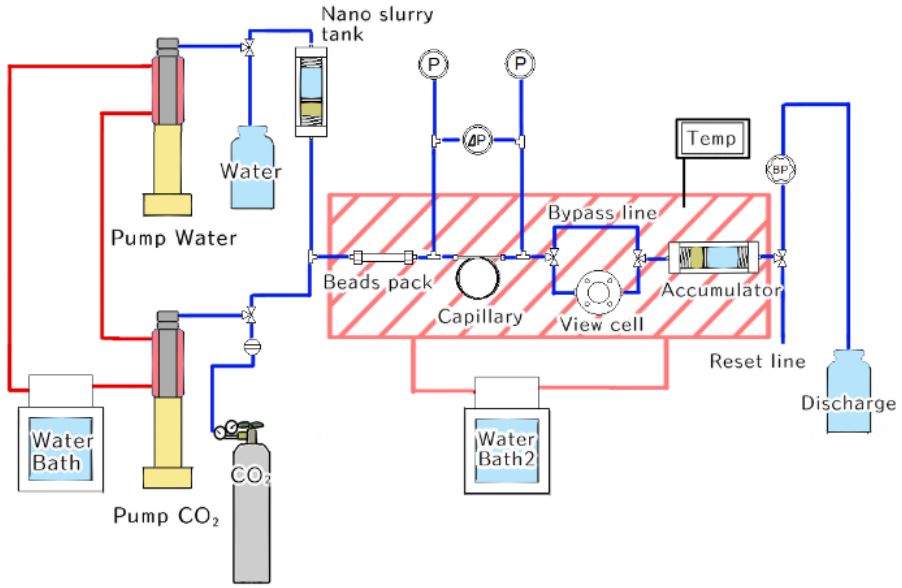

Figure 3.21. Schematic of continuous injection equipment

3.2. Experimental Results

3.2.1. Batch-type emulsion/foam generator

3.2.1.1. CO_2/ water emulsion stabilized with fly ash

Aqueous dispersions of fly ash nanoparticles were prepared at different solid concentrations of up to 10 wt%. The dispersions were agitated with equal amounts of liquid CO_2 in the batch cell at 800 psi and 286 K.

The liquid CO_2 was fully emulsified and very stable when the solid loading was greater than 10 wt% for all three types of fly ashes. As the concentration of solids decreased, the volume of the emulsion decreased rapidly, and no emulsion was formed when the solid concentration was less than 5 wt%.

The results of emulsification with 10 wt% solid loading of the three different fly ash types are shown in Figure 3.22. For the TTFA particles, the large and small droplets were sparsely distributed. On the other hand, the raw fly ash and +140 mesh fly ash particles displayed very dense emulsions; the respective cells were filled with uniform fine droplets. These samples contained more hydrophobic carbonaceous materials, which led to the conclusion that the size of the droplets decreased progressively with an increase in the hydrophobicity of the particles.

(a)

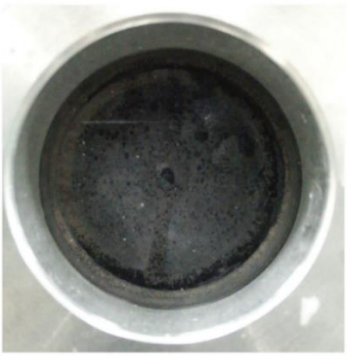

(b)

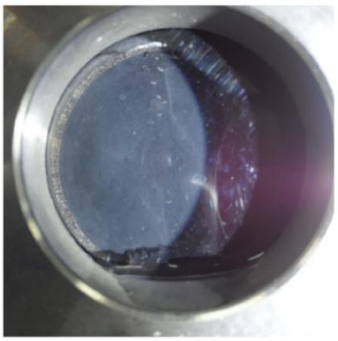

(c)

Figure 3.22. Images of the CO_2/water emulsion stabilized by using three different types of fly ash nanoparticles: (a) TTFA, (b) raw fly ash, and (c) +140 mesh fly ash (generated at 800 psi, 286 K).

3.2.1.2. CO_2/water foam stabilized with fly ash

Experiments were carried out with gaseous or supercritical CO_2 at various temperatures and pressures. However, stable foam was not observed when the mixed with fly ash dispersion. The gas or supercritical state has much higher interfacial tension with water (up to 3 to 4 times) than the liquid state (Espinoza and Santamarina, 2010). As described by Binks (Binks, 2002), unlike surfactants, solids need to overcome the adsorption energy barrier which is proportional to the CO_2 /water interfacial tension. Previous studies have shown that nanoparticles either do not affect the interfacial tension (Wang et al., 2004) or affect it to only a small extent (a few millinewtons per meter) (Schramm and Hepler, 1994).

3.2.1.3. Fly ash–surfactant synergy

The experimental results of Section 3.2.1.2 showed that none of the fly ash samples were able to form a stable CO_2 foam, which suggests that fly ash by itself is not effective in readily being adsorbed at the CO_2 (g)–water interface and stabilizing the CO_2 bubbles; that the addition of materials that adsorb onto the fly ash particles and impart the required surface characteristics is needed.

From the testing of various combinations of the different types of fly ashes and surfactants, a synergistic effect of fly ash and

surfactant was observed in the case of TTFA-dodecyl-trimethylammonium bromide (DTAB; Sigma-Aldrich, USA) combination.

Initial experiments to derive the combination involved mixing the nanoparticle dispersion and CO_2 gas by manually shaking them in a tube at atmospheric pressure. As illustrated in Figure 3.23, CO_2 gas was injected at atmospheric pressure into 15 ㎖ test tubes containing 6 ㎖ of the fly ash nanoparticle dispersion. Then, the test tubes were sealed tightly and vigorously shaken 50 times with hand. Foam stability was examined by observing the change in the foam height over a period of 2 h.

Figure 3.24 shows the ratio of the foam volume to the volume of the water phase when DTAB was added in the amount of 1 wt% of particles. It can be seen that DTAB was unable to form stable foams by itself, but when used in combination with the fly ash particles, it led to a noticeable improvement in the formation of stable CO_2 foams. However, in the case of the +70 mesh fly ash sample, which represents a sample with 28% carbonaceous materials, no stable foam was observed. Obviously, DTAB absorbed more favorably onto the surfaces of the fly ash mineral particles rather than onto the surfaces of the carbonaceous materials of the fly ash.

Based on previous experiments on CO_2 (g)-water foams, a batch test on the CO_2 (sc)-water foam was conducted. The tests

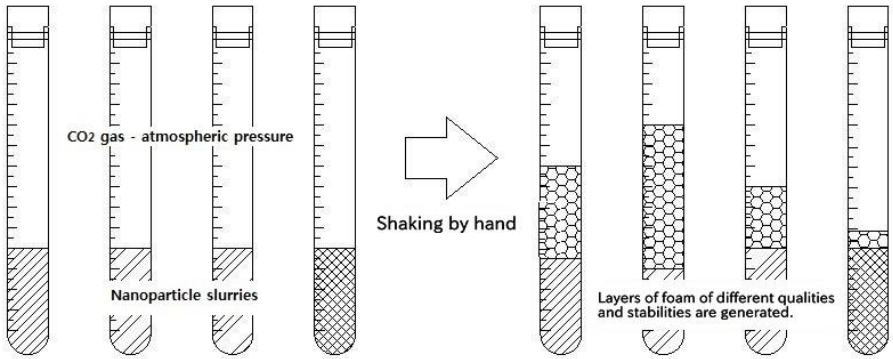

Figure 3.23. Outline of the CO_2 foam test used to find the synergistic fly ash–surfactant combinations.

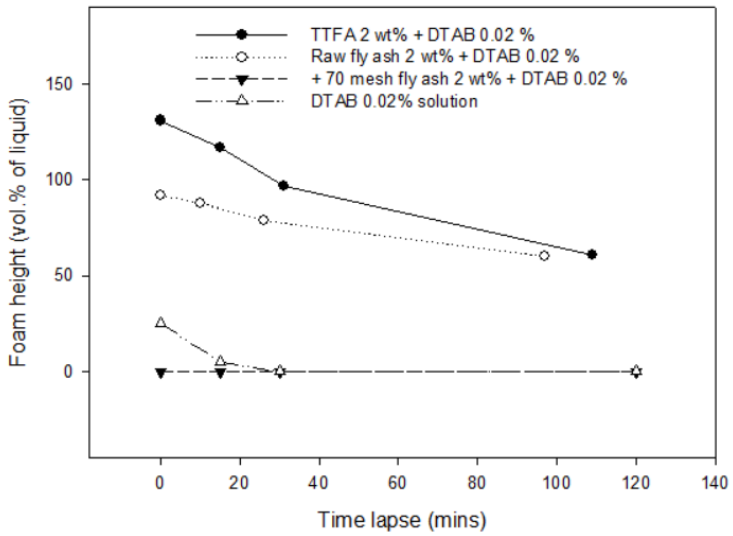

Figure 3.24. Relative volume of the foam formed through the addition of DTAB into the slurries of the fly ash nanoparticles obtained by grinding three different types of fly ash samples.

were conducted mainly at 317 K and 1378 psi (96.9 kgf/㎠). In the independent experiments for each material, DTAB hardly stabilized the CO_2 (sc)−water foam at less than 0.1 wt%, and no foam was formed when TTFA alone was added up to 10 wt%. However, when both the materials were added together, the foam started to stabilize in the mixture of 0.5 wt% TTFA and 0.005 wt% DTAB, and, at 3% TTFA and 0.03% DTAB, a sufficiently fine texture foam was produced (Figure 3.25).

In atmospheric pressure experiments, the carbonaceous components negatively affected foam formation, and this tendency was also observed in the supercritical foam experiments. Figure 3.26 shows that the texture of the foam becomes coarse as the carbonaceous material content increases. It can be inferred that there is a large cavity inside at +70 mesh fly ash case (Figure 3.26(c)), based on the transmission of the backlight, which cannot pass through the other samples.

3.2.1.4. Fly ash−oil coating synergy

Unlike what was mentioned in Section 3.2.1, the carbonaceous material showed only a negative impact on foam stabilization, as reported in Section 3.2.1.3. Various attempts have been made to increase the CO_2 affinity of the carbonaceous materials in fly ash, and some positive effects have been confirmed in the turpentine oil coating method.

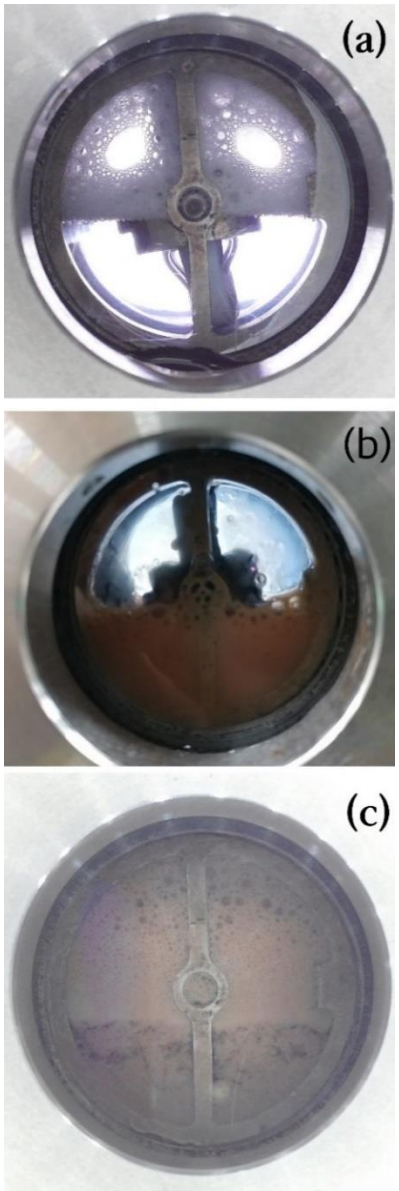

Figure 3.25. Neither the (a) 0.1% DTAB solution nor (b) 3% TTFA dispersion formed a stable foam with supercritical CO_2, but a stable fine-textured foam was obtained in (c) a mixed solution of 3% TTFA and 0.03% DTAB.

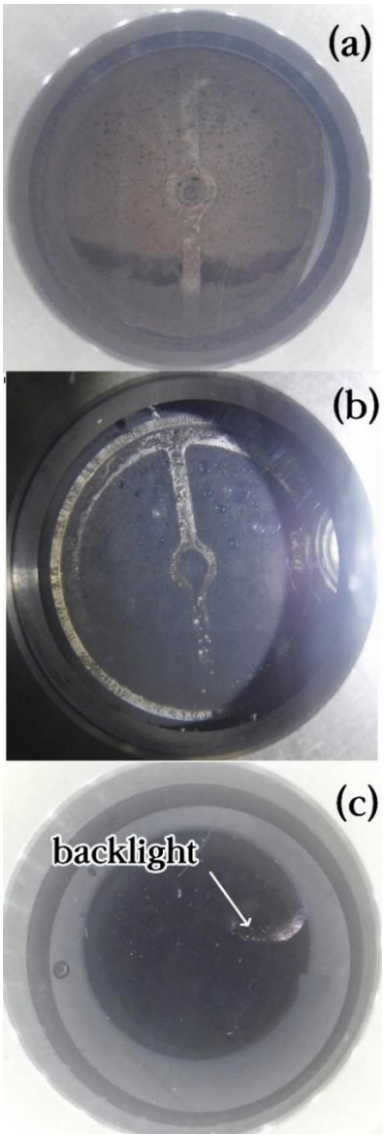

Figure 3.26. Supercritical CO_2 foam stabilized with 0.05% DTAB and different fly ash: (a) 5 wt% TTFA, (b) 5 wt% raw fly ash, (c) 5 wt% +70 mesh fly ash mixtures. There are large cavities inside the foam in figure (c); consequently the backlight is visible, while it is invisible in the other samples.

As noted in Section 3.1.2.2, the carbonaceous materials in fly ash are hydrophobic and have been well associated with oily collectors such as kerosene. CO_2 also has high affinities to many types of oils and sometimes even acts as a solvent, therefore, it can be used to extract oil from various plants (Bravi et al., 2002; Friedrich et al., 1982; Marrone et al., 1998; Reverchon and Senatore, 1992; Sovová, 1994). Based on these two pieces of information, various fuel oils and vegetable oils were added to coat the carbonaceous component of fly ash before CO_2 foam tests were conducted.

When using turpentine oil (Sigma Aldrich, USA) as an additive, the best results were obtained for the samples with the highest amounts of carbonaceous materials. Figure 3.27 shows the ratio of the foam volume to the volume of the liquid obtained with various concentrations of fly ash particles for the addition of 0.15 ㎖ of turpentine oil. It can be seen that there is no or minimal beneficial effect on the thermally-treated or raw fly ash particles, but considerable improvement is observed for the +70 mesh fly ash particles. The foam height is not remarkably high, but the fact that foam can be formed through a synergy between the oil and the nanoparticles is a positive result for the petroleum industry.

Unfortunately, turpentine oil failed to produce supercritical CO_2 foam even when the fly ash carbon content exceeded 50% and the solid concentration was 5% (Figure 3.28). This suggests

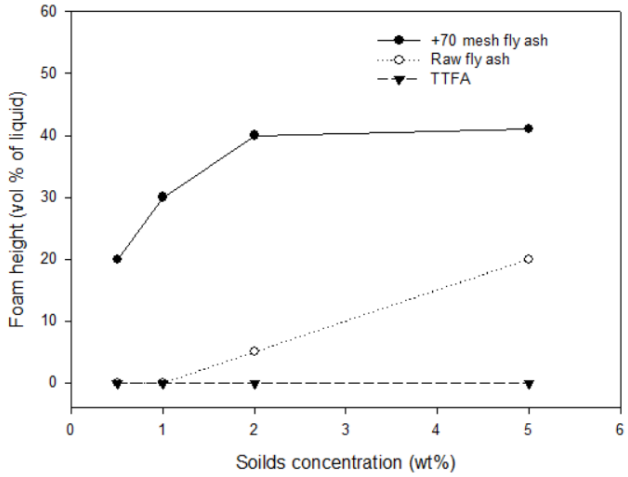

Figure 3.27. Foam stabilization effect of oil-coated fly ash obtained from a CO_2 foam test performed under atmospheric pressure.

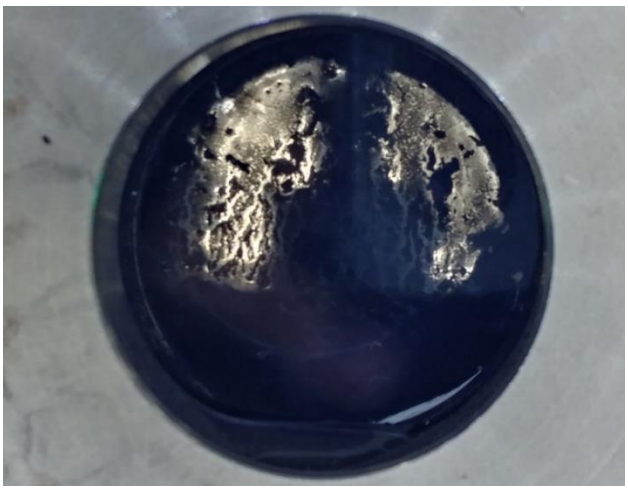

Figure 3.28. When 5 wt% of fly ash (50% LOI) with 0.5 ㎖ of turpentine oil was mixed with supercritical CO_2 , no foam was observed.

that the studies on gaseous CO_2 can only be a reference for the supercritical experiments, and that they do not predict the results of the supercritical state firmly.

3.2.2. Continuous injection test

3.2.2.1. Bead pack flooding

The DTAB-TTFA synergy observed in the batch experiments reported in Section 3.2.1.3 was also confirmed in continuous injection experiment. In the supercritical CO_2 injection experiments using the equipment shown in Figure 3.21 at 1500 psi and 323 K, the pressure drop baseline corresponding to 80 vol% of CO_2 (sc) and 20 vol% of deionized (D.I.) water was measured to be 0.22 psi. The pressure drop was increased to 1.09 psi when 0.01 wt% DTAB was added, which further increased to about 2.18 psi when 1 wt% of TTFA was also added (Figure 3.29). This means that the resistance factor (RF, see Section 2.1.3.1) of sthe DTAB solution doubled with the addition of TTFA, indicating that a denser foam was formed within the pipeline.

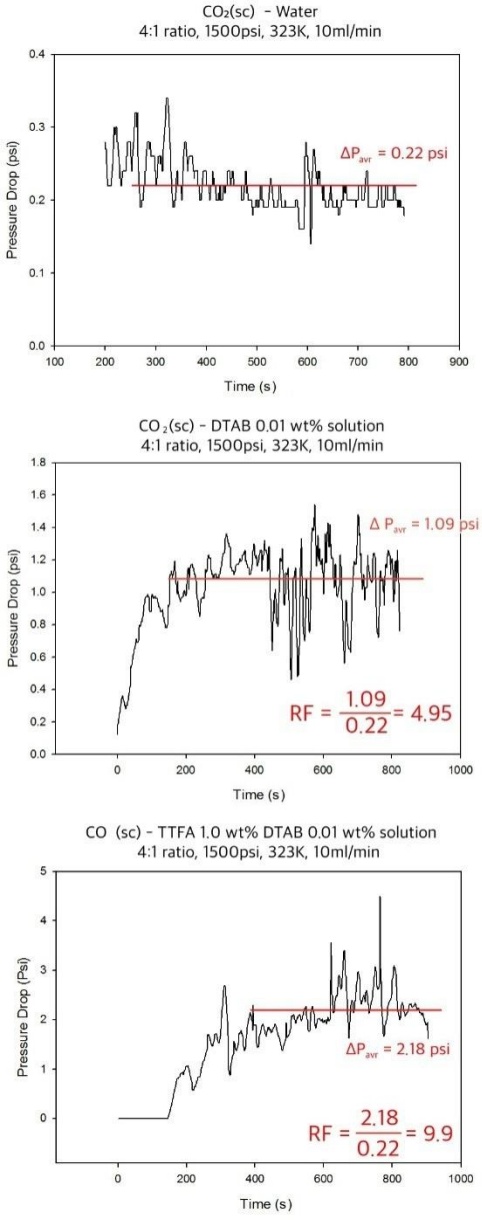

Figure 3.29. Supercritical CO_2 injection test results.

Sandstone-core flooding

Information on the dynamic properties of a foam passing through porous media can be obtained by injecting the mixture of CO_2 and aqueous nanoparticle dispersion into a sandstone core. Experiments to inject fly ash nanoparticles into the sandstone core were conducted by Robin Singh, a researcher at the UT Austin, which is an international collaborative research partner in this study, as mentioned earlier.

UT Austin is one of the pioneers in petroleum research and has been setting up various experimental apparatus for core injection. The major difference between this equipment and the equipment corresponding to Section 3.1.6 is that it includes a core holder that contains a Berea sandstone core instead of a capillary (Figure 3.30).

To prevent damage and clogging of the core, centrifuged TTFA ($d_{50} = 180\ nm,\ d_{90} = 280\ nm$) was used in core flooding. Experiments were carried out by comparing the pressure differences produced in three different conditions: when only brine and CO_2 were injected (as the base case), when surfactant was added to it, and when surfactant and nanoparticles are both added to it.

A variety of surfactant combinations have been attempted, and there have been two cases in which the nanoparticles caused a noticeable change in the RF.

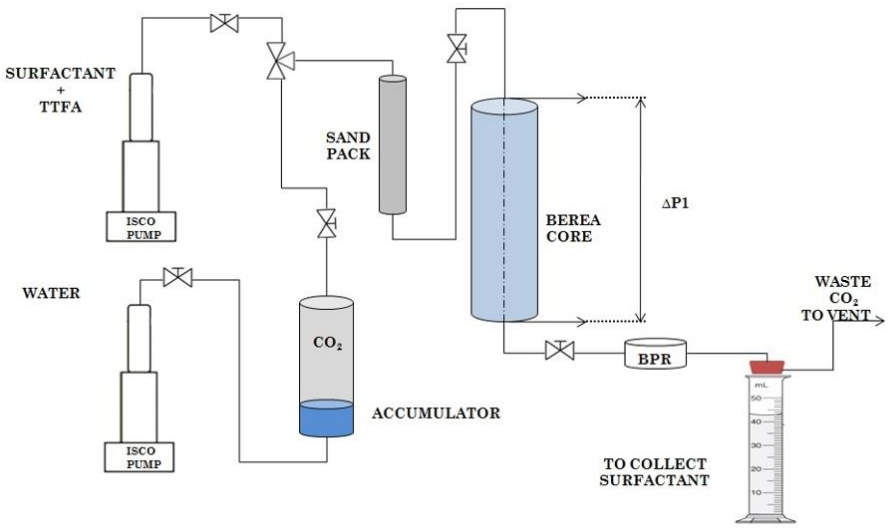

Figure 3.30. Schematic of the core flooding equipment of UT Austin.

.

The first case was the synergy with anionic surfactants (Bio-terge AS-40, Stepan Company, US). When the differential pressure of the base case (90% foam quality, injection rate 4 ft/day, room temperature, 100 psi) was 0.85 psi, the addition of 0.4 wt% anionic surfactant increased it to 5.9 psi, which further increased to 21.9 psi when 0.4 wt% of the nanoparticles were added together (Figure 3.31). This implies that the effect of the anionic surfactant represented by the RF value increased 3.7 times owing to the nanoparticles.

In the second case, the nanoparticles had a negative impact on non-ionic surfactants (Triton CG-110, Spectrum Chemical Mfg. Corp., US). The selected nonionic surfactant had a high RF value of 24.95, but this value decreased to 8.7 after the addition of the nanoparticles (Figure 3.32).

In both the cases, there was no decrease in the permeability of the core after the experiment and no face-plugging due to the TTFA particles occurred. This indicates that most of the nanoparticles successfully traveled through the sandstone core.

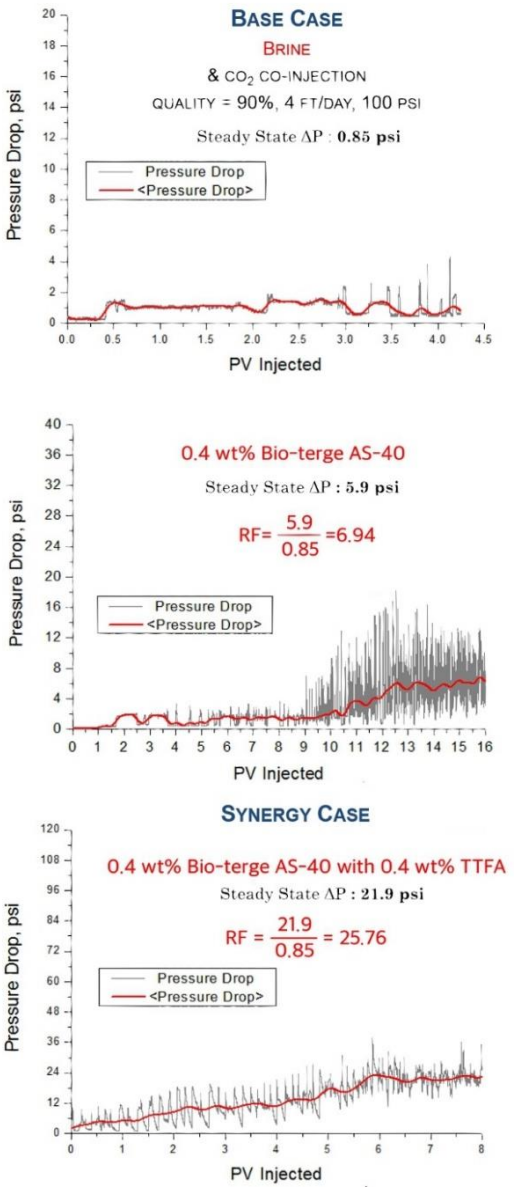

Figure 3.31. Synergy case of TTFA nanoparticles with an anionic surfactant (Bio-terge AS-40). (Modified from the annual research report of UT Austin, Aug 2014; not published)

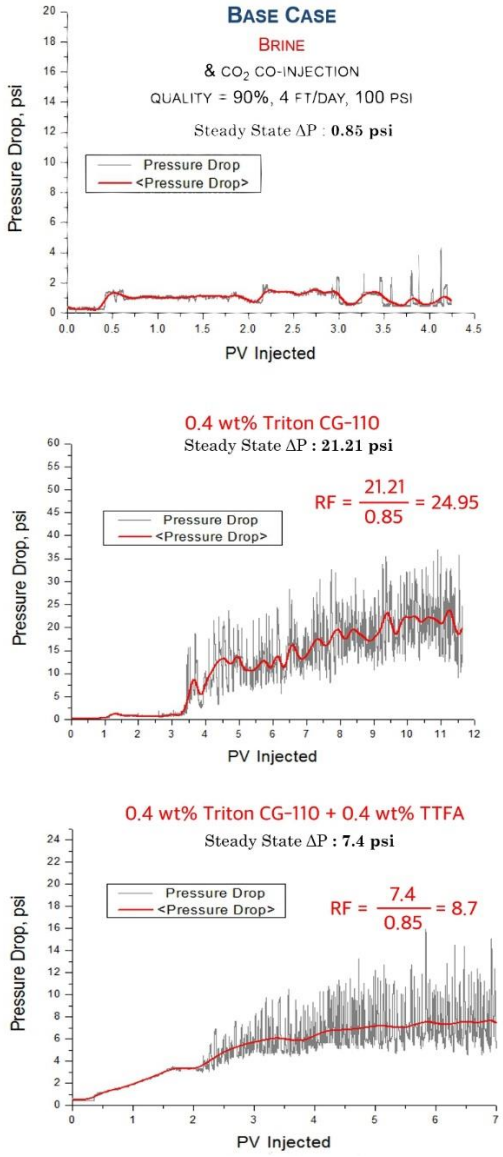

Figure 3.32. Experimental case where nanoparticles have a negative effect on nonionic surfactants. (Modified from the annual research report of UT Austin, Aug 2014; not published)

4 . Utilization of the Carbonaceous Material in Fly Ash

In Chapter 3, fly ash nanoparticles have been studied as substitutes for synthetic silica for EOR applications. Various physical and chemical properties of fly ash particles systematically characterized to achieve the above task. In the course of the research, the possibility of utilizing the different forms of fly ash that have been prepared and characterized, for other potential applications, was discovered.

Among the many applications, including the topics covered in background studies, oil wastewater treatment was the most promising topic. The characteristics of fly ash that are relevant for these applications:

1. Fly ash absorbs various organic matters. (Section 2.4.3)
2. Fly ash contains hydrophobic (lipophilic) components. (Section 3.1.2.2)
3. The nano-milled fly ash has a large surface area, especially when the carbon content is high. (Section 2.4.3.2)
4. The carbonaceous components can be further concentrated. (Section 3.1.2.2)

5. The removal of carbonaceous materials increases the value of fly ash as a construction material. (Section 2.4.2)

6. Nano-milled fly ash particles can be adsorbed at appropriate interfaces. (Sections 2.1.4 and 3.2.1)

In Section 4.1 below, experiments were conducted to better understand the o/w interfacial properties that are particularly important for the targeted application, so that its feasibility can be properly characterized. In section 4.2, the possibility of using HCCFA for oil spill cleanup investigated. In section 4.3, the possibility of using HCCFA for treatment of oilfield produced water is investigated.

4.1. Fly Ash at the O/W Interface

To understand the behavior of fly ash at the O/W interface, the nanoparticle slurries obtained from the second-stage grinding were diluted with D.I. water at various solid concentrations of 1% to 5%. The nanoparticle dispersions were then mixed with equal amounts of different oils (alkanes with 6-10 carbon atoms) in a 20 ㎖ vial and emulsified by using a sonication gun (VC505, Sonics & Materials, USA) for 30 sec at 560 J/min. The stability of the resulting emulsions was examined by observing the extent of phase separation over a period of several days.

As expected, the TTFA sample did not stabilize the o/w emulsion even when the concentration was increased up to 5%, since it does not have any hydrophobic components. However, stable o/w emulsion layers were observed in the tests using the raw fly ash and all the other carbon-concentrated samples. The typical results obtained with decane are shown in Figure 4.1, and the appearance of the emulsion is observed in Figure 4.2.

The +140 mesh fly ash sample with the solid concentration of 0.31 wt% stabilized about half of the total volume as an emulsion. As the concentration of solids increased, larger volumes of the emulsion phase were formed, and it almost reached 100% at 5% solid concentration. The height of the emulsion phase was larger for the +70 mesh and +140 mesh fly ash samples, indicating that the presence of carbonaceous material promoted the formation of the emulsion. However, it does not directly guarantee that higher concentrations of carbon stabilize larger amounts of emulsion, since the +70 mesh samples contain more carbonaceous material (28%) than the +140 mesh samples (18%), even though they stabilized less emulsion. The same experiment was even carried out by using activated carbon consisting of almost pure carbon, but it did not yield better results than the +140 mesh sample. It seems that the carbon content has little effect on the volume of the stabilized emulsion at about 20% or more. However, the higher the carbon content, the lower is the amount of sediment that sinks to the bottom. In

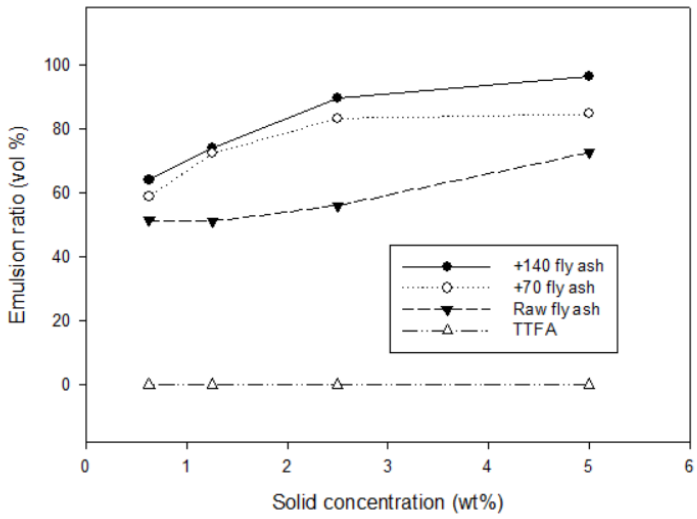

Figure 4.1. Relative volume of the o/w emulsion phase formed when decane was mixed with the dispersion of fly ash nanoparticles of various solid concentrations after the lapse of 5000 min.

Figure 4.2. Visual demonstration of the o/w emulsion phase formed for solid concentrations of (a) 0.31 wt%, (b) 0.62 wt%, and (c) 1.25 wt% in +140 fly ash samples.

Figure 4.2, the black particles in the emulsion phase are the carbonaceous material, and the light gray matter that sinks to the bottom is the mineral component. More research is needed to understand why the concentration of the solids present in the emulsion phase increases as the type of fly ash changes, even though the volume of the emulsion does not increase.

There are several characteristics of the stabilized emulsions obtained by using fly ash.

First, the volume of a stabilized emulsion is hardly affected by the oil type used (C_6 to C_{10} alkane). Figure 4.3 shows that the emulsion stabilized by raw fly ash was not affected by the type of alkane in both the stabilized volume and the change over time. This offers a practical advantage in using fly ash particles for the formation of a crude o/w emulsion, considering the heterogeneous nature of crude oil and the possibility of using raw fly ash particles directly without pretreatment. For comparison, additional tests were conducted by using Bioterge AS-40, which is one of the most commonly used anionic surfactants in the petroleum industry. The results are shown in Figure 4.4. When using the surfactant as a stabilizer, the volume fraction of the emulsion was heavily influenced by the oil type and decreased gradually over time.

Second, the emulsions formed with fly ash nanoparticles are stable for an extremely long time compared to that formed with

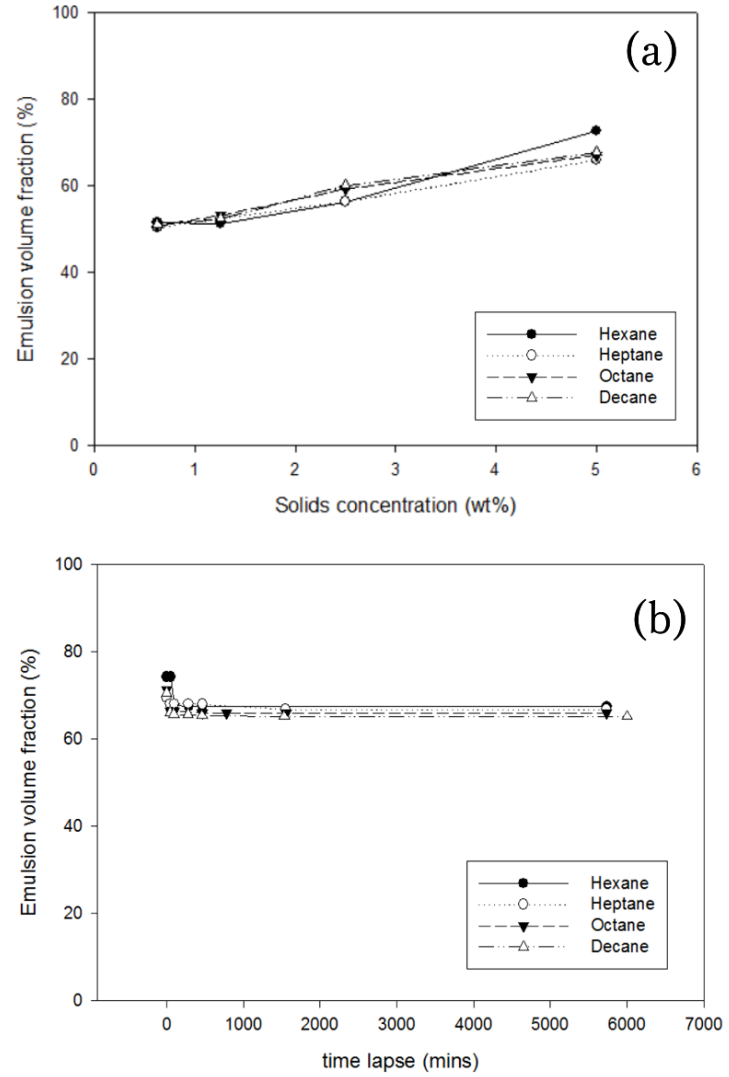

Figure 4.3. (a) Relative volume of the o/w emulsion phase formed when different types of alkanes were mixed with the dispersion of fly ash nanoparticles at various solid concentrations after the lapse of 2000 min. (b) Plots as functions of time for the different alkanes.

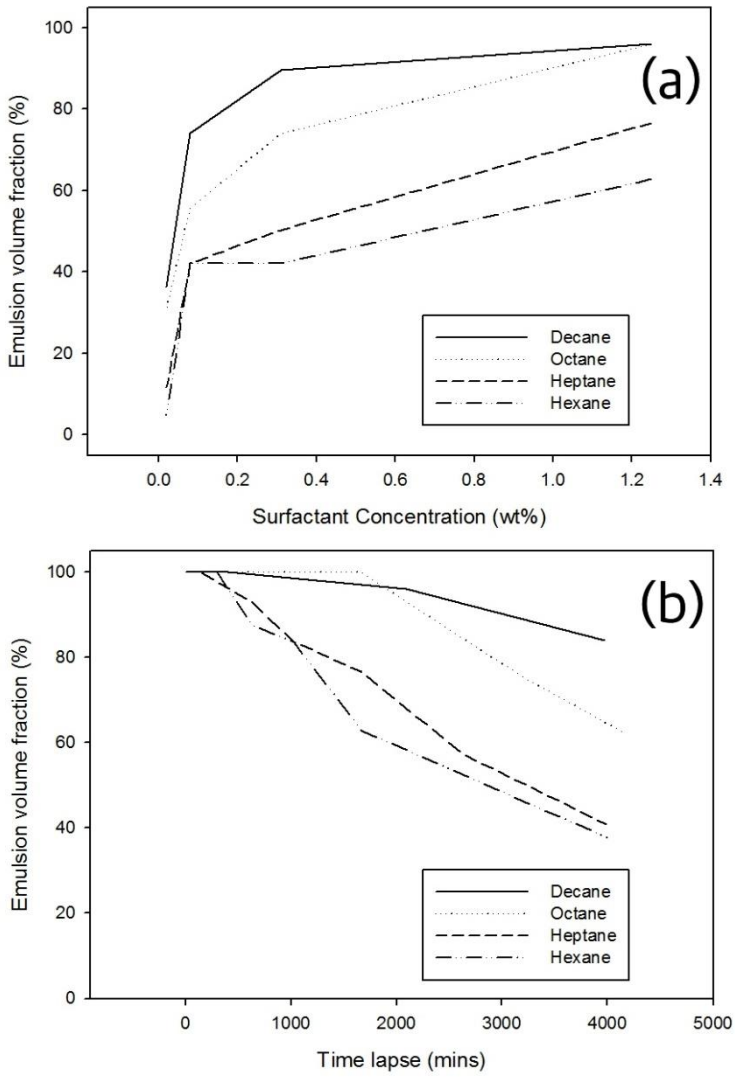

Figure 4.4. (a) Relative volume of the o/w emulsion phase formed when different types of alkanes were mixed with an anionic surfactant (Bioterge AS-40) at various concentrations after the lapse of 1600 min. (b) Plots as functions of time for the different alkanes.

surfactant (For example, Bioterge AS-40). After 5000 min of analysis, the samples were left on one side of the laboratory, and no changes were observed after more than a few months. Although the initial volume of the emulsion phase was low when compared to that with the surfactant, much more emulsion remained after a few months. It is generally known that particles are difficult to remove when they are adsorbed at the interface. These particles form a physical barrier that prevents the coalescence of droplets over time.

4.2. Oil Spill Cleanup by Using HCCFA

4.2.1. Experimental method

In this experiment, the HCCFA reported in Section 3.1.2.2 was used after grinding (d_{50} = 500 ㎚) to reduce the amount of sediment deposits at the bottom. Three crude oils of different origins were used to identify the differences in the interaction based on oil type, and the oil characteristics are summarized in Table 8. Brine (3.0% NaCl), crude oil, and HCCFA were placed in 20 ㎖ vials in the weight ratio of 100: 10: 1 and shaken strongly by hand for 30 sec to form an o/w emulsion. After a few minutes, the emulsion floated to the surface, and was then injected into the tidal flushing and the surface scraping test equipment.

4.2.1.1. Tidal flushing experiment

Tidal flushing experiments were conducted to examine whether oil-HCCFA aggregates (OHA) could escape from sand through a low-energy water stream. Figure 4.5 shows the experimental scheme.

First, standard sand (The grain size is distributed between 80 ㎛ and 2 ㎜ and the SiO_2 content should be more than 98%) of volume 40 cc was prepared in a cylinder.

Second, pour a mixture (brine: crude oil = 10: 1 mixture or brine: crude oil: HCCFA = 100: 10: 1 mixture) of 0.8 pore volume (PV) onto the sand pack.

Third, wait 24 hours for oil to penetrate into the sand.

Forth, 4 PV of brine was injected from the bottom of the cylinder at the rate of 2 ㎖/min to simulate the sandy beach's water level change due to tide. Since the inner diameter of the cylinder is 28 ㎜, the rising speed of the water level was 3.2 ㎜/min in this experiment.

Fifth, after the injection, the liquid above the sand surface was removed by suction. Any oil or OHA floating in the water is removed during this process.

Finally, the remaining sand was subjected to total petroleum hydrocarbon analysis (TPH analysis) to determine the concentration of the remaining oil.

4.2.1.2. Surface-scraping experiment

Surface-scraping experiments were carried out to confirm the effect of OHA on the decrease in oil penetration. The experimental procedure is presented in Figure 4.6. Same as in the tidal flushing experiment, a 0.8 PV brine-crude oil or brine-OHA sample was added to the sand pack. After 24 h, the upper part of the sand was removed by scraping by a depth of 5 ㎜ from the initial dry sand height. The actual scraped height was thicker than 5 ㎜ when the OHA was piled on the sand surface. The sand was pushed up to a specified height by using a piston, and the protruding part was removed with a sharp knife. The remaining samples were subjected to TPH analysis and compared to those that were not scraped.

4.2.2. Experimental results

4.2.2.1. Tidal flushing

The experimental results show that the rate of penetration of the sand is much lower when crude oil is present in the form of OHA as a result of agitation with HCCFA. The OHA remaining on

Table 8. Origin and properties of the crude oil used in the experiment

Name	Origin	API	Sulfur (%)	Viscosity (㎟/s at 37.8 ℃)
AEL	Saudi Arabia	38.9	1.2	36.3
SOK	Russia	38.3	0.2	2.7
KWT	Kuwait	30.6	2.67	7.74

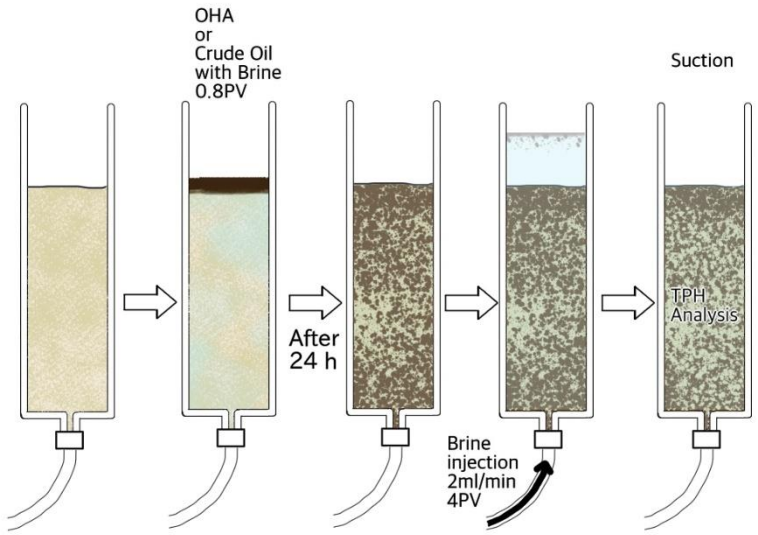

Figure 4.5. Schematic of tidal flushing experiment.

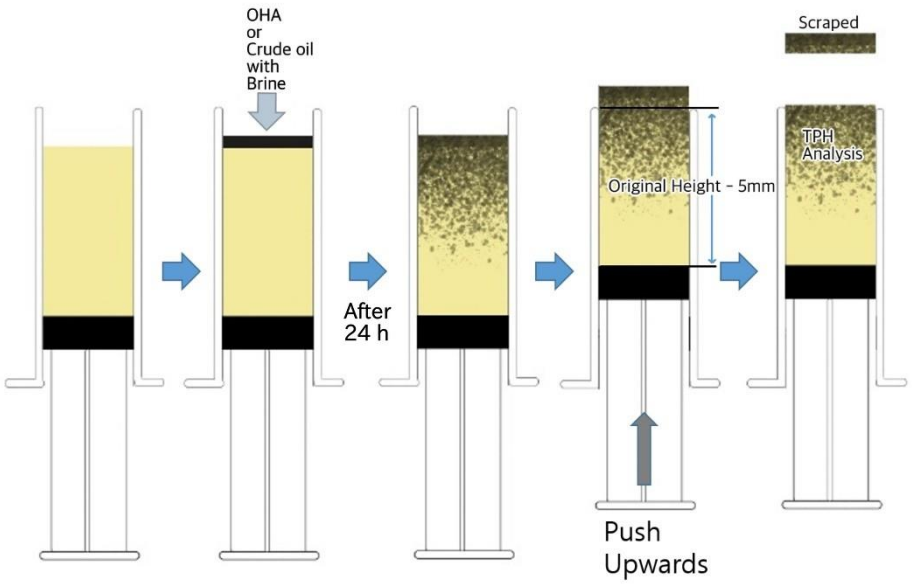

Figure 4.6. Schematic of surface-scraping experiment.

the sand surface were also easily removed by the slow injection of brine even when the thickness of the OHA was as low as 2 ㎜. In Figure 4.7, there is a clear effect of increasing the removal efficiency by forming OHA, but the efficiency varied depending on the oil type. The relative removal efficiency increased in the order of SOK (151%) > AEL (137%) > KWT (112%), but no clear correlation was found between the relative removal efficiency and the oil properties such as specific gravity or viscosity.

These effects were more prominent as the amount of OHA increased. In an experiment using 5 ㎖ of oil, HCCFA formed a 1.6 ㎝-thick OHA, which was about twice the original oil thickness. After 24-hour penetration, the sand below the OHA was also contaminated with crude oil, but a significant amount of OHA remained on the surface. When the water level increased by 3.2 ㎜/min upon injecting 2 ㎖ of water per minute, most of the OHA on the surface were separated from the sand (Figure 4.8).

4.2.2.2. Surface-scraping

The oil removal efficiency of surface scraping showed a great difference between when the oil was incorporated in the liquid state and when it existed in the OHA state. Twenty-four hours after the addition of crude oil and brine to the sand, oil penetrated

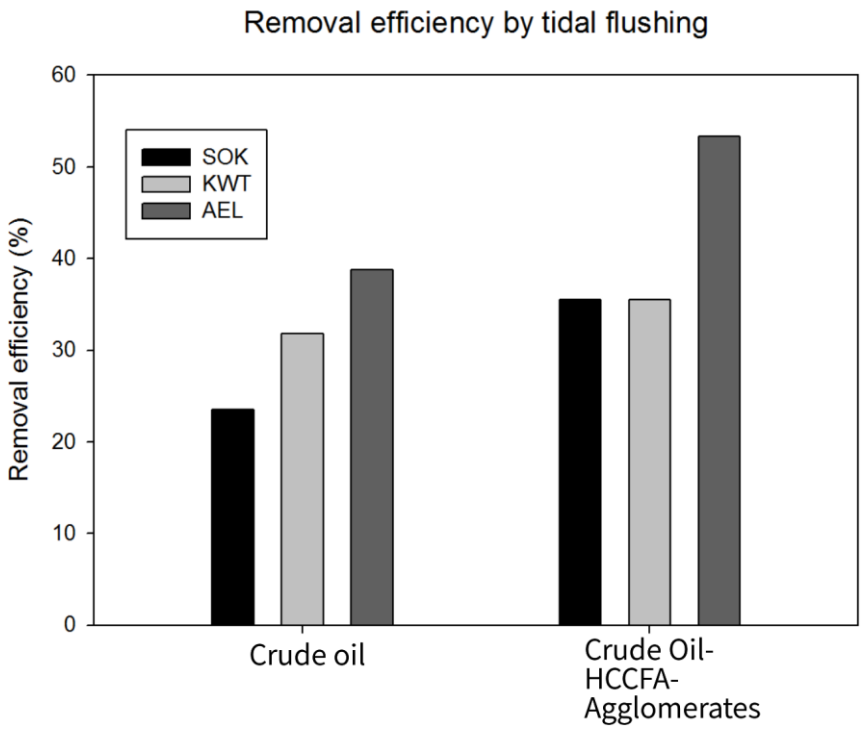

Figure 4.7. Percentage of oil removed by tidal flushing.

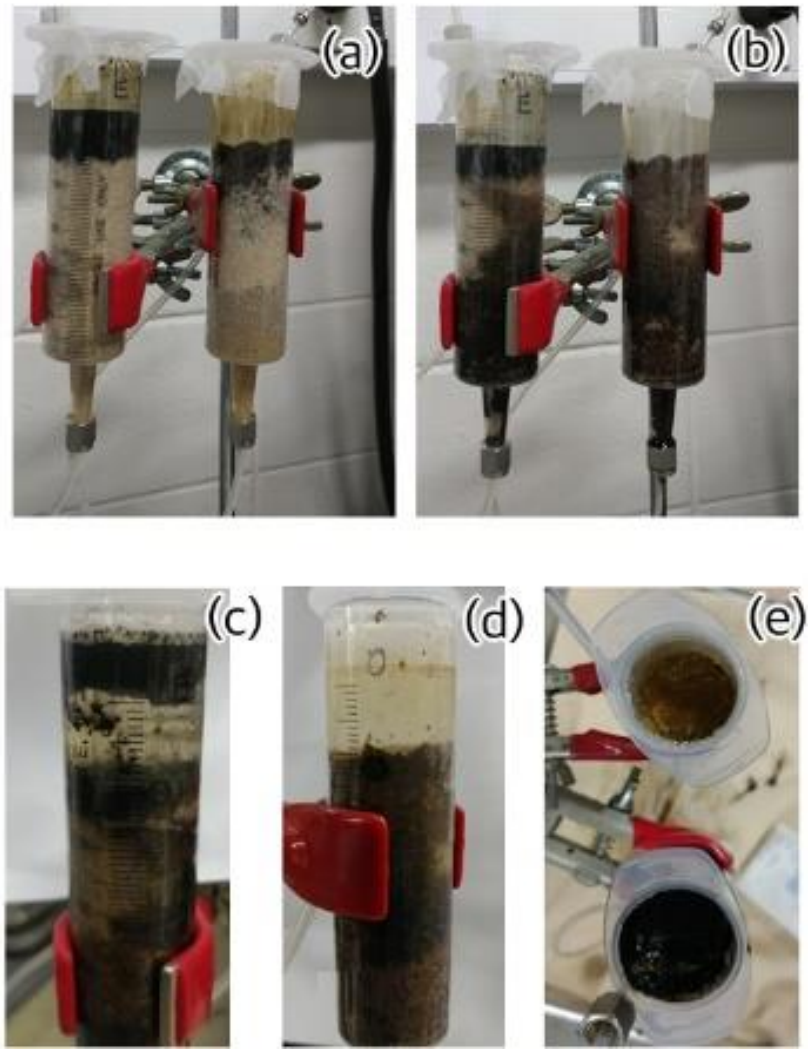

Figure 4.8. (a) The left side shows a sand pack with OHA and brine, and the right side is a sand pack with crude oil and brine; (b) After 24 h, the oil settled at the bottom; (c) The OHA remaining on the surface floated, due to water injection; (d) In the sand pack with crude oil, contaminated brine is elevated, but no oil layer is observed; (e) Top view.

the sand almost evenly, and scraping the surface did not help in reducing the concentration. TPH analysis showed an average 2-5% concentration decrease, though it increased sometimes; which is thought to be comparable to an analysis error.

When oil was added in the OHA state, a significant amount of the OHA remained near the surface, as noted in Section 4.2.2.1. Since the scraping height was set at 5 ㎜ from the initial height of the sand pack, the actual amount removed from the OHA input sample was about 1 ㎝; the corresponding image is shown in Figure 4.9. TPH analysis of the scraped samples showed that at least 78% and up to 92% of the oil was removed. SOK crude oil showed the lowest removal efficiency of 78%, whereas the highest 92% was measured with the KWT sample; the AEL oil had a moderate removal efficiency of 88.7%.

This suggests that the OHA facilitate the natural self-purifying process involving low-energy sources such as tides and waves, but more effective removal is by aggressive cleanup work, such as surface scraping.

4.3. Treatment of Produced Water by Using HCCFA

4.3.1. Experimental method

Four different types of artificial produced water (APW) samples were prepared for the experiment: AEL, SOK, KWT, and BTEX. AEL, SOK, and KWT are the dispersions of the three crude oils

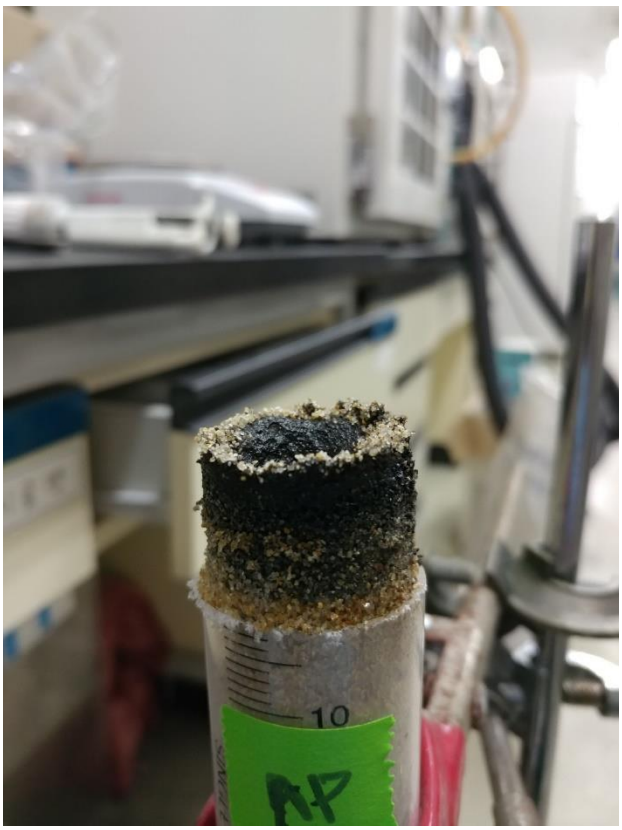

Figure 4.9. Appearance of the sample pushed up for surface-scraping (for the case of AEL OHA).

introduced in Section 4.2.1, whereas BTEX is a mixture of benzene, toluene, ethylbenzene, and xylene in 1: 1: 1: 1 ratio.

There are some differences between an actual produced water and the APW. First, the APW has a higher organic concentration than the typical produced water. Although the organic content of the actual produced water is of the order of hundreds ppm, that of the APW is mostly maintained at 2000 ppm in order to reduce the measurement errors such as due to evaporation. Secondly, well-characterized surfactants were added to the APW, while actual produced water contains various natural surfactants that disperse the droplets. Since the surfactant components in the crude oil samples have already been neutralized during the demulsification process, 200 ppm of a non-ionic surfactant (IGEPAL CA-630, Fluka, US) was added to APW samples.

Oil or BTEX components are dispersed in 50 ㎖ of 3.0% NaCl brine by using ultrasonicator (VC505, Sonics & Materials, USA) for 30 sec at 560 J/min. The dispersed state of the droplets of size less than 10 ㎛ diameter was confirmed by optical microscopy, and it was also observed that the dispersion was stable for several days. The sample showed a light brown to dark brown color depending on the type of crude oil, and the BTEX sample turned turbid white immediately after the ultrasonic treatment and subsequently became transparent.

Equal amounts of HCCFA particles were added to adsorb the oil and BTEX components. Since the specific gravity of HCCFA is about 2 g/㎤, the HCCFA-attached emulsion sinks when the proportion of HCCFA increases above 20%. In a basic dosage test, when HCCFA was added in the same amount of oil, the entire emulsion precipitated without leaving any oil rims or clusters on the water surface. The sample loaded with HCCFA was again sonicated for 30 sec at 560 J/min and left standing for 24 h. After the precipitation was completed, 40 ㎖ of the sample was recovered from the top and TPH or BTEX analysis was performed.

Additional experiments were conducted on 1 to 5 wt% of cationic surfactant (DTAB) added HCCFA when the adsorption rate was not sufficiently high. Since BTEX droplets has a weak negative charge of about from −3 to −11 mV under the experimental conditions, it is expected that the cationic surfactant will increase the adsorption rate by reducing the electrostatic repulsion between HCCFA and BTEX droplets.

4.3.2. Experimental results

4.3.2.1. Crude oil APW treatment

Figure 4.10 summarizes the crude oil APW treatment process and the results obtained. In the supernatant portion of the samples, almost all the oily components visually disappeared, and

3-5 ㎖ of sediment accumulated at the bottom. Considering that the amount of injected oil and HCCFA solids is about 0.2 g, the sediment seems to have quite a flimsy structure.

Figure 4.11 shows the microscope image of each sample. In the supernatant recovered after the HCCFA precipitation reaction, only a small amount of oil droplets was observed around 1 ㎛, and most of the droplets were removed. HCCFA combined with the oil component to form aggregates in the form of branches that displayed sizes of several hundred micrometers.

As a result of TPH analysis, 93-97% of the oil components were removed: 93.4% for SOK, 96.4% for KWT, and 97.3% for AEL. Considering the difference in the physical properties of the three oils, the effect of oil type on the adsorption and precipitation induced by HCCFA appears to be insignificant.

4.3.2.2. BTEX APW treatment

The adsorption efficiency of HCCFA towards BTEX was lower than that of crude oil. On average, 52% of BTEX was adsorbed, and the adsorption efficiency of each component was significantly different. Benzene, the least adsorbed, was removed about 23%, whereas the most adsorbed was xylene at 71%.

The same experiment was carried out on samples with median sizes of 1 ㎛ and 2 ㎛ in order to examine the effect of fly ash

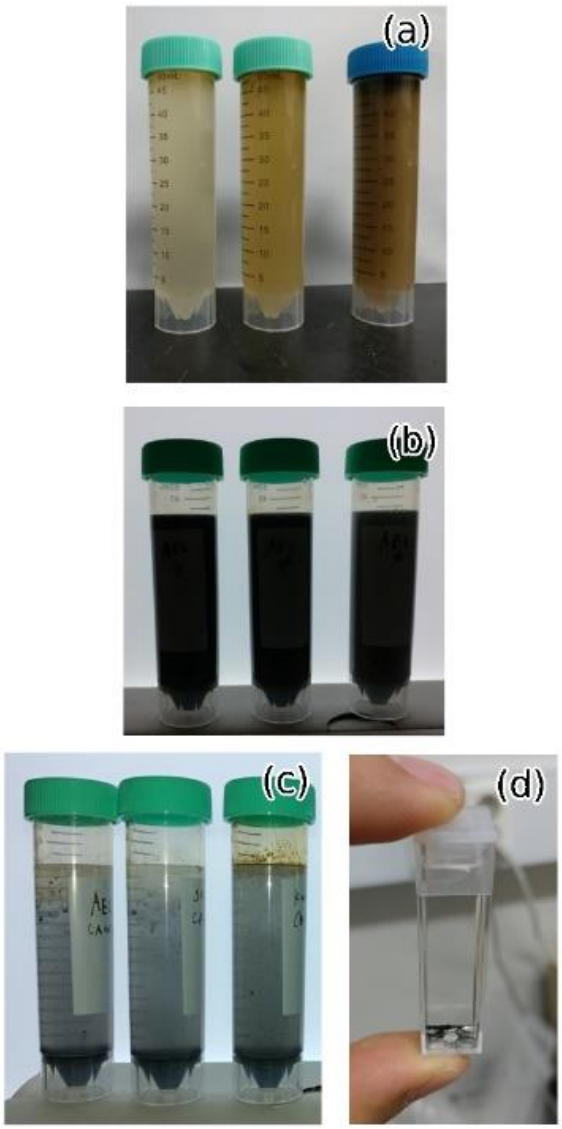

Figure 4.10. (a) APW samples with 2000 ppm of crude oil dispersed. AEL is on the left, SOK in the middle, and KWT on the right. (b) After HCCFA was added in 1:1 ratio with oil. (c) After 24 h; and (d) Appearance of the separated supernatant, which is almost transparent.

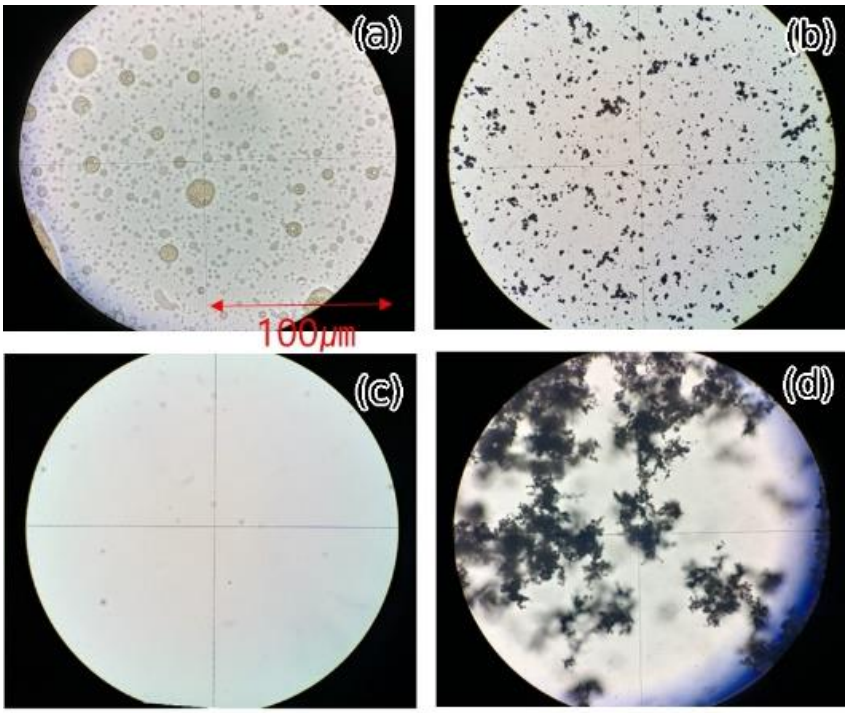

Figure 4.11. (a) Optical microscopy image of APW with dispersed crude oil at 1000 magnification; (b) HCCFA particles with $\mathbf{d_{50}}$ = 500 ㎜; (c) An image (at 1000 magnification) of the supernatant recovered after HCCFA precipitation reaction; (d) Appearance of the precipitated HCCFA particles.

particle size. Smaller grain sizes tend to increase the adsorption rate, but do not offset the energy cost associated with the size reduction or the longer settling time.

There are many reasons why HCCFA cannot effectively absorb BTEX compared to crude oil, but the biggest difference that was visually confirmed is that the coagulation that occurred in the crude oil APW did not occur in the BTEX APW (Figure 4.13). If aggregation does not occur, it will be very difficult to separate the HCCFA particles from the solution in a continuous process, which renders HCCFA difficult to use as an adsorbent.

DTAB treated HCCFA showed higher adsorption rate for BTEX (Figure 4.14). The average adsorption rate was about 75% when DTAB was added at 1% and 5% relative to HCCFA solids. The increase in DTAB input showed a positive effect on benzene adsorption and a slightly negative effect on adsorption for the remaining components. No branch-like aggregation phenomenon was observed under DTAB addition conditions. These results show that the adsorption rate of HCCFA can be changed depending on the type and concentration of the natural surfactant present in the produced water, and the it suggests that branch-like agglomeration has a low correlation with the adsorption rate itself.

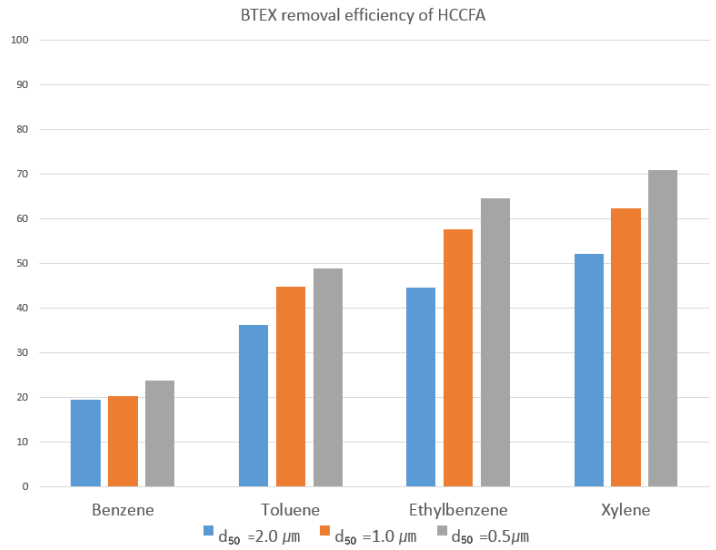

Figure 4.12. Removal efficiency of HCCFA particles corresponding to each BTEX component with different average particle sizes.

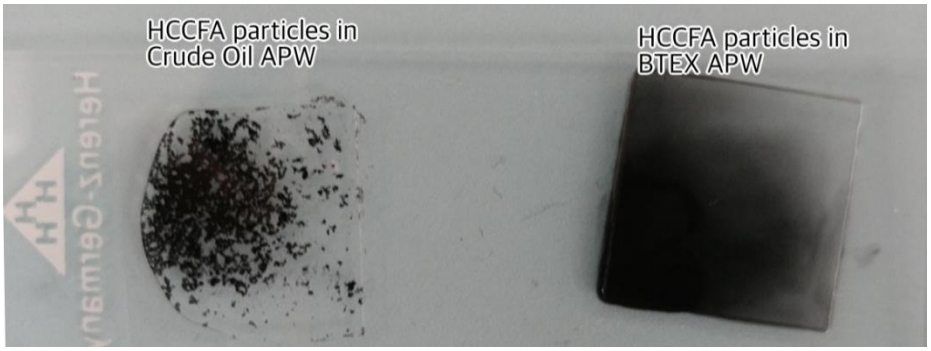

Figure 4.13. Appearance of the HCCFA particles recovered from the bottom.

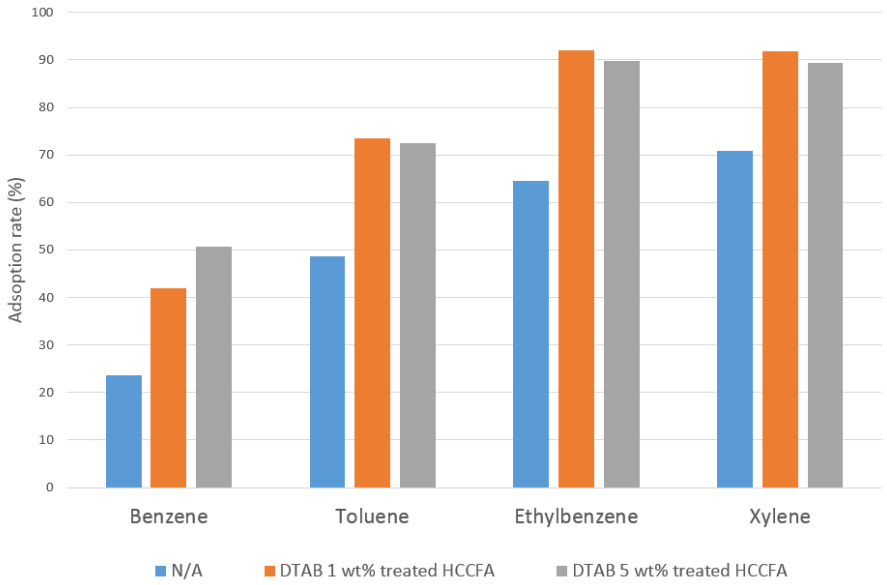

Figure 4.14. Change of adsorption rate on BTEX by addition of DTAB. In both cases, the average adsorption rate increased from 52% to 75%.

5. Conclusions and Recommendations

5.1. Conclusions

In this research, two main themes were discussed. The first is the replacement of synthetic silica nanoparticles used for EOR with nanoparticles obtained from fly ash; the second is finding new methods to utilize the components of fly ash that are typically difficult to recycle by conventional method. To achieve these goals, the separation, grinding characteristics, adsorption characteristics, and interfacial behavior of fly ash were systematically studied.

Fly ash is a heterogeneous material that exhibits various compositions, depending on the raw coal composition and combustion condition. The components of fly ash can largely be divided into mineral components and unburned carbon components. The mineral components are mostly hydrophilic, whereas the unburned carbon components are mostly hydrophobic. Thermal treatment of fly ash under oxygen conditions removes the unburned carbon and leaves behind the mineral components. The concentration of unburned carbon can be achieved by a combination of methods such as sieving, hindered settling, and float flotation.

After controlling the chemical composition, fly ash can be ground to an average particle size of 200 ㎚ using the two-stage

grinding method that employs an attrition mill and a bead mill. Two-stage grinding drastically reduced the energy consumption and time required to obtain nanoparticles from fly ash. Higher efficiencies were achieved with large-scale laboratory equipment; the addition of milling aids also helped improve efficiency. The energy cost of producing fly ash nanoparticles with a median size of 200 ㎚ was approximately one-tenth the price of synthetic silica.

The fly ash nanoparticle dispersion containing a large amount of hydrophobic components successfully formed an emulsion with liquid phase CO_2 . However, none of the fly ash nanoparticles produced in this experiment could stabilize the gas or supercritical CO_2 without an additive.

Several synergies were observed depending on the combination of additives and the chemical composition of fly ash nanoparticles. The TTFA dispersion injected together with a cationic surfactant (DTAB) generated stable supercritical CO_2 foam at a very low concentration; stable bubbles were not observed when DTAB was injected alone. This synergistic effect was also observed in experiments using continuous injection equipment. The addition of 1.0 wt% TTFA nanoparticles and 0.01 wt% DTAB solution produced a stable supercritical CO_2 foam through the shear stress generated upon the passage of CO_2 through porous media.

The foam had a resistance factor (RF) value that was twice as high as that of the 0.01 wt% DTAB solution.

The fly ash containing a large amount of hydrophobic components produced gaseous CO_2 foams when turpentine oil was added, but it could not stabilize the supercritical CO_2 foam.

In the sandstone core injection experiment, the TTFA nanoparticles (d_{50}=180 ㎚) showed the synergistic effect of increasing the RF of the anionic surfactant (Bioterge AS-40), which did not cause any injection problems such as face plugging and clogging. These results show that the synergistic effects observed in previous studies between synthetic silica and surfactants can also be found in fly ash nanoparticles.

Fly ash nanoparticles, including the hydrophobic components, were well adsorbed on the oil surface by short mixing, producing a very stable o/w emulsion. This emulsion was less affected by the oil type than the surfactant, and reached a steady state within a relatively short time that persisted for several months. Since the interfacial adsorption of nanoparticles is determined by the surface tension and contact angle, it is not significantly influenced by ordinary seawater temperature (6-30 ℃). This property is particularly useful when strong waves and low temperatures render conventional solidifiers useless. The emulsion holds the oil strongly and facilitates the cleanup of an oil spill by delaying the penetration of oil into the sand, which is

then separated from the sand by tidal flushing. The oil penetration delay effect was confirmed by surface scraping, and the removal of 5 ㎜ of the surface resulted in oil removal rates of 78% to 92%.

Increasing the amount of fly ash added to the oil increased the bulk density of the emulsion, causing it to sink into the water. This phenomenon can be used to remove oil droplets or BTEX components in produced water. HCCFA (d_{50} = 500 ㎚, 1:1 ratio to oil) adsorbed 93–97% of crude oil droplets (d < 10 ㎛) and produced aggregates in the form of branches that were several hundred micrometers in size. These results show that the carbonaceous compounds of fly ash can be used for the purification of water contaminated by oil waste.

However, the adsorption rate of HCCFA to BTEX, which is one of the major pollutants in produced water, was lower than the adsorption rate to crude oil, and no branch-like coagulation occurred. The coagulation does not seem to occur well for organic materials including aromatic rings. Addition of a small amount of cationic surfactant (DTAB) was effective to increase the adsorption rate of HCCFA to BTEX (from 52% to 75%).

5.2. Recommandations

In the course of the research, surfactants such as SDS, which had been used in conventional synthetic silica nanoparticle

research, were applied to fly ash, but no synergistic effect was observed. At this point, fly ash nanoparticles and synthetic silica are not identical; they cannot be simply replaced at a ratio of 1:1. Further surface modification of fly ash and research on synergetic surfactants combination should be conducted to enable fly ash nanoparticles to compete against synthetic silica as nanoparticles that can be produced inexpensively. Although DTAB showed synergistic effect with TTFA, problems such as salinity resistance and colloidal stability still remain. On the assumption that these problems are solved, fly ash nanoparticle will be an attractive option, especially when the particle size required for injection is not too small. Since the energy cost in top-down method increases exponentially as the target particle size is reduced, fly ash nanoparticles may not be an economical choice if an average particle size of less than 150 nanometers is required.

In an application for oil spill cleanup, the vials were shaken by hand to make an o/w emulsion. However, the actual movements of the sea are very complex and the types of waves vary. Even if the height of the wave is high, it is difficult to expect the formation of the o/w emulsion in the case of waves without agitation of the surface like seiche waves or spilling waves. If HCCFA particles failed to produce o/w emulsion within a short time, they will sink and be lost. Depending on the application conditions, additional artificial agitation process and

pretreatment could be required to improve the adsorption rate and to prevent the loss of the particles due to sedimentation. On the other hand, in the shallow coast, steady agitation occurs due to collapsing waves, and the HCCFA particles will not easily be lost since it is likely to be on the sand after sink and float again by wave. For this reason, HCCFA particles should be studied specifically to prevent beach contamination rather than marine pollution.

The most deficient part of the research on produced water treatment was the absence of demonstration on the real samples. The experiment showed that the adsorption rate of the BTEX components can vary depending on the type and concentration of surfactants in the solution. Actual produced water contains much more complex surfactant components than artificial samples, and the compositions vary from site to site, so experiments on actual samples are essential to assess applicability.

References

2017a. ASTM C618-17a Standard Specification for Coal Fly Ash and Raw or Calcined Natural Pozzolan for Use in Concrete, in: A. International (Ed.), West Conshohocken, PA.

2017b. Typical Bills and average rates report-summer 2017. Edison Electric institute, Washington, D.C. .

2018a. Annual energy outlook 2018. US Energy Information Administration.

2018b, "Electricity prices for households in Germany from 2010 to 2018, semi-annually (in euro cents per kilowatt-hour)", statista, Jan 08, 2019, https://www.statista.com/statistics/418078/electricity-prices-for-households-in-germany/

2018c, 2016.12.01, "한글 전기요금표(산업용-갑/을)", Korean-Electric-Power-Coporation, accessed Dec 11, 2018, http://cyber.kepco.co.kr/ckepco/front/jsp/CY/E/E/CYEEHP00101.jsp

Aguado, S., Polo, A.C., Bernal, M.a.P., Coronas, J.n., Santamarı□a, J.J.J.o.M.S., 2004. Removal of pollutants from indoor air using zeolite membranes. 240, 159-166.

Ahmaruzzaman, M., 2010. A review on the utilization of fly ash. Progress in energy combustion science 36, 327–363.

Akgerman, A., Zardkoohi, M., 1996. Adsorption of phenolic compounds on fly ash. Journal of Chemical & Engineering Data 41, 185–187.

Al–Shawabkeh, A., Maisuda, H., Hasatani, M., 1995. Comparative reactivity of treated FBC– and PCC–Fly ash for SO2 removal. The Canadian Journal of Chemical Engineering 73, 678–685.

Alemany, L., Jimenez, M., Larrubia, M., Delgado, F., Blasco, J., 1996. Removal of phenol from aqueous solution by adsorption on to coal fly ash. Adsorption Science & Technology 13, 527–536.

Alvarado, V., Manrique, E., 2010. Enhanced oil recovery: an update review. Energies 3, 1529–1575.

AlYousef, Z., Almobarky, M., Schechter, D., 2017. Enhancing the Stability of Foam by the Use of Nanoparticles. Energy & Fuels 31, 10620–10627.

American–Coal–Ash–Association., 2012. Coal Combustion Product (CCP) production & use survey report. ACAA: Aurora, CO.

American–Coal–Ash–Association., 2018. Ash at Work. ACAA: Aurora, CO.

Andreani, T., de Souza, A.L.R., Kiill, C.P., Lorenzón, E.N., Fangueiro, J.F., Calpena, A.C., Chaud, M.V., Garcia, M.L., Gremião, M.P.D., Silva, A.M.J.I.j.o.p., 2014. Preparation and characterization of PEG-coated silica nanoparticles for oral insulin delivery. 473, 627-635.

Annut, A., 2018, Dec 20, "International industrial energy prices", GOV.UK, Jan 08, 2019, https://www.gov.uk/government/statistical-data-sets/international-industrial-energy-prices

Antiohos, S., Papageorgiou, A., Papadakis, V., Tsimas, S., 2008. Influence of quicklime addition on the mechanical properties and hydration degree of blended cements containing different fly ashes. Construction Building Materials 22, 1191-1200.

Atiş, C., Sevim, U., Özcan, F., Bilim, C., Karahan, O., Tanrikulu, A., Ekşi, A., 2004. Strength properties of roller compacted concrete containing a non-standard high calcium fly ash. Materials Letters 58, 1446-1450.

Babamahmoudi, S., Riahi, S., 2018. Application of nano particle for enhancement of foam stability in the presence of crude oil: Experimental investigation. Journal of Molecular Liquids.

Baker, A., 2016, Jan 27, "Argentina to raise electricity rates in February amid 'energy emergency'", BNamericas, Jan 1, 2019, https://www.bnamericas.com/en/news/electricpower/argentina

-to-raise-electricity-rates-in-february-amid-energy-emergency

Batabyal, D., Sahu, A., Chaudhuri, S., 1995. Kinetics and mechanism of removal of 2, 4-dimethyl phenol from aqueous solutions with coal fly ash. Separations Technology 5, 179-186.

Binks, B.P., 2002. Particles as surfactants—similarities and differences. Current Opinion in Colloid & Interface Science 7, 21-41.

Binks, B.P., Horozov, T.S., 2005. Aqueous Foams Stabilized Solely by Silica Nanoparticles. Angewandte Chemie International Edition 44, 3722-3725.

Binks, B.P., Lumsdon, S.O., 2000. Influence of Particle Wettability on the Type and Stability of Surfactant-Free Emulsions. Langmuir 16, 8622-8631.

Boud, D.C., Holbrook, O.C., 1958. Gas drive oil recovery process. Google Patents.

Bravi, M., Bubbico, R., Manna, F., Verdone, N., 2002. Process optimisation in sunflower oil extraction by supercritical CO_2 . Chemical Engineering Science 57, 2753-2764.

Britt, D.W., Hlady, V., 1996. An AFM study of the effects of silanization temperature, hydration, and annealing on the

nucleation and aggregation of condensed OTS domains on mica. Journal of colloid interface science 178, 775-784.

Bryk, M.T., Yakovenko, N.M., 1987. Magnetic Adsobent Based on Iron-containing Clay for Removal of Petroleum from Water. Soviet journal of water chemistry and technology 9, 126-128.

Buecker, B., 2011. Qualities of Limestone That Influence Wet FGD Performance. Power Engineering 115, 34-37.

Cai, J., Chenevert, M.E., Sharma, M.M., Friedheim, J.E., 2012. Decreasing water invasion into Atoka shale using nonmodified silica nanoparticles. SPE Drilling Completion 27, 103-112.

Cheung, K., Venkitachalam, T., 2000. Improving phosphate removal of sand infiltration system using alkaline fly ash. Chemosphere 41, 243-249.

Choi, H.-M., Kwon, H.-J., Moreau, J.P., 1993. Cotton Nonwovens as Oil Spill Cleanup Sorbents. Textile Research Journal 63, 211-218.

Choolaei, M., Rashidi, A.M., Ardjmand, M., Yadegari, A., Soltanian, H., 2012. The effect of nanosilica on the physical properties of oil well cement. Materials Science Engineering: A 538, 288-294.

Chovelon, J., Aarch, L.E., Charbonnier, M., Romand, M., 1995. Silanization of stainless steel surfaces: influence of application parameters. The Journal of Adhesion 50, 43-58.

Cicek, T., Tanrıverdi, M., 2007. Lime based steam autoclaved fly ash bricks. Construction and Building Materials 21, 1295–1300.

Clogston, J.D., Patri, A.K., 2011. Zeta potential measurement, Characterization of nanoparticles intended for drug delivery. Springer, 63–70.

Cultrone, G., Sebastián, E., 2009. Fly ash addition in clayey materials to improve the quality of solid bricks. Construction and Building Materials 23, 1178–1184.

Dahl, W.A., Lessard, R.R., Cardello, E.A., Fritz, D.E., Norman, F.S., Twyman, J.D., Clayton, E.W., Knight, B.L., Crane, R.D., Johnson, S.J., Martin, B.R., 1996. Solidifiers for Oil Spill Response, SPE Health, Safety and Environment in Oil and Gas Exploration and Production Conference. Society of Petroleum Engineers, New Orleans, Louisiana.

Davidovits, J., 1994. Global warming impact on the cement and aggregates industries. World Resource Review 6, 263–278.

Davini, P., 2002. Flue gas treatment by activated carbon obtained from oil–fired fly ash. Carbon 40, 1973–1979.

de Vries, A.S., Wit, K., 1990. Rheology of gas/water foam in the quality range relevant to steam foam. SPE–28733–PA 5, 185–192.

Denkov, N.D., 2004. Mechanisms of Foam Destruction by Oil-Based Antifoams. Langmuir 20, 9463-9505.

Derosa, R., Trapasso, J., 2002. Poly (ethylene glycol) interactions with alumina and silica powders determined via DRIFT. Journal of materials science 37, 1079-1082.

Diamadopoulos, E., Ioannidis, S., Sakellaropoulos, G.P., 1993. As (V) removal from aqueous solutions by fly ash. Water Research 27, 1773-1777.

Dickson, J.L., Binks, B.P., Johnston, K.P., 2004. Stabilization of Carbon Dioxide-in-Water Emulsions with Silica Nanoparticles. Langmuir 20, 7976-7983.

Donaldson, E.C., Chilingarian, G.V., Yen, T.F., 1989. Enhanced oil recovery, II: Processes and operations. Elsevier.

Dooley, J.J., Dahowski, R.T., Davidson, C.L., 2010. CO_2 -driven Enhanced Oil Recovery as a Stepping Stone to What?, in: U.d.o. energy (Ed.).

EIA, 2012. Annual energy review 2011. Government Printing Office.

EIA, 2018. Annual Coal Report 2017 (November 2, 2018). 1, 17-18.

Emrani, A.S., Nasr-El-Din, H.A., 2017. Stabilizing CO_2 foam by Use of nanoparticles. SPE Journal 22, 494-504.

Erdem, E., Karapinar, N., Donat, R., 2004. The removal of heavy metal cations by natural zeolites. Journal of Colloid and Interface Science 280, 309−314.

Ershadi, V., Ebadi, T., Rabani, A., Ershadi, L., Soltanian, H., 2011. The effect of nanosilica on cement matrix permeability in oil well to decrease the pollution of receptive environment. International Journal of Environmental Science Development 2, 128.

Espinoza, D.N., Santamarina, J.C., 2010. Water-CO_2 -mineral systems: Interfacial tension, contact angle, and diffusion—Implications to CO_2 geological storage. Water resources research 46.

Ewers, W., Sutherland, K., 1952. The role of surface transport in the stability and breakdown of foams. Australian Journal of Chemistry 5, 697−710.

Fassihi, M.R., Yannimaras, D.V., Kumar, V.K., 1997. Estimation of Recovery Factor in Light−Oil Air−Injection Projects. SPE−28733−PA 12, 173−178.

Ferro, B.D., Smith, M., 2007. Global onshore and offshore water production. Oil and Gas Review, OTC edition.

Flood, C., Cosgrove, T., Espidel, Y., Howell, I., Revell, P., 2007. Sodium Polyacrylate Adsorption onto Anionic and Cationic Silica in the Presence of Salts. Langmuir 23, 6191−6197.

Friedmann, F., Chen, W., Gauglitz, P., 1991. Experimental and simulation study of high-temperature foam displacement in porous media. SPE-28733-PA 6, 37-45.

Friedrich, J., List, G., Heakin, A., 1982. Petroleum-free extraction of oil from soybeans with supercritical CO_2 . Journal of the American Oil Chemists' Society 59, 288-292.

Galbreath, K.C., Zygarlicke, C.J., 2000. Mercury transformations in coal combustion flue gas. Fuel Processing Technology 65-66, 289-310.

Gao, M.-W., Forssberg, E., 1993. A study on the effect of parameters in stirred ball milling. International journal of mineral processing 37, 45-59.

Gashi, S., Daci, N., Ahmeti, X.M., Selimi, T., Hoxha, E., 1988. Removal of heavy metals from industrial wastewaters. Elsevier Publishers Amsterdam.

Giaccio, G.M., Malhotra, V., 1988. Concrete incorporating high volumes of ASTM Class F fly ash. Cement, concrete aggregates 10, 88-95.

Graham, D., 1988. Crude oil emulsions: their stability and resolution. Spec. Publ. R. Soc. Chem 67, 155.

Grice, T.J.P.o.t.n.A.S.-M.T.D.S., 1998. Underground mining with backfill. 216, 234-239.

Griffith, C., Daigle, H., 2017. Stability of polyvinyl alcohol–coated biochar nanoparticles in brine. Journal of Nanoparticle Research 19, 23.

Grutters, M., van Dijk, M., Dubey, S., Adamski, R., Gelin, F., Cornelisse, P., 2007. Asphaltene induced W/O emusilon: False or true? Journal of dispersion science and technology 28, 357–360.

Handy, L.L., Amaefule, J.O., Ziegler, V.M., Ershaghi, I., 1982. Thermal Stability of Surfactants for Reservoir Application (includes associated papers 11323 and 11597). SPE–7867–PA 22, 722–730.

Heidrich, C., Feuerborn, H.–J., Weir, A., 2013. Coal combustion products: a global perspective, World of Coal Ash Conference, 22–25.

Heller, J.P., 1994. CO_2 Foams in Enhanced Oil Recovery, Foams: Fundamentals and Applications in the Petroleum Industry. American Chemical Society, 201–234.

Hirasaki, G.J., Lawson, J.B., 1985. Mechanisms of Foam Flow in Porous Media: Apparent Viscosity in Smooth Capillaries.

Hoelscher, K.P., De Stefano, G., Riley, M., Young, S., 2012. Application of nanotechnology in drilling fluids, SPE international oilfield nanotechnology conference and exhibition. Society of Petroleum Engineers.

Holler, H., Wirsching, U., 1985. Zeolite formation from fly-ash. Fortschritte der mineralogie 63, 21-43.

Holm, L.W., Josendal, V.A., 1974. Mechanisms of Oil Displacement By Carbon Dioxide. SPE-4736-PA 26, 1427-1438.

Horozov, T.S., 2008. Foams and foam films stabilised by solid particles. Current Opinion in Colloid & Interface Science 13, 134-140.

Hower, J.C., Maroto-Valer, M.M., Taulbee, D.N., Sakulpitakphon, T., 2000. Mercury capture by distinct fly ash carbon forms. Energy Fuels 14, 224-226.

Hunter, T.N., Pugh, R.J., Franks, G.V., Jameson, G.J., 2008. The role of particles in stabilising foams and emulsions. Advances in Colloid and Interface Science 137, 57-81.

Jarrell, P.M., Fox, C.E., Stein, M.H., Webb, S.L., 2002. Practical aspects of CO_2 flooding. Society of Petroleum Engineers Richardson, TX.

Jensen, J.A., Friedmann, F., 1987. Physical and Chemical Effects of an Oil Phase on the Propagation of Foam in Porous Media, SPE California Regional Meeting. Society of Petroleum Engineers, Ventura, California.

Johnston, K.P., Da Rocha, S.R.P., 2009. Colloids in supercritical fluids over the last 20 years and future directions. Journal of Supercritical Fluids 47, 523–530.

Joshi, R.C., Lohita, R., 1997. Fly ash in concrete: production, properties and uses. CRC Press.

Jung, J.H., Chu, Y.S., 2016. Characteristics of Mortar using Reject Fly Ash and Paper Sludge Ash. Journal of Korea Society of Waste Management 33, 778–785.

Kam, S.I., Rossen, W.R., 1999. Anomalous Capillary Pressure, Stress, and Stability of Solids–Coated Bubbles. Journal of Colloid and Interface Science 213, 329–339.

Kang, S., Jeon, S., Kang, H., Song, M., Kim, K., 2012. A Study on the Basic Characteristics of Fire Resistant Material using Slaked Fly Ash. Korea Concrete Institute, 331–332.

Kao, P.C., Tzeng, J.H., Huang, T.L., 2000. Removal of chlorophenols from aqueous solution by fly ash. Journal of hazardous materials 76, 237–249.

Kaptay, G., 2003. Interfacial criteria for stabilization of liquid foams by solid particles. Colloids Surfaces A: Physicochemical Engineering Aspects 230, 67–80.

Karakashev, S.I., Ozdemir, O., Hampton, M.A., Nguyen, A.V., 2011. Formation and stability of foams stabilized by fine particles with similar size, contact angle and different shapes.

Colloids and Surfaces A: Physicochemical and Engineering Aspects 382, 132–138.

Kelland, M.A., 2014. Production chemicals for the oil and gas industry. CRC press.

Khan, F.I., Kr. Ghoshal, A., 2000. Removal of Volatile Organic Compounds from polluted air. Journal of Loss Prevention in the Process Industries 13, 527–545.

Khanna, P., Malhotra, S., 1977. Kinetics and mechanism of phenol adsorption on fly ash. Indian J. Environ. Health 19, 224–237.

Kikuchi, R., 1999. Application of coal ash to environmental improvement: Transformation into zeolite, potassium fertilizer, and FGD absorbent. Resources, Conservation and Recycling 27, 333–346.

Kılınçkale, F., Ayhan, S., Apak, R., 1997. Solidification/ Stabilization of Heavy Metal-Loaded Red Muds and Fly Ashes. Journal of Chemical Technology Biotechnology 69, 240–246.

Kim, B., Prezzi, M., Salgado, R., 2005. Geotechnical Properties of Fly and Bottom Ash Mixtures for Use in Highway Embankments. 131, 914–924.

Kim, M., Yim, U.H., Hong, S.H., Jung, J.–H., Choi, H.–W., An, J., Won, J., Shim, W.J., 2010. Hebei Spirit oil spill monitored on site by fluorometric detection of residual oil in coastal waters off Taean, Korea. Marine Pollution Bulletin 60, 383–389.

Kovscek, A.R., Tadeusz, W.P., Radke, C.J., 1997. Mechanistic foam flow simulation in heterogeneous and multidimensional porous media. SPE Journal 2, 511-526.

Kumar, S., Upadhyay, S.N., Upadhya, Y.D., 1987. Removal of phenols by adsorption on fly ash. Journal of Chemical Technology & Biotechnology 37, 281-290.

Kurihara, M., Ikeda, K., Izawa, Y., Deguchi, Y., Tarui, H., 2003. Optimal boiler control through real-time monitoring of unburned carbon in fly ash by laser-induced breakdown spectroscopy. Appl. Opt. 42, 6159-6165.

Kuziemska, I., 1980. Application of water extract of brown coal fly ash to phosphate precipitation from polluted waters. Water Research 14, 1289-1293.

Lake, L., Schmidt, R.L., Venuto, P.B., 1992. A niche for enhanced oil recovery in the 1990s.

Lake, L.W., 1989. Enhanced oil recovery. Prentice Hall, Englewood Cliffs, N.J.

Lazaro, A., Brouwers, H.J.H., Quercia, G., Geus, J.W., 2012. The properties of amorphous nano-silica synthesized by the dissolution of olivine. Chemical Engineering Journal 211-212, 112-121.

Le Floch, S., Guyomarch, J., Merlin, F.-X., Stoffyn-Egli, P., Dixon, J., Lee, K., 2002. The Influence of Salinity on Oil-

Mineral Aggregate Formation. Spill Science & Technology Bulletin 8, 65-71.

Lee, J.M., Frankiewicz, T.C., 2005. Treatment of produced water with an ultrafiltration (UF) membrane-a field trial, SPE Annual Technical Conference and Exhibition. Society of Petroleum Engineers.

Lee, K., Lunel, T., Wood, P., Swannell, R., Stoffyn-Egli, P., 1997. Shoreline Cleanup by Acceleration of Clay-Oil Flocculation Processes. International Oil Spill Conference Proceedings 1997, 235-240.

Lee, K., Stoffyn-Egli, P., Wood, P.A., Lunel, T., 1998. Formation and structure of oil-mineral fines aggregates in coastal environments, twenty-first Arctic and marine oilspill program (AMOP) technical seminar. Environment Canada, Canada, 962.

Lee, S., Lee, D., Kim, J., Kim, J., 2017. Possible Usage of Waste Incineration Fly Ash Added Cementitious Material in 3D Printing. KOREAN SOCIETY OF CIVIL ENGINEERS, 1200-1201.

Lemly, A.D.J.E.p., 2015. Damage cost of the Dan River coal ash spill. 197, 55-61.

Li, Z., Liu, Z., Li, B., Li, S., Sun, Q., Wang, S., 2012. Aqueous Foams Stabilized with Particles and Surfactants, SPE Saudi

Arabia Section Technical Symposium and Exhibition. Society of Petroleum Engineers, Al-Khobar, Saudi Arabia, 9.

Lingling, X., Wei, G., Tao, W., Nanru, Y., 2005. Study on fired bricks with replacing clay by fly ash in high volume ratio. Construction building materials 19, 243-247.

Liou, T.-H., Yang, C.-C., 2011. Synthesis and surface characteristics of nanosilica produced from alkali-extracted rice husk ash. Materials Science and Engineering: B 176, 521-529.

Liu, Y., Li, Y., Li, X.-M., He, T., 2013. Kinetics of (3-aminopropyl) triethoxylsilane (APTES) silanization of superparamagnetic iron oxide nanoparticles. Langmuir 29, 15275-15282.

Maestro, A., Rio, E., Drenckhan, W., Langevin, D., Salonen, A., 2014. Foams stabilised by mixtures of nanoparticles and oppositely charged surfactants: relationship between bubble shrinkage and foam coarsening. Soft Matter 10, 6975-6983.

Manz, O.E., 1999. Coal fly ash: a retrospective and future look. Fuel 78, 133-136.

Mao, H., Qiu, Z., Shen, Z., Huang, W., 2015. Hydrophobic associated polymer based silica nanoparticles composite with core-shell structure as a filtrate reducer for drilling fluid at

utra-high temperature. Journal of Petroleum Science Engineering 129, 1-14.

Marangoni, C., 1865. Sull'espansione delle goccie d'un liquido galleggianti sulla superfice di altro liquido.

Maroto-Valer, M.M., Taulbee, D.N., Schobert, H.H., Hower, J.C., Andersen, J., 1999. Use of unburned carbon in fly ash as precursor for the development of activated carbons, International ash utilization symposium, paper.

Marrone, C., Poletto, M., Reverchon, E., Stassi, A., 1998. Almond oil extraction by supercritical CO_2 : experiments and modelling. Chemical Engineering Science 53, 3711-3718.

Maslehuddin, M., Al-Mana, A.I., Shamim, M., Saricimen, H., 1989. Effect of sand replacement on the early-age strength gain and long-term corrosion-resisting characteristics of Fy ash concrete. Materials Journal 86, 58-62.

Mishra, M.K., Karanam, U.R., 2006. Geotechnical characterization of fly ash composites for backfilling mine voids. Geotechnical Geological Engineering 24, 1749-1765.

Mo, D., Yu, J., Liu, N., Lee, R.L., 2012. Study of the effect of different factors on nanoparticle-stablized CO_2 foam for mobility control, SPE Annual Technical Conference and Exhibition. Society of Petroleum Engineers.

Morawska, L., Zhang, J.J., 2002. Combustion sources of particles. 1. Health relevance and source signatures. Chemosphere 49, 1045-1058.

Moreno, N., Querol, X., Ayora, C., Pereira, C.F., Janssen-Jurkovicová, M., 2001. Utilization of Zeolites Synthesized from Coal Fly Ash for the Purification of Acid Mine Waters. Environmental Science & Technology 35, 3526-3534.

Mukherjee, A.B., Zevenhoven, R., Bhattacharya, P., Sajwan, K.S., Kikuchi, R.J.R., Conservation, Recycling, 2008. Mercury flow via coal and coal utilization by-products: a global perspective. 52, 571-591.

Obla, K.H., Hill, R.L., Thomas, M.D., Shashiprakash, S.G., Perebatova, O., 2003. Properties of concrete containing ultra-fine fly ash. ACI materials journal 100, 426-433.

Oner, A., Akyuz, S., Yildiz, R., 2005. An experimental study on strength development of concrete containing fly ash and optimum usage of fly ash in concrete. Cement Concrete Research 35, 1165-1171.

OPEC, 2017. World Oil Outlook 2040.

Pei-Wei, G., Xiao-Lin, L., Hui, L., Xiaoyan, L., Jie, H., 2007. Effects of fly ash on the properties of environmentally friendly dam concrete. Fuel 86, 1208-1211.

Peloso, A., Rovatti, M., Ferraiolo, G., 1983. Fly ash as adsorbent material for toluene vapours. Resources conservation 10, 211–220.

Pichot, R., Spyropoulos, F., Norton, I.T., 2012. Competitive adsorption of surfactants and hydrophilic silica particles at the oil–water interface: Interfacial tension and contact angle studies. Journal of Colloid and Interface Science 377, 396–405.

Pickering, S.U., 1907. CXCVI.—Emulsions. Journal of the Chemical Society, Transactions 91, 2001–2021.

Pickles, C., McLean, A., Alcock, C., Nikolic, R., 1990. Plasma recovery of metal values from flyash. Canadian Metallurgical Quarterly 29, 193–200.

Princen, H., Aronson, M., Moser, J., 1980. Highly concentrated emulsions. II. Real systems. The effect of film thickness and contact angle on the volume fraction in creamed emulsions. Journal of Colloid and Interface Science 75, 246–270.

Princen, H., Science, I., 1979. Highly concentrated emulsions. I. Cylindrical systems. Journal of Colloid and Interface Science 71, 55–66.

Pugh, R.J., 1996. Foaming, foam films, antifoaming and defoaming. Advances in Colloid and Interface Science 64, 67–142.

Querol, X., Alastuey, A., Moreno, N., Alvarez-Ayuso, E., Garcıa-Sánchez, A., Cama, J., Ayora, C., Simón, M., 2006. Immobilization of heavy metals in polluted soils by the addition of zeolitic material synthesized from coal fly ash. Chemosphere 62, 171-180.

Querol, X., Moreno, N., Umaña, J.t., Alastuey, A., Hernández, E., Lopez-Soler, A., Plana, F., 2002. Synthesis of zeolites from coal fly ash: an overview. International Journal of coal geology 50, 413-423.

Ramsden, W., 1903. Separation of solids in the surface-layers of solutions and 'suspensions' (observations on surface-membranes, bubbles, emulsions, and mechanical coagulation).—Preliminary account. 72, 156-164.

Ranka, M., Brown, P., Hatton, T.A., 2015. Responsive Stabilization of Nanoparticles for Extreme Salinity and High-Temperature Reservoir Applications. ACS Applied Materials & Interfaces 7, 19651-19658.

Rankine, R.P., M & Sivakugan, Nagaratnam, 2007. Underground mining with backfills. Soils and Rocks 30, 93-101.

Ravina, D., Mehta, P.K., 1986. Properties of fresh concrete containing large amounts of fly ash. Cement Concrete Research 16, 227-238.

Reijnders, L., 2005. Disposal, uses and treatments of combustion ashes: a review. Resources, Conservation and Recycling 43, 313-336.

Reverchon, E., Senatore, F., 1992. Isolation of rosemary oil: comparison between hydrodistillation and supercritical CO_2 extraction. Flavour fragrance journal 7, 227-230.

Reynolds, R.R., Kiker, R.D., 2003. Produced water and associated issues. Oklahoma Geological Survey.

Rio, S., Delebarre, A., Hequet, V., Cloirec, P.L., Blondin, J., 2002. Metallic ion removal from aqueous solutions by fly ashes: multicomponent studies. Journal of Chemical Technology Biotechnology 77, 382-388.

Rossen, W.R., 1996. Foams in Enhanced Oil Recovery, in: R.K. Prud'homme, S.A. Khan (Eds.), Foams: Theory, Measurements, and Applications. Marcel Dekker, New York.

Rothenberg, S.J., Mettzler, G., Poliner, J., Bechtold, W.E., Eidson, A.F., Newton, G.J., 1991. Adsorption kinetics of vapor-phase m-xylene on coal fly ash. Environmental science technology 25, 930-935.

Rubel, A., Andrews, R., Gonzalez, R., Groppo, J., Robl, T., 2005. Adsorption of Hg and NOX on coal by-products. Fuel 84, 911-916.

Rubio, B., Izquierdo, M.T., Mayoral, M.C., Bona, M.T., Andres, J.M., 2007. Unburnt carbon from coal fly ashes as a precursor of activated carbon for nitric oxide removal. Journal of Hazardous Materials 143, 561–566.

Ruhl, L., Vengosh, A., Dwyer, G.S., Hsu–Kim, H., Deonarine, A., 2010. Environmental impacts of the coal ash spill in Kingston, Tennessee: an 18–month survey. Environmental science technology 44, 9272–9278.

Sarma, D.S.R., Khilar, K.C.J.I., research, e.c., 1988. Effects of initial gas volume fraction on stability of aqueous air foams. 27, 892–894.

Schramm, L.L., Hepler, L.G., 1994. Surface and interfacial tensions of aqueous dispersions of charged colloidal (clay) particles. Canadian Journal of Chemistry 72, 1915–1920.

Schroeder, W.H., Munthe, J., 1998. Atmospheric mercury—an overview. Atmospheric environment 32, 809–822.

Sethumadhavan, G.N., Nikolov, A.D., Wasan, D.T., 2001. Stability of Liquid Films Containing Monodisperse Colloidal Particles. Journal of Colloid and Interface Science 240, 105–112.

Sheng, J., 2013. Enhanced oil recovery field case studies. Gulf Professional Publishing.

Shi, C., Qian, J., 2003. Increasing coal fly ash use in cement and concrete through chemical activation of reactivity of fly ash. Energy Sources 25, 617–628.

Shi, Z., Zhang, Y., Liu, M., Hanaor, D.A.H., Gan, Y., 2018. Dynamic contact angle hysteresis in liquid bridges. Colloids and Surfaces A: Physicochemical and Engineering Aspects 555, 365–371.

Simsiman, G.V., Chesters, G., Andren, A.W., 1987. Effect of ash disposal ponds on groundwater quality at a coal–fired power plant. Water Research 21, 417–426.

Singh, R., Mohanty, K.K., 2015. Synergy between Nanoparticles and Surfactants in Stabilizing Foams for Oil Recovery. Energy & Fuels 29, 467–479.

Singh, R., Mohanty, K.K., 2017. Nanoparticle–stabilized foams for high–temperature, high–salinity oil reservoirs, SPE Annual Technical Conference and Exhibition. Society of Petroleum Engineers.

Sirivedhin, T., McCue, J., Dallbauman, L., 2004. Reclaiming produced water for beneficial use: salt removal by electrodialysis. Journal of Membrane Science 243, 335–343.

Sovová, H., 1994. Rate of the vegetable oil extraction with supercritical CO_2 —I. Modelling of extraction curves. Chemical Engineering Science 49, 409–414.

Stowe, G.B., 1991. Oil spill water treatment. CLNZALL Corp, US.

Sun, R., Sun, X., Sun, J., Zhu, Q., 2004. Effect of tertiary amine catalysts on the acetylation of wheat straw for the production of oil sorption-active materials. Comptes Rendus Chimie 7, 125-134.

Taber, J.J., Martin, F.D., Seright, R.S., 1997. EOR Screening Criteria Revisited - Part 1: Introduction to Screening Criteria and Enhanced Recovery Field Projects.

Teal, J.M., Howarth, R.W.J.E.M., 1984. Oil spill studies: a review of ecological effects. 8, 27-43.

Theis, T.L., Gardner, K.H.J.C.R.i.E.S., Technology, 1990. Environmental assessment of ash disposal. 20, 21-42.

Tikalsky, P., Carrasquillo, P., Carrasquillo, R., 1988. Strength and durability considerations affecting mix proportioning of concrete containing fly ash. ACI Materials Journal 85, 505-511.

USEPA, 2017. Inventory of US greenhouse gas emissions and sinks: 1990-2015, in: EPA (Ed.), Washington, DC, USA.

Van der Meer, B., 2005. Carbon dioxide storage in natural gas reservoir. Oil gas science technology 60, 527-536.

Veil, J.A., Puder, M.G., Elcock, D., Redweik Jr, R.J., 2004. A white paper describing produced water from production of crude oil,

natural gas, and coal bed methane. Argonne National Lab., IL (US).

Velikov, K.P., Durst, F., Velev, O.D., 1998. Direct Observation of the Dynamics of Latex Particles Confined inside Thinning Water–Air Films. Langmuir 14, 1148–1155.

Wang, W., Zhou, Z., Nandakumar, K., Xu, Z., Masliyah, J.H., 2004. Effect of charged colloidal particles on adsorption of surfactants at oil–water interface. Journal of Colloid and Interface Science 274, 625–630.

Warheit, D.B., Sayes, C.M., Reed, K.L., Swain, K.A., 2008. Health effects related to nanoparticle exposures: environmental, health and safety considerations for assessing hazards and risks. Pharmacology therapeutics 120, 35–42.

Weaire, D., Hutzler, S., 1999. The Physics of Foams: Oxford University Press, New York.

Wolcott, E.R., 1923. Method of increasing the yield of oil wells. Google Patents.

Worthen, A.J., Bagaria, H.G., Chen, Y., Bryant, S.L., Huh, C., Johnston, K.P., 2013a. Nanoparticle–stabilized carbon dioxide–in–water foams with fine texture. Journal of Colloid and Interface Science 391, 142–151.

Worthen, A.J., Bagaria, H.G., Chen, Y., Bryant, S.L., Huh, C., Johnston, K.P., 2013b. Nanoparticle–stabilized carbon

dioxide-in-water foams with fine texture. Journal of Colloid and Interface Science 391, 142-151.

Worthen, A.J., Bryant, S.L., Huh, C., Johnston, K.P., 2013c. Carbon dioxide-in-water foams stabilized with nanoparticles and surfactant acting in synergy. 59, 3490-3501.

Worthen, A.J., Vu, C., Cornell, K.A., Truskett, T.M., Johnston, K., 2016. Steric stabilization of nanoparticles with grafted low molecular weight ligands in highly concentrated brines including divalent ions.

Xu, H., Yan, F., Monson, E.E., Kopelman, R., 2003. Room-temperature preparation and characterization of poly (ethylene glycol)-coated silica nanoparticles for biomedical applications. Journal of Biomedical Materials Research Part A 66, 870-879.

Xue, Z., Worthen, A., Qajar, A., Robert, I., Bryant, S.L., Huh, C., Prodanović, M., Johnston, K.P., 2016. Viscosity and stability of ultra-high internal phase CO_2 -in-water foams stabilized with surfactants and nanoparticles with or without polyelectrolytes. Journal of Colloid and Interface Science 461, 383-395.

Yekeen, N., Idris, A.K., Manan, M.A., Samin, A.M., Risal, A.R., Kun, T.X., 2017. Bulk and bubble-scale experimental studies of influence of nanoparticles on foam stability. Chinese Journal of Chemical Engineering 25, 347-357.

Yellig, W., Metcalfe, R., 1980. Determination and Prediction of CO_2 Minimum Miscibility Pressures (includes associated paper 8876). SPE-4736-PA 32, 160-168.

Yusuf, S., Manan, M., Jaafar, M., 2013. Aqueous foams stabilized by hydrophilic silica nanoparticles via in-situ physisorption of nonionic TX100 Surfactant. Iran Energy Environ. 4, 08-16.

Zorpas, A., Constantinides, T., Vlyssides, A., Haralambous, I., Loizidou, M.J.B.T., 2000. Heavy metal uptake by natural zeolite and metals partitioning in sewage sludge compost. 72, 113-119.

김강주, 이은규, 이재철, 황수연, 김창현, 2012. 태안화력발전소 비산재로부터 리튬용출연구. 한국광물학회지 25, 117-122.

이종근, 김재영, 2013. 석탄재 내 희토류 회수 가능성 검토. Journal of Korea Society of Waste Management 30, 94-99.

Appendix.

Estimation of energy cost for fly ash nanoparticle production.

Energy costs can be estimated from electricity rates and vary from country to country. The type and accessibility of energy sources are the main factors affecting the electricity rates, but sometimes political and economic factors play a larger role. By 2016, for example, the electric price per kilowatt-hour(kWh) of Argentina was only 3 cents(Baker, 2016), which is only a tenth of Germany in the same period (2018b). There are differences in the energy policies of the two countries, which are abbreviated as nuclear power plants and renewable energy, but the main reason is the subsidies funded by the Argentine government.

For estimating the objective energy cost, industrial electricity rates in the U.S. and Korea were used in the calculations. The U. S. is politically and economically stable oil producing country, and Korea was chosen because its electricity rate is the closest to the IEA average (Annut, 2018).

Electric price varies by region to region in the U.S., the average industrial rates by state ranged from 4.64 to 20.87 cents per kWh. The national average was 6.92 cents per kWh in the U.S. (2017b). In Korea, there are no regional differences, but the calculation is more complicated because the rates vary depending on the time of operation, season, and maximum power demand (2018c). The high-voltage C-3 contract is the most economical choice when

the factory using 500,000 kWh per month operates 24 hours every day with the contract capacity at 120% of the required capacity considering the peak power demand for restart or cooling. In this assumption, the energy cost in Korea is 12.1 cents / kWh (Assuming that the exchange rate is 1,218 won per dollar).

In section 3.1.3.2, the specific energy to produce fly ash nanoparticles with a median size of 200 ㎚ was 8000 kJ/kg. In terms of kWh, 2,222 kWh/ton of energy is required to produce fly ash nanoparticles. When it is multiplied by the energy cost obtained above, the cost of producing one ton of fly ash nanoparticles can be obtained. The average energy cost is about 153 $/ton in the United States and about 269 $/ton in Korea. This is a rough estimate of the average energy cost per country and may vary depending on the region and the operating strategy. Additionally, actual energy need includes idling losses, equipment cooling, feeding of raw materials and transfer of product, which can result in a slight increase in energy costs. Although it is still competitive with synthetic silica, which costs more than $ 1,500 per ton.

초록

본 연구는 비산재의 선별 및 분쇄를 통해 석유 산업에 적용 가능한 나노입자를 생산하는 것을 목표로 하였다. 주요 적용 방안은 CO_2 기반 석유 증진 회수 연구에 쓰이는 합성 실리카 나노입자의 대체, 석유 생산 과정에서 발생하는 오일 폐수의 정화, 원유 유출 처리의 3 가지이다.

어트리션밀과 비드밀을 이용한 2 단계 분쇄 과정에서 비산재는 합성 실리카 가격의 약 10 분의 1 에 해당하는 에너지 비용을 소비하여 평균 입도 200 나노미터에 도달하였다. 별도의 처리를 거치지 않은 나노 입자는 초임계 CO_2 거품을 안정화시키기에 적합한 물성을 가지지 않아 계면활성제를 이용한 표면 개질을 시도했다. 열처리를 통해 광물 성분을 주로 남긴 비산재(TTFA)는 양이온계 계면활성제인 dodecyltrimethylammonium bromide (DTAB) 또는 음이온계 계면활성제인 Bioterge AS-40 와 만나 더 안정적인 초임계 CO_2 거품을 만드는 시너지 효과를 보였다. TTFA 나노입자가 해당 계면활성제와 함께 존재하면 거품의 밀도와 안정성이 증가하여 계면활성제가 단독으로 주입된 경우보다 저항 계수가 2 에서 4 배 증가하는 것이 연속 주입 실험에서 확인되었다.

고탄소 함량의 비산재 나노입자는 원유와 혼합했을 때 매우 안정한 응집물을 만들었다. 응집물은 원유가 모래에 침투하는 것을 지연시키고 조수나 파도에 의해 모래에서 원유가 분리되는 것을 촉진하여 원유 유출 처리에 도움을 주었다. 이 같은 특성은 파도가

치는 해변 근처에서 발생한 원유 유출 방제에 특히 효과적일 것으로 보인다.

고탄소 함량의 비산재는 10 ㎛ 이하로 분산된 오일이 포함된 생산수 처리에도 활용될 수 있었다. 고탄소 함량의 비산재를 오일량 대비 1:1 비율로 투입했을 때 수 백 마이크로 미터 크기의 가지 모양 응집체가 만들어졌으며 93 에서 97%의 오일 성분이 흡착된 후 침전하였다.

본 연구는 비산재의 탄소 성분과 광물 성분 각각에 대한 활용 방안을 탐색함으로써 비산재의 재활용률을 높이고 환경적 영향은 줄일 수 있는 가능성을 제시하였는데 그 의의가 있다.

핵심어: 비산재, 나노분쇄, 석유증진회수, 원유유출, 생산수 정화, CO_2 거품.

학번: 2010-21041